(12)

AD

AD-E400 956

AD A123793

CONTRACTOR REPORT ARLCD-CR-82060

EXPLOSION PREVENTION IN DRY DUST COLLECTION SYSTEMS

J. C. HOKANSON
R. J. MAGOTT
O. TRANBARGER
SOUTHWEST RESEARCH INSTITUTE
P. O. DRAWER 28510
6220 CULEBRA ROAD
SAN ANTONIO, TX 78284

G. PETINO
HAZARDS RESEARCH CORPORATION
ROCKAWAY, NJ 07866

W. O. SEALS
PROJECT ENGINEER
ARRADCOM

JANUARY 1983

US ARMY ARMAMENT RESEARCH AND DEVELOPMENT COMMAND
LARGE CALIBER
WEAPON SYSTEMS LABORATORY
DOVER, NEW JERSEY

The views, opinions, and/or findings contained in this report are those of the author(s) and should not be construed as an official Department of the Army position, policy, or decision, unless so designated by other documentation.

The citation in this report of the names of commercial firms or commercially available products or services does not constitute official endorsement by or approval of the U.S. Government.

Destroy this report when no longer needed. Do not return to the originator.

UNCLASSIFIED

SECURITY CLASSIFICATION OF THIS PAGE (When Data Entered)

REPORT DOCUMENTATION PAGE		READ INSTRUCTIONS BEFORE COMPLETING FORM
1. REPORT NUMBER Contractor Report ARLCD-CR-82060	2. GOVT ACCESSION NO. AD-A123	3. RECIPIENT'S CATALOG NUMBER 743
4. TITLE (and Subtitle) EXPLOSION PREVENTION IN DRY DUST COLLECTION SYSTEMS		5. TYPE OF REPORT & PERIOD COVERED Final Report July 1980 - July 1982 6. PERFORMING ORG. REPORT NUMBER 02-6180
7. AUTHOR(s) J.C. Hokanson, R.J. Magott, and O. Tranbarger, Southwest Research Institute; G. Petino, Hazards Research Corp.; W.O. Seals, Proj Engr, ARRADCOM		8. CONTRACT OR GRANT NUMBER(s) DAAK10-80-C-0176
9. PERFORMING ORGANIZATION NAME AND ADDRESS Southwest Research Institute P.O. Drawer 28510, 6220 Culebra Road San Antonio, TX 78284		10. PROGRAM ELEMENT, PROJECT, TASK AREA & WORK UNIT NUMBERS MMT-5804288
11. CONTROLLING OFFICE NAME AND ADDRESS ARRADCOM, TSD STINFO Div (DRDAR-TSS) Dover, NJ 07801		12. REPORT DATE January 1983 13. NUMBER OF PAGES 182
14. MONITORING AGENCY NAME & ADDRESS(if different from Controlling Office) ARRADCOM, LCL Energetic Systems Proc Div (DRDAR-LCM-SA) Dover, NJ 07801		15. SECURITY CLASS. (of this report) Unclassified 15a. DECLASSIFICATION/DOWNGRADING SCHEDULE

16. DISTRIBUTION STATEMENT (of this Report)

Approved for public release; distribution unlimited.

17. DISTRIBUTION STATEMENT (of the abstract entered in Block 20, if different from Report)

18. SUPPLEMENTARY NOTES

This project was accomplished as part of the U.S. Army's Manufacturing Methods and Technology Program. The primary objective of this program is to develop, on a timely basis, manufacturing processes, techniques, and equipment for use in production of Army materiel. (cont)

19. KEY WORDS (Continue on reverse side if necessary and identify by block number)

Minimum ignition energy
Minimum explosive concentration
Explosion severity
Composition B
Composition A-5
Static electricity
MMT - Dust explosion

20. ABSTRACT (Continue on reverse side if necessary and identify by block number)

To reduce the risk of dust explosions in propellant and explosive manufacturing plants, dust is captured as it is generated and transported through ducts to filters, separators, or collectors. However, the dust collection systems may potentially contribute to the accident potential within the plant. A series of site visits was made to measure the electrostatic potential buildup and the dust concentration levels in ducting actually present during normal plant operations. These data provide a base of plant operating conditions upon which one may evaluate the safety of dry dust collection systems.

DD FORM 1 JAN 73 1473 EDITION OF 1 NOV 65 IS OBSOLETE

UNCLASSIFIED

SECURITY CLASSIFICATION OF THIS PAGE (When Data Entered)

18. SUPPLEMENTARY NOTES (cont)

Hazards Research Corporation, 200 E. Main Street, Rockaway, N.J. was the subcontractor on this project.

20. ABSTRACT (cont)

A survey was conducted to determine if off-the-shelf instrumentation exists which will measure dust concentrations dynamically at levels within the explosive range. After an extensive search, one such instrument was located and evaluated.

Most dust explosive characterizations are conducted using the Hartmann apparatus. This instrument is useful for evaluating relative characteristics of dusts. However, it has been shown that this instrument underpredicts both the peak pressure and the pressure rise rate for full-scale explosions. In designing explosion venting or explosion-resistant structures, data obtained in larger chambers are needed to allow the prediction of full-scale trends. A series of experiments was conducted using 40- and 1000-liter vessels to characterize the peak pressure and pressure rise rate for several explosive dusts.

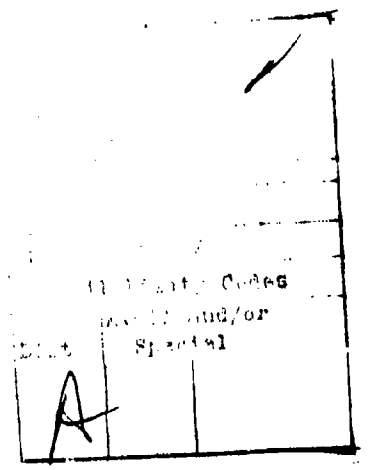

CONTENTS

	Page
Introduction	1
Army Ammunition Plant Testing	3
Test Objectives	3
Preliminary Plant Visits	3
Test Equipment and Procedures	4
Plant Visits and Sampling Results	18
Louisiana AAP	18
Longhorn AAP	36
Lone Star AAP	46
Summary of Plant Sampling	67
Selection of Dust Detection Equipment	72
Survey	72
Characterization of Explosive Dusts	76
Overview	76
Ignition	79
Explosibility Test Results	81
Conclusions	97
Plant Sampling	97
Survey of Concentration Equipment Measurement	97
Explosion Tests	98
Recommendations	100
References	101
Appendix	
A Calculation of Duct Velocity	103
B Derivation of Electrostatic Energy Contained in a Dust-Filled Dust; Electrostatic Instrument Calibration; Development of Sampling Procedures	107
C Dust Detection Instrumentation Data Sheets	119
D Dust Explosion Characteristics of Composition A-5, TNT, and, Sodium Nitrate (Subcontractor's Report)	123
E Comprehensive Test Data	165
Distribution List	171

FIGURES

		Page
1	Pitot-Static Velocity Probe	5
2	Duct Flow Velocity Sample Locations	6
3	Temperature and Humidity Measurement Technique in a Typical Duct	8
4	Dust Sampling Probe	9
5	Duct Velocity and Dust Sample Flow Rate Panel Board	11
6	Charge Density Sensor	13
7	Charge Density Control and Readout Unit	14
8	Power Supply	15
9	Charge Density Measurement	16
10	Dust and Electrostatic Sampling Location in the Composition B Screening and Bin Loading Operation of Building 1611, Louisiana AAP	19
11a	Fixtures Used to Penetrate the Building 1611 Ducting	21
11b	Fixtures Used to Penetrate the Building 1611 Ducting	22
12	Dust and Electrostatic Sample Locations in the Drilling Operation of Building 1619, Louisiana AAP	23
13	Instrumented Duct Section Installed at Sample Location 5 at Building 1619, Louisiana AAP	24
14	Electrostatic Measurements at Building 1611 in 30.5 cm Diameter Duct at Location 1	29
15	Charge Density Measurements at Building 1611 in 10.2 cm Diameter Duct at Location 2	30
16	Electrostatic Measurements at Building 1611 in 30.5 cm Diameter Duct at Location 3	31
17	Charge Density Measurements at Location 4 During Deep Drilling Operations at Building 1619	33

		Page
18	Charge Density Measurements at Location 5 During Shallow Drilling Operations at Building 1619	34
19	Dust and Electrostatic Sampling Locations in 4.2 Aluminum Candle Production Process in Building B-7, Longhorn AAP	37
20	Dust and Electrostatic Sampling Locations in the Signal Flare Production Process in Building 34-Y, Longhorn AAP	38
21	Charge Density Measurements at Building B-7 at Sample Location 6	44
22	Charge Density Measurements at Building B-7 at Sample Location 7	45
23	Charge Density Measurements at Building 34-T at Sample Location 8	47
24	Charge Density Measurements at Building 34-Y at Sample Location 9	48
25	Vacuum Exhaust Ducting and Dust Collection System for Burster Facing Operation in Building 04-M-40	51
26	Dust Exhaust Line on Drill Head in 04-M-40	52
27	Vacuum Exhaust and Dust Collection System for Grenade Press Operation in Building B-46	53
28	Rotary Pellet Press and Dust Collection Lines in Building B-46	54
29	Probe Attachment Fixture Installed at Building B-46	56
30	Charge Density Measurements at Building 04-M-40 at Sample Location 10	62
31	Charge Density Measurements at Building 04-M-40 at Sample Location 11	63
32	Charge Doublets Measured at Building B-46 at Sample Location 14	65
33	Charge Density Measurements at Buildings B-46 at Sample	66
34	Charge Density Dependence on Mass Flow Rate Through the Duct	71
35	Minimum Ignition Energy Tests Using the SwRI Lucite Hartmann Apparatus	80

		Page
36	Hartmann Bomb Apparatus	82
37	40 Liter Explosion Chamber	83
38	Pressure Wave Forms Obtained in Composition B Explosives Ignited by the AC Arc in the 40-Liter Chamber	85
39a	Maximum Pressure in Composition B Explosions Ignited by the AC Arc in the 40 Liter Chamber	86
39b	Pressure Rise Rate in Composition B Explosions Ignited by the AC Arc in the 40 Liter Chamber	87
40a	Maximum Pressure in Composition B Explosions Initiated by the BEM in the 40 Liter Chamber	88
40b	Pressure Rise Rate in Composition B Explosions Ignited by the BEM in the 40 Liter Chamber	89
41a	Maximum Pressure in Composition A-5 Explosions Ignited by the BEM in the 40 Liter Chamber	90
41b	Pressure Rise Rate in Composition A-5 Explosions Ignited by the BEM in the 40 Liter Chamber	91
42	Picture of $1m^3$ Vessel	93
43	Pressure Wave Forms Obtained in Composition B Explosives Ignited by the AC Arc in the $1m^3$ Vessel	94
44a	Comparison of Maximum Pressures Obtained in Composition B Explosives and Vessels of Different Volumes	95
44b	Comparison of Pressure Rise Rates Obtained in Composition B Explosions in Vessels of Different Volumes	96

TABLES

		Page
1	Duct Velocity and Flow Rate Data for Buildings 1611 and 1619 Louisiana AAP	25
2	Duct Sampling Data at Louisiana AAP	27
3	Charge Density and Energy Levels Measured in Louisiana AAP	35
4	Duct Velocity and Flow Rate at Building B-7 at Longhorn AAP	40
5	Duct Velocity and Flow Rate Data at Building 34-Y at Longhorn AAP	41
6	Dust Sampling Data in Building B-7 and B-34, Longhorn AAP	42
7	Charge Density and Energy Levels Measured in Longhorn AAP	49
8	Duct Velocity and Flow Rata Data for Building 04-M-40 at Lone Star AAP	57
9	Duct Velocity and Flow Rate for Building B-46 at Lone Star AAP	58
10	Dust Sampling Data at Building 04-M-40	59
11	Dust Sampling Data in Building B-46	60
12	Charge and Energy Levels Measured in Lone Star AAP	68
13	Summary of Measurements Taken During the Plant Sampling	69
14	Dust Detection Equipment	73
15	Comparison of Dust Explosion Test Vessels	78

INTRODUCTION

Dust explosions occur when particular levels of concentration, ignition energy, air and confinement are present. To reduce the risk of dust explosions in propellant and explosive manufacturing plants, dust is captured as it is generated and transported through ducts to filters, separators or collectors. As dust flows through ducts, static electricity is generated by the collisions of dust particles with each other and with the ducting. If this electrostatic energy is of a sufficient level, it could initiate burning or explosive reactions within the dust. If the electrostatic energy level is less than that required to initiate the energetic reaction directly, it can still contribute to initiation by reducing the energy required from some other ignition source. Bonding and grounding techniques can mitigate these effects if the static electricity can be bled off at a higher rate than it is generated. However, flow conditions within the duct could be such that insulation of the static electricity from the grounding system could inhibit the full potential of grounding.

Another potential hazard exists within the dust collection system. If the dust concentration is above the lower explosive limit, and if the dust is initiated, the duct could be the basis of transporting explosive reactions to other operations and stations within the plant, or out to the dust collector. The interrelations of duct size, concentration levels, and flow conditions have not been investigated in terms of initiating and propagating reactions within ducts.

Dusts which do not contain their own oxidizer have an upper explosive limit. That is, if the dust concentration is sufficiently high, the fuel-air ratio of the cloud is sufficiently rich to preclude sustaining an energetic reaction. With dusts made from explosives and propellants, however, the oxidizers within the materials can contribute to sustaining energetic reactions at high concentrations. This, in turn, can provide a more energetic explosion than would be expected from dust with no internal oxygen.

It appears reasonable to expect that dust collection systems can contribute to the accident potential within the plants. It is also reasonable to expect that the initiation of explosive reactions and propagations within the dust collection ducts are much more complex in the dynamic environment than in one that is static. What was needed, then, was a characterization of the environment within the dust collection systems so that controls can be postulated and evaluated. To this end, a series of site visits was made to ascertain the electrostatic potential buildup in representative dust collection ducts. Also measured were dust concentration levels on time-average bases.

Since high dust concentrations can contribute to the violence of the explosive reactions, it was determined that it would be desirable to measure the concentration levels in dust collection ducts dynamically. A survey was conducted to determine if off-the-shelf instrumentation

exists which will measure dust concentrations at levels within the explosive range. After an extensive search, one such instrument was evaluated.

Most dust explosive potential characterizations are conducted using the Hartmann apparatus. This instrument is useful for evaluating relative characteristics between dust types. However, it has been shown that this instrument underpredicts both the peak pressure and the pressure rise rate for full scale explosions. Both parameters are important in designing explosion venting or explosion-resistant structures, and larger chambers are needed to allow the full-scale trends to be predicted. A series of experiments was conducted using 40ℓ and 1000ℓ vessels to characterize the peak pressure and pressure rise rate for explosive dust.

The remaining sections of this report describe: the site visits, the instrumentation used and the data collected, an assessment of the data gathered from the site visits, the results of the survey of concentration measurement instruments, explosion characterization experiments with Hartmann 40ℓ and 1000ℓ chambers, conclusions and recommendations.

ARMY AMMUNITION PLANT TESTING

Test Objectives

The objective of the sampling conducted in the Army Ammunition Plants (AAP) was to characterize the explosion potential in the ducts used to transport explosive dust generated from selected munitions manufacturing processes during actual plant operation. The essential measurements made were aimed at quantifying the concentration of explosive dust and the level of electrical energy resulting from electrostatic charge accumulation in the duct. The three plants visited were

Louisiana AAP, Shreveport, Louisiana
Longhorn AAP, Marshall, Texas
Lone Star AAP, Texarkana, Texas.

Preliminary Plant Visits

Prior to actual testing, a preliminary visit was made to each plant to become familiar with the type of manufacturing processes, to select those processes where sampling would subsequently be performed, and to determine the logistical requirements necessary to interface measurement equipment with the in-process dust collection systems.

A summary of the important aspects of the preliminary plant visits is enumerated below:

- The majority of dust exhaust ducting used to transport explosive dust from the manufacturing process is of small [$\leq$ 5.08 cm (2 in.)] diameter.
- The internal static pressures within the ducting ranged from 2.29 to 152 mm Hg (0.09 to 6.0 in. Hg) vacuum.
- Plant operating safety requirements do not allow personnel in the production area during operation. This requires the implementation of remote sampling techniques.
- Most production processes operate on a half-day production schedule, with blocks of time set aside for start-up, housekeeping, shutdown, breaks, and lunch. The operational schedule effectively limits the sampling that can be performed in one day.
- All of the plants required that the data collection be designed for minimum interruption of production. In some cases shutdown of production was not allowed for servicing or inspection of the sampling equipment.
- Typically, production schedules are short-term and notice of production start-up cannot be given more than one week in advance.

- Each duct sample location required the fabrication of a replacement duct section in which the necessary dust and electrostatic sampling ports were installed. The replacement sections were removed at the completion of the sampling and the original ducting was replaced.

Test Equipment and Procedures

After the initial plant visits, a sampling strategy was developed which would enable the measurement of the critical parameters affecting the explosibility of the dust in the duct. The critical parameters which, by contract, were measured included:

- Duct Velocity
- Flow Rate
- Dust Concentration
- Duct Temperature
- Duct Humidity
- Charge Density
- Electric Field.

The test equipment and procedures used to measure the above parameters are described in the following sections.

Dust Sampling Equipment

To characterize the concentration of dust flowing inside a duct, two criteria must be considered. First, one must be able to withdraw a measured amount of the dust from the duct over a known period of time. The collection velocity must be the same as the internal duct flow velocity so that it does not alter the distribution of dust particle sizes. By meeting these conditions, one can obtain an accurate measurement of dust concentration at one point in the duct. In order to define the overall dust concentration, a reasonable number of points must be sampled over the entire duct cross section. The above sampling techniques, known as gravimetric sampling under isokinetic conditions, was used in the determination of dust concentration at selected locations within the dust collection systems of several processes in the three Army Ammunition Plants mentioned above.

Duct Velocity and Flow Rate.

Dust sampling was initiated by measuring the internal flow velocity in the duct at various points along the vertical diameter of the selected duct sample location. The equipment used to accomplish this was a pitot static tube and a magnehelic gage as shown in Figure 1. Based on standard practices, the duct cross section was divided into three concentric annulli with equal areas and the velocity pressure was measured at the centers of these areas on each side of the duct centerline. An additional measurement was also taken at the duct centerline. The sample locations are shown in Figure 2. (In some cases, the top and

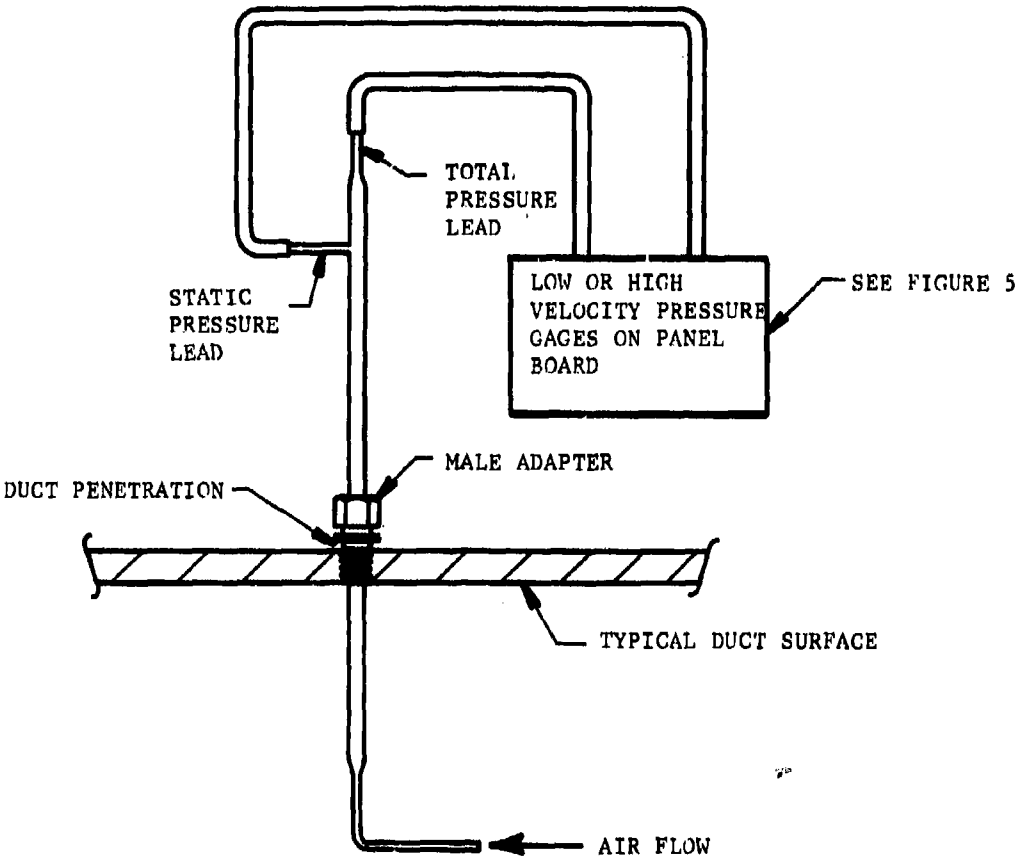

Figure 1. Pitot-Static Velocity Probe

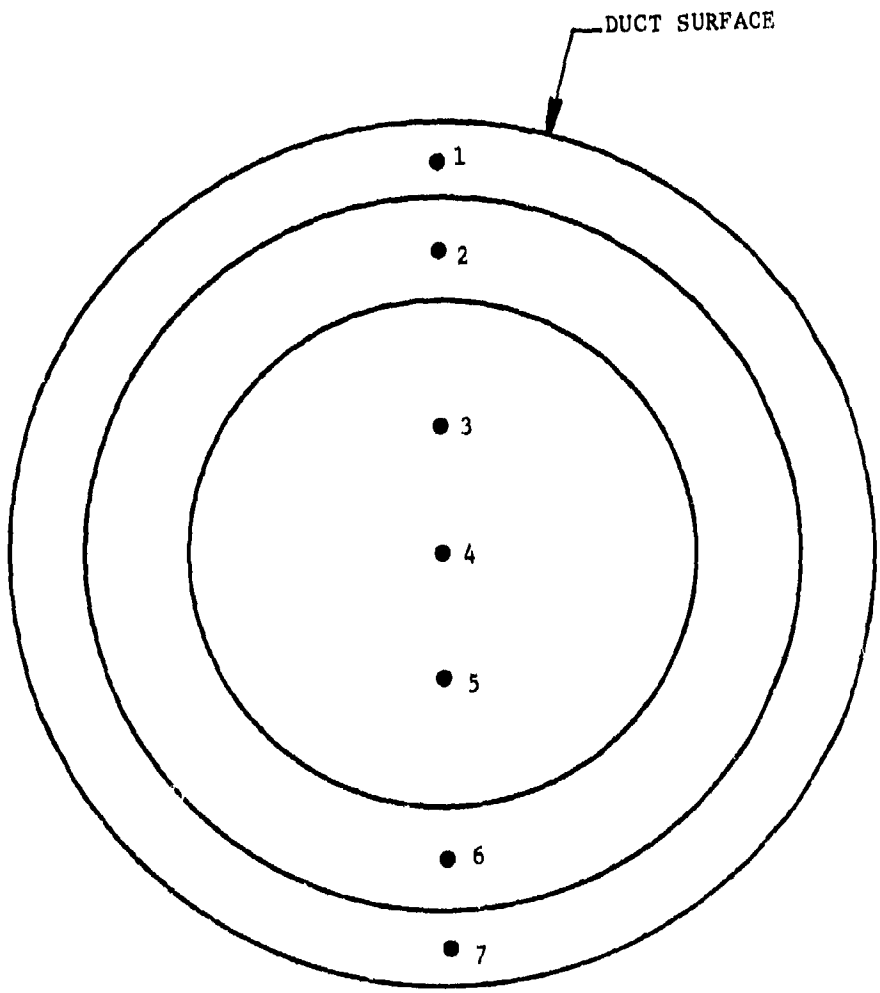

Figure 2. Duct Flow Velocity Sample Locations

bottom locations could not be sampled because the probe could not be physically positioned at these locations due to the design of the probe.) The velocity at each point was then calculated by the following equation:

$$V_i = 1096\sqrt{\frac{VP_i}{\rho}} \qquad (1)$$

where

VP_i = velocity pressure at the i^{th} traverse point

ρ = density of the gas at the duct sample location.

To calculate the gas density, the duct humidity, temperature, and static pressure were measured. The method for determining the humidity consisted of measuring the wet and dry bulb temperature of a continuous sample stream that was withdrawn from the duct through a 6.35 mm (0.25 in.) stainless steel tube as shown in Figure 3. An inline metal filter (5 micron pore size) was used to prevent dust build-up on the wick of the wet bulb thermometer. Provided no moisture condensed out in the sample tubing, the absolute humidity obtained from the wet and dry bulb reading taken in the 2.54 cm (1.0 in.) pipe cross fixture would be the same as that in the duct. A more detailed velocity equation, which includes the calculation of the gas density in the duct is given in Appendix A.

The total duct flow rate, Q, was obtained by multiplying the average of the velocity measured at the seven points, $\overline{V}$, by the duct cross section, A_d, as shown below:

$$\overline{V} = \frac{1}{7}\sum_{i=1}^{7} V_i \qquad (2)$$

$$Q = \overline{V} \cdot A_d \qquad (3)$$

Dust Concentration.

To obtain dust concentrations within the duct, dust samples were collected using the probe/filter arrangement shown in Figure 4. The locations where the samples were withdrawn coincided with the velocity traverse points. The probe was fabricated from standard 6.35 mm (0.25 in.) stainless steel tubing long enough to traverse the entire duct diameter. The filter on which the explosive dust was trapped was a Millipore® 37-mm plastic filter casette. Each casette contained a backing pad which supported a pre-weighed acetate filter paper. These filters are typically used for ambient particulate sampling. The inlet

® Registered Trademark of Millipore Corporation, Bedforth, MA.

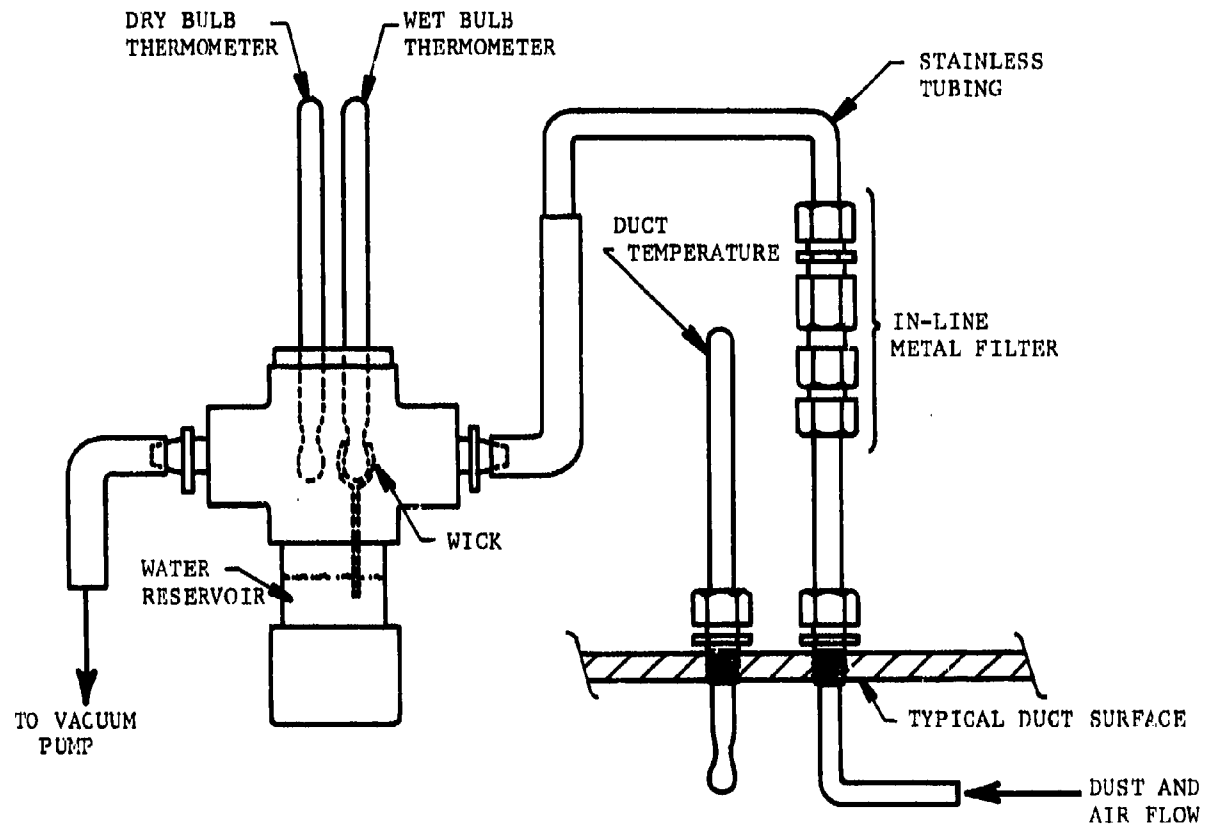

Figure 3. Temperature and Humidity Measurement Technique in a Typical Duct

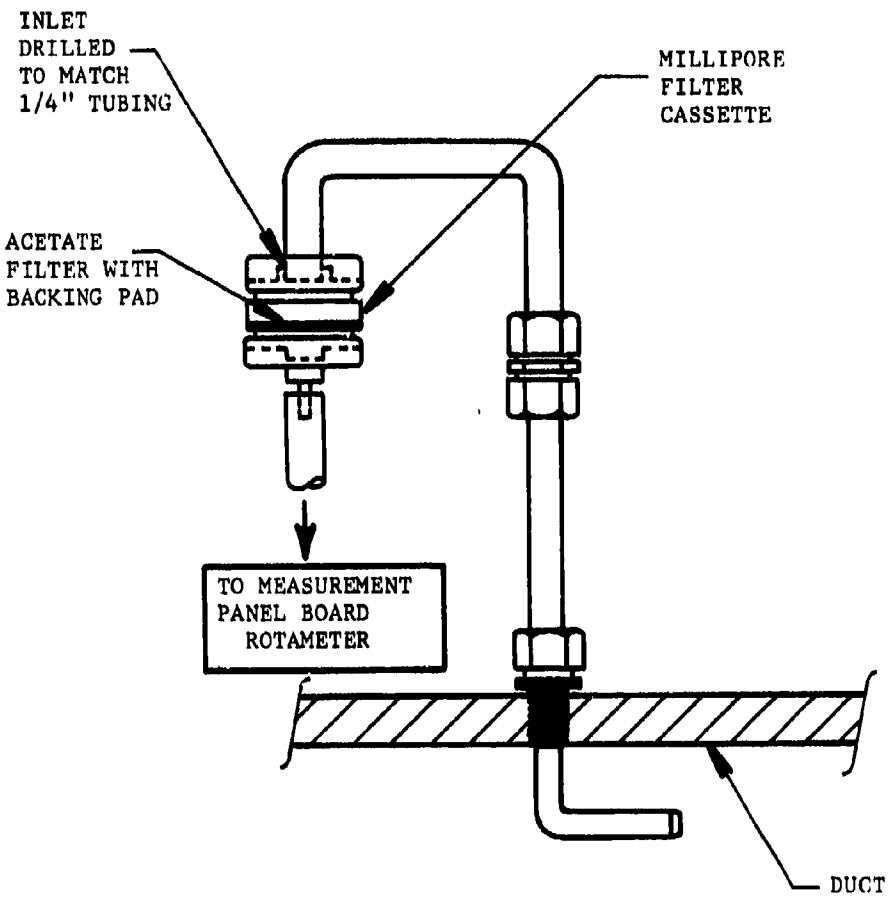

Figure 4. Dust Sampling Probe

was drilled out to slightly less than 6.35 mm (0.25 in.) to allow for a friction fit between the probe and filter cassette.

Once the velocity, V_i, was determined at a particular traverse point inside the duct, the sample flow rate, Q_{si}, required to extract a dust sample isokinetically was calculated by Equation 4:

$$Q_{si} = V_i \cdot A_p \tag{4}$$

where

A_p = the cross-sectional area of the dust sampling probe.

The rotameter on the measurement panel board in Figure 5 was used to moniter the actual sampling flow rate.

Calculation of the dust concentration at each traverse point was obtained by Equation 5:

$$C_i = \frac{W_{Di}}{Q_{si}\Delta t_{si}} \tag{5}$$

where

C_i = dust concentration in the duct

W_{Di} = weight of dust collected on the filter cassette

Q_{si} = probe sample flow rate

Δt_{si} = sampling time,

and the subscript i represents the value at the i^{th} traverse point.

Electrostatic Instrumentation.

The objectives of the electrostatic sampling were to measure the electrostatic conditions in representative explosive and pyrotechnic dust collection systems and to assess the potential hazards imposed by the observed electrostatic levels. To accomplish these objectives, the electrostatic charge levels within selected dust collection systems

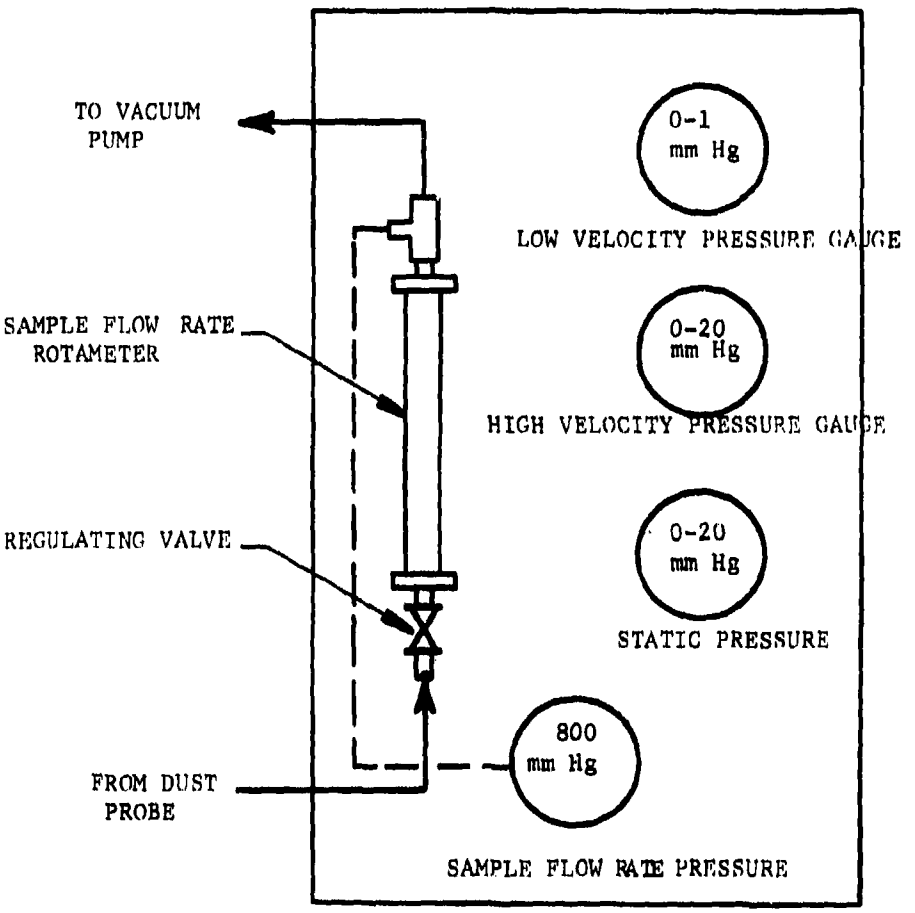

Figure 5. Duct Velocity and Dust Sample Flow Rate Panel Board

were monitored with instrumentation that measured the charge density of the dust being transported through the ducts and the resulting electric fields at the duct inner walls. An instrument designed originally for measuring the space charge density of charged water aerosols [1,2,3] was used for making the charge density measurements. A Monroe Electronics, Inc., Model 171 electric fieldmeter was used for the electric fieldmeter measurements. A theoretical equation was derived for circular geometries that allows estimation of the electrical energy in the ducting which is potentially available for discharge from the measurements of the charge density and the electric field. The derivation of this equation is provided in Appendix B. Calibration of the electrostatics instrumentation is also discussed in Appendix B.

Charge Density Measurement.

Charge density measurements were made with a charge density meter designed and built by SwRI for the purpose of measuring electrostatic space charge on water and hydrocarbon aerosols within the cargo tanks of crude oil tankships. The instrument was designed and fabricated to comply with the requirements of the National Fire Protection Association (NFPA) Standard 460. The charge density meter consists of a Sensor Unit, a Control and Readout Unit and a Power Supply. These units are shown in Figures 6, 7 and 8.

Operation of the instrument requires ingesting a sample of the dust flow in the duct through the sensor unit. The sensor contains a series of steel screens which trap the charge laden dust particles. The charge is removed from the steel screens to ground to avoid the build-up of hazardous energies in the sensor. This creates a picoampere current flow which is converted to a voltage for display on the control and readout unit and for recording. Both the sensor and the control and readout units are powered by the power supply.

A dust sample was extracted from the dust collection duct and transferred to the charge density meter through a 30.5 m (100 ft) long conductive rubber hose. Sample withdrawal was initiated by activating a pneumatically controlled three-way ball valve. One valve inlet was connected to the duct, and the other inlet went to the atmosphere and was used to purge the charge density meter before measurements were made. In practice, the dust was extracted from the duct for 30 to 60 seconds and transported through the conductive rubber hose to the sensor where the steel screens trapped the majority of the dust particles. An industrial vacuum cleaner drum was located downstream of the charge density meter to prevent any residual dust from getting into the vacuum pump or discharging to the atmosphere. Sampling flow rates were monitored by a turbine flow meter installed between the dust collector and the vacuum pump. Figure 9 shows schematically the equipment to obtain the charge density measurements.

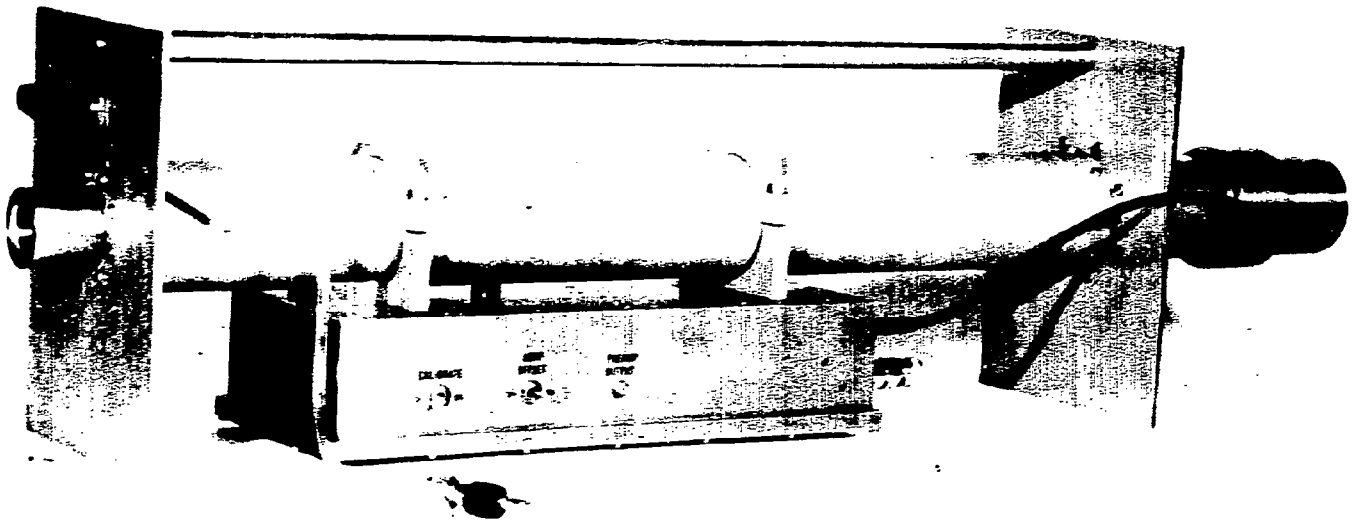

Figure 6. Charge Density Sensor

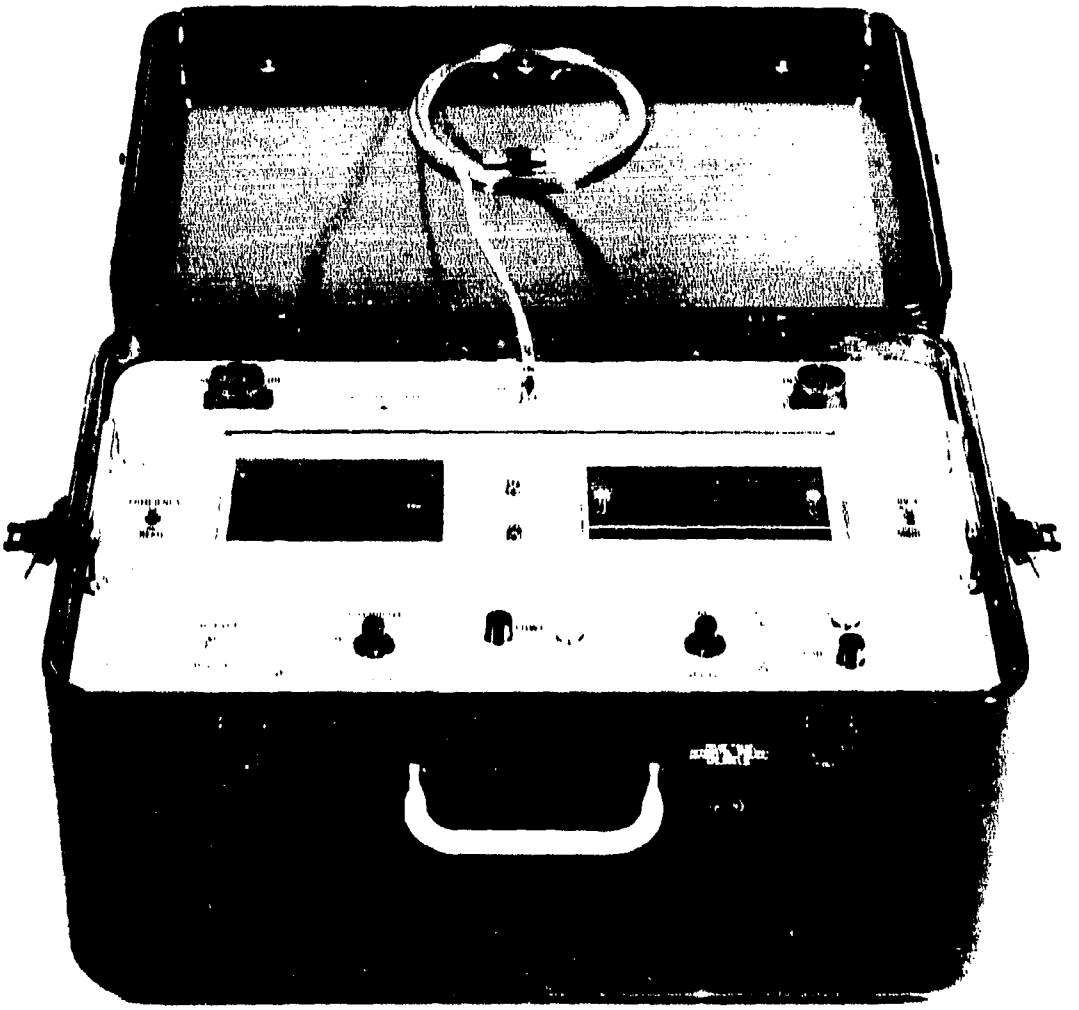

Figure 7. Charge Density Control and Readout Unit

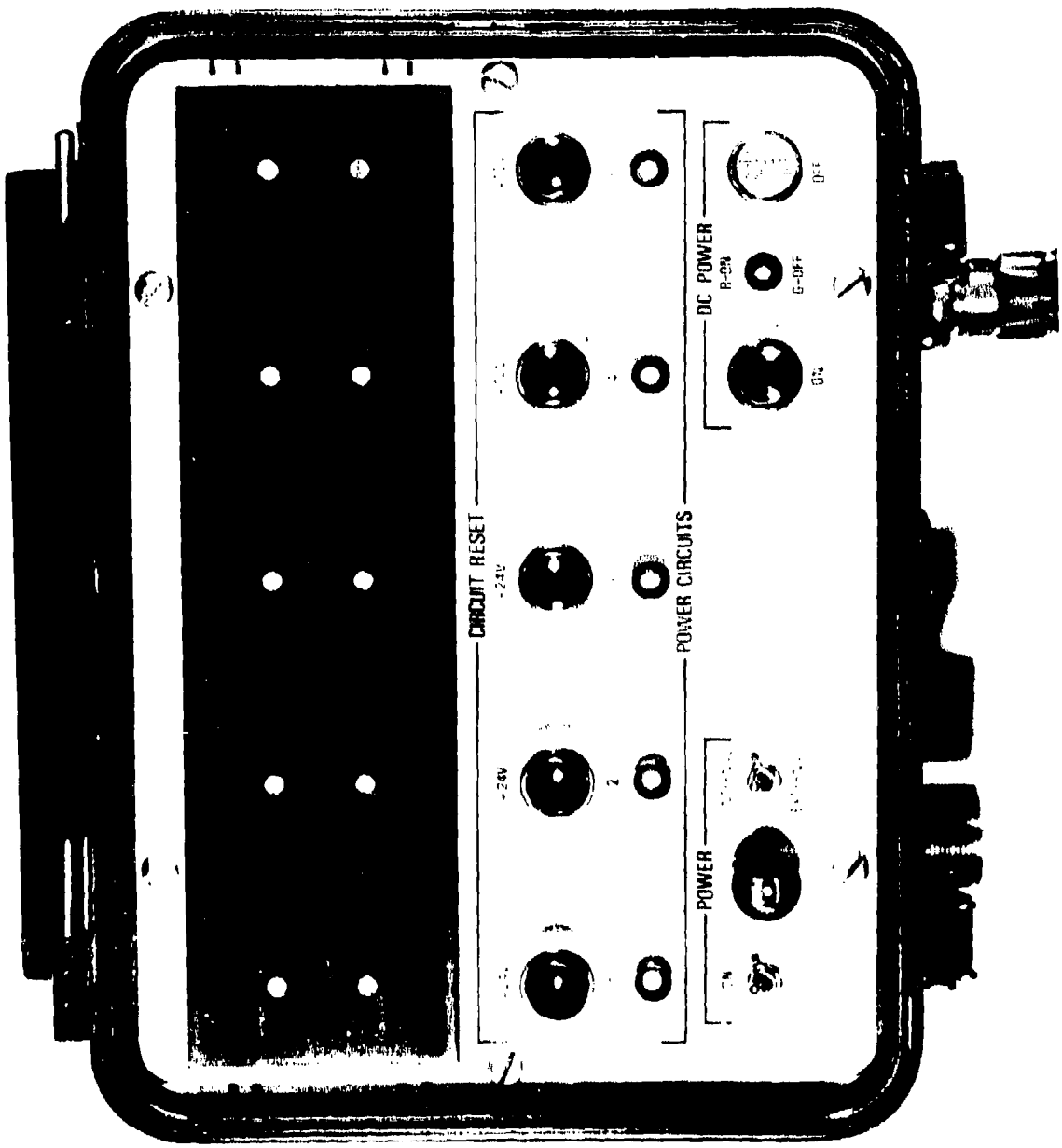

Figure 8. Power Supply

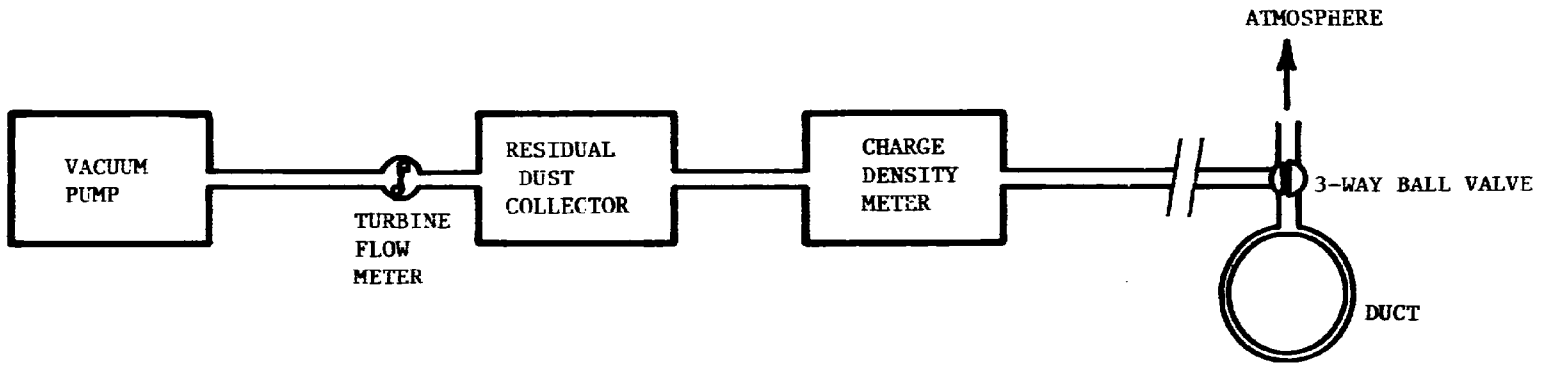

Figure 9. Charge Density Measurement

Electric Field Measurement.

The Model 171 Monroe Electronics Electric Fieldmeter was used in conjunction with a Model 1019B sensor probe to measure the electric field at the inner surface of the duct. The Model 1019B sensor contains a vibrating electrode enclosed in a capped, cylindrically-shaped probe. The environment in which the probe is positioned is viewed by the sensor through an opening on the face of the probe. An electric field from the charged dust particles around the sensor creates a voltage on the electrode, which is amplified. The amplified signal is sent to the Model 171 mainframe for demodulation and readout. A feedback voltage to the sensor head automatically nulls the electric field being measured. This feedback voltage is proportional to the field intensity at the probe. A constant low-pressure filtered air flow is provided to the probe for purging to reduce the deposition of dust on to the sensor.

Measurements with the electric field meter were confined to those plants sampling locations with large diameter ducts. Due to the physical dimensions of the sensor [approximately 5.1 cm (2.0 in.) diameter], sampling in small ducts was precluded because the probe would lead to distorted electric field measurements.

PLANT VISITS AND SAMPLING RESULTS

Prior to initiating the actual sampling, a test plan was developed for each of the three Army Ammunition Plants chosen for study. The test plans were submitted to ARRADCOM and ARRCOM for review and approval. Once the test plans were approved, each plant was contacted individually and arrangement for plant support, dimensions of the ducting to be replaced by test sections, specifications of the dust control systems and a date for the plant sampling were obtained. The following sections describe the plant processes in which sampling was performed and detail the results of the measurements. A short summary at the end of this section compares the measurements taken at all sampling locations.

Louisiana AAP

The dust exhaust ducting of two different processes in the Louisiana AAP was sampled for both dust concentration and electrostatic charge accumulation. The two processes were (a) the Composition B screening and bin loading in Building 1611 and (b) the 155 mm shell drill out operation in Building 1619. Along with investigating the above parameters based on the differences in the processes conducted in the two buildings, the visit to Louisiana AAP also afforded sampling in a variety of different duct sizes. Large diameter ducts of 30.5 cm (12.0 in.) and 10.2 cm (4.0 in.) were prevalent in 1611 as compared to the small 5.1 cm (2.0 in.) ducting utilized in 1619.

Process Descriptions and Sample Locations

Building 1611.

In Building 1611, bulk Composition B explosive is received in 27.4 kg (60 lb) boxes and conveyed to the second floor of the building. The boxes are dumped onto a shaker table and the explosive is screened for removal of foreign matter. Dust generated by this operation is contained by vent hoods above the shaker table and transferred through 30.5 cm (12.0 in.) diameter ducts to the wet collector shown in Figure 10. After screening, the explosive material drops through a duct into a loading bin on the first floor. To assure even filling of the hopper, one plant employee stirs the contents with a paddle. The dropping of the flake material produces explosive dust which is removed in a 10.2 cm (4.0 in.) duct attached to the hopper. The 30.5 cm (12.0 in.) and 10.2 cm (4.0 in.) ducts connect in a Y-configuration on the first floor and continue on toward the wet collector. The duct diameter downstream of the Y was also 30.5 cm (12.0 in.).

As shown in Figure 11, three locations were sampled at 1611. Sample location No. 1 was located in the second floor exhaust ducting servicing the shaker table, while location No. 2 was in the ducting connected directly to the loading bin on the first floor. The combined effects of these two activities were investigated at location No. 3 which was near the wet collector. Each location coincided with a duct cleanout opening

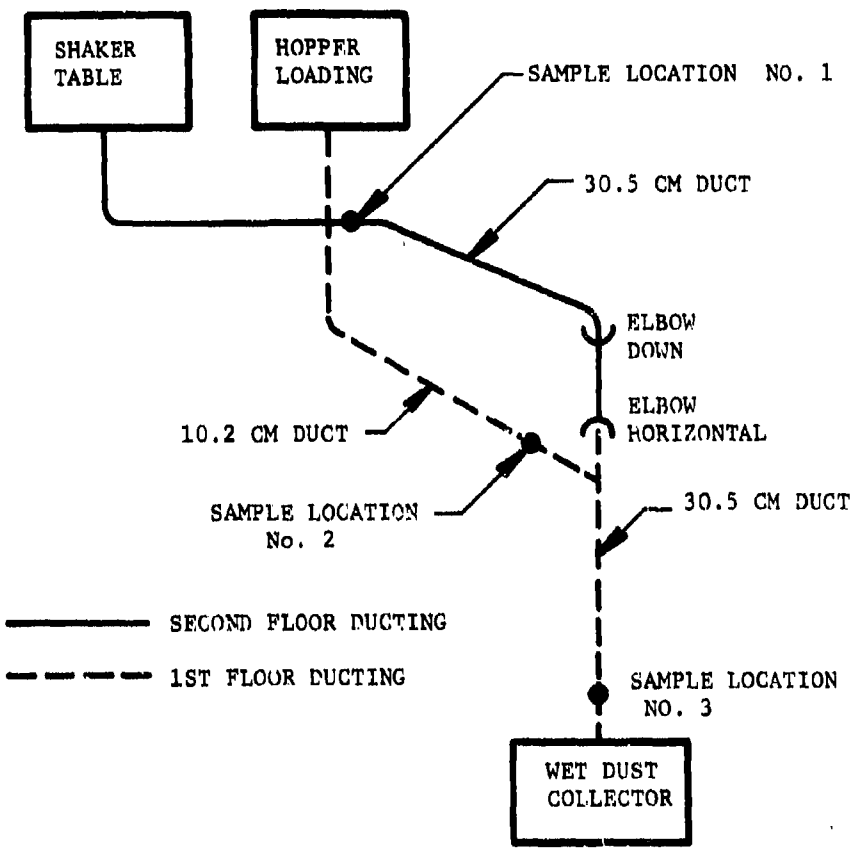

Figure 10. Dust and Electrostatic Sampling Location in the Composition B Screening and Bin Loading Operation of Building 1611, Louisiana AAP

as shown in Figure 11a. These openings are used to facilitate removal of dust accumulations in the ducting; this cleaning operation is performed once a week. The cleanouts for sample locations No. 1 and 2 were on the bottom side of the duct while sample location No. 3 had a cleanout on the top of the duct. The probe attachment fixture used to interface the dust and electrostatic sampling equipment is shown in Figure 11b, and installed in the duct in Figure 11a. The essential feature in its design was the round bottom which was required to provide a continuous cylindrical surface with the existing ducting to prevent disturbances in the flow during normal operation.

Building 1619.

The process in Building 1619 was the drill out of Composition B which had been cast into the body of 155 mm shells. The explosive material is removed to provide room for the installation of a fuze in a subsequent operation. Typically, a skid containing twenty-four 155 mm shells is moved to one of the drilling cubicals shown in Figure 12. An air driven drill, which has internal passages for dust ejection inside the drilling head, is used to drill and face the explosive in the nose of the shell. Dust generated by this operation is removed by suction down a 5.1 cm (2.0 in.) exhaust line to a Hoffmann primary dry dust collector. Downstream of the primary collector is a secondary collector and a high capacity vacuum pump.

For normal drilling, approximately 11.3 kg (25 lb) of dust is exhausted from two skids of 155 mm shells. In some cases, "deep drilling" is performed to remove the Composition B when flaws or voids are found in the casting. During the sampling activity, both types of drilling operations were investigated. Two sampling locations were selected in 1619 and they are shown in Figure 12. Sample location No. 4 was located near the drilling operation. Sample Location No. 5 was downstream of No. 4. Attachment of the sampling probes was accommodated by replacing the existing ducting with instrumented duct section. Figure 13 illustrates one such replacement duct installed at sample Location No. 5. At the completion of the sampling efforts, the original ducting was reinstalled.

Dust Concentration Measurements

Table 1 illustrates the dust velocity and flow rates obtained in Buildings 1611 and 1619. For all sample locations, a blunt shape velocity profile was obtained, indicating that the duct flow was turbulent. The accuracy of the velocity measurements is indicated by the approximate equality of the sum of the flow rates in the duct at sample locations 1 and 2 [63.3 + 4.9 = 68.2 m^3/min (2237 + 172 = 2409 ft^3/min)] as compared to the flow rate at location 3 [67.6 m^3/min (2388 + 4.9 ft^3/min)] of building 1611. Significantly higher flow velocities and negative static

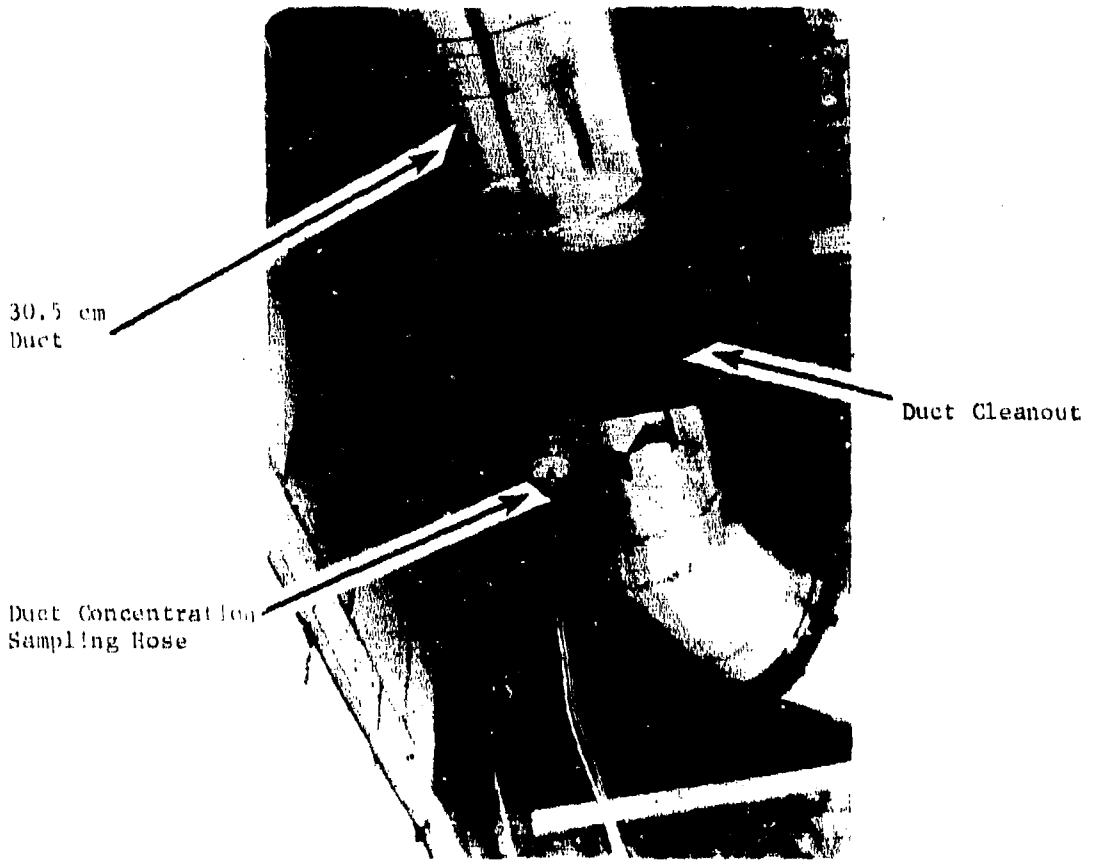

(a)

Typical Cleanout with Probe Attachment Fixture Installed

Figure 11a. Fixtures Used to Penetrate the Building 1611 Ducting

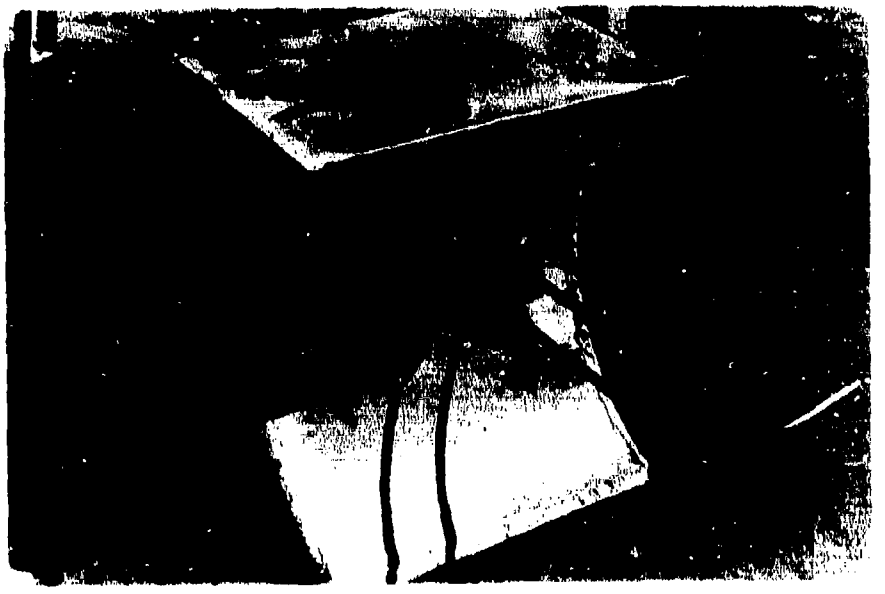

(b)

Probe Attachment Fixture with Velocity and Dust
Sampling Probes Installed

Figure 11b. Fixtures Used to Penetrate the Building 1611 Ducting

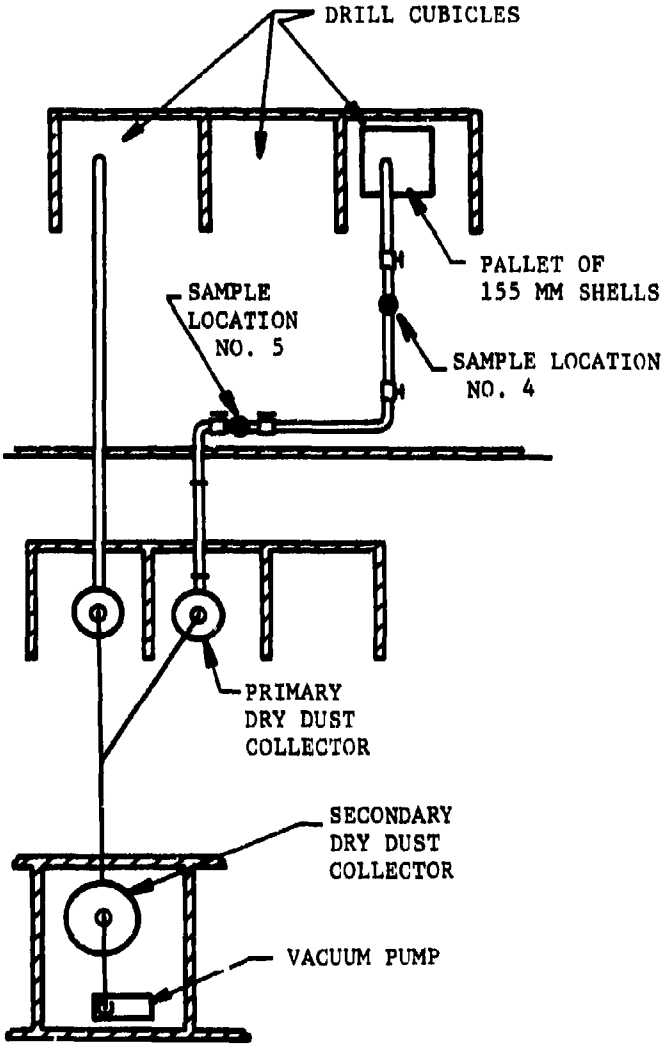

Figure 12. Dust and Electrostatic Sample Locations in the Drilling Operation of Building 1619, Louisiana AAP

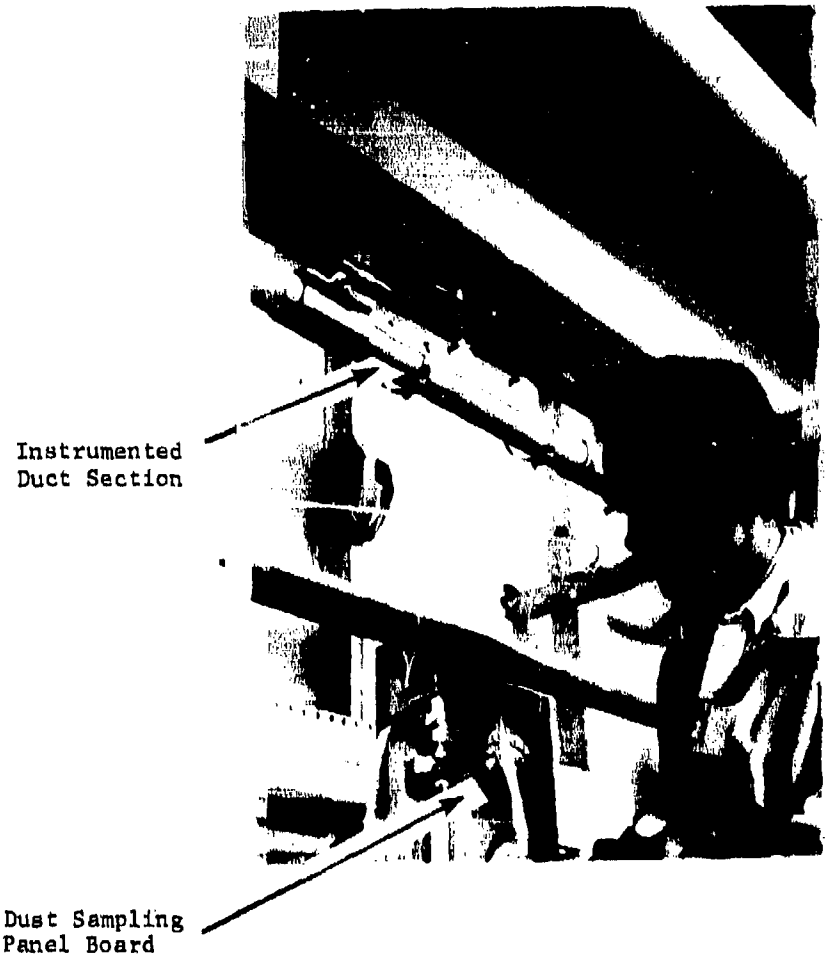

Figure 13. Instrumented Duct Section Installed at Sample Location No. 5 at Building 1619, Louisiana AAP

Table 1. Duct Velocity and Flow Rate Data for Buildings 1611 and 1619, Louisiana AAP

Bldg. No. 1611 Sample Location 1 Duct Size 30.5 cm			Bldg. No. 1611 Sample Location 2 Duct Size 10.2 cm			Bldg. No. 1611 Sample Location 3 Duct Size 30.5 cm			Bldg. No. 1619 Sample Location 5 Duct Size 5.1 cm		
Traverse[1] Point Location (cm)	VP_i (mmHg)	V_i[2] (m/min)	Traverse[1] Point Location (cm)	VP_i (mmHg)	V_i[2] (m/min)	Traverse[1] Point Location (cm)	VP_i (mmHg)	V_i[2] (m/min)	Traverse[1] Point Location (cm)	VP_i (mmHg)	V_i[2] (m/min)
1.9	0.861	822	1.9	1.011	900	.32	0.345	522	0.32	2.997	1739
4.5	0.899	840	4.5	1.085	933	1.6	0.488	619	0.76	3.734	1944
8.9	0.955	860	8.9	1.085	933	2.9	0.561	665	1.4	4.115	2034
15.2	0.935	857	15.2	1.123	948	5.1	0.599	686	2.5	4.293	2085
21.6	0.917	847	21.6	1.123	948	7.3	0.579	675	3.6	4.496	2128
26.0	0.935	857	26.0	1.123	948	8.6	0.505	630	4.3	3.734	1942
28.6	1.217	977	28.6	1.011	902	9.8	0.345	522	4.8	2.997	1737
Humidity Measurement W_B/D_B = 45.5°F/52°F W_H = 35 grains/lb dry air X_H = .008 **Duct Temperature** t = 62°F **Duct Humidity** R.H. = 41% @ 62°F **Duct Static Pressure** P = -2.3 mm Hg **Duct Flow Rate** Q = 63.3 m^3/min			**Humidity Measurement** W_B/D_B = 54°F/62°F W_H = 42 grains/lb dry air X_H = .0096 **Duct Temperature** t = 63°F **Duct Humidity** R.H. = 50% @ 63°F **Duct Static Pressure** P = -2.3 mm Hg **Duct Flow Rate** Q = 5.7 m^3/min			**Humidity Measurement** Same as Position 2 Bldg. 1611 **Duct Temperature** t = 72°F **Duct Humidity** R.H. = 36% @ 72°F **Duct Static Pressure** P = -2.3 mm Hg **Duct Flow Rate** Q = 67.6 m^3/min			**Humidity Measurement** W_B/D_B = 56/69 W_H = 46 grains/lb dry air X_H = .0105 **Duct Temperature** t = 75°F **Duct Humidity** R.H. = 35% @ 75°F **Duct Static Pressure** P = -152 mm Hg **Duct Flow Rate** Q = 3.8 m^3/min		

(1) Distance from duct bottom.

(2) See equation in Appendix A.

pressures (vacuum) were measured in the drilling operation exhaust ducting of 1619 as compared to 1611. The magnitude of the differences in these two parameters stems from the differences in the duct diameters and the relative size and number of dust inlets in the two dust removal systems.

The gravimetric dust sampling data obtained at the two plant processes is shown in Table 2. Dust samples were obtained at each sample location in the ducting of 1611. However, only one location was sampled in 1619. Low dust loading at 1611 required relatively long sample periods. Consequently, reduction of the number of dust concentration samples was made to allow reasonable description of dust flow with the short working schedule at 1611. Essentially, three of the velocity traverse points were sampled in the large ducting in Building 1611 at each sample location. The reduced sampling effort was aimed at inspecting the dust concentration gradient by sampling at the duct centerline and one point above and below the centerline. On the other hand, high dust loading and the small diameter ducting precluded taking samples at multiple points across the duct centerline in 1619. Consequently, each dust sample was taken at the centerline of the 5.1 cm (2.0 in.) duct.

As seen in Table 2, dust concentrations for the drilling operation in 1619 were approximately three orders of magnitude higher than the concentrations obtained in the hopper loading operation of 1611. When one analyzes the type of activity and the quantity of dust being generated from both processes, this finding is not unreasonable. The concentrations obtained at 1619 also agree well when compared to concentrations obtained from the overall loading rates into the primary collector. Earlier in this report it was mentioned that drilling of 48 shells accumulated 25 lb (11.34 kg) of explosive dust. Based on an observed time of 0.15 minutes to drill one shell, and an overall duct flow rate of 3.77 m^3/min (133 ft^3/min), a calculated dust concentration of 0.42 oz/ft^3 is obtained during the drilling of one shell.

Since the operation in 1611 utilized a wet dust collector, a comparison similar to that noted above could not be performed to validate the measured concentrations. However, a close inspection of the data illustrates that a concentration profile does exist in the duct measurements at 1611. With the exception of location 1, higher dust concentrations were observed at the bottom of the duct with predominately constant levels from the top of the duct to the centerline.

Electrostatic Measurements

Building 1611.

The electrostatic sampling performed at Building 1611 included both electric field and charge density measurements. This process was the only sample area in all three plants where both types of measurements could be taken because of the large duct sizes. At sample location No. 1, the electrostatic measurements were performed in the clean-

Table 2. Duct Sampling Data at Louisiana AAP

Duct Sample Location	Traverse Point Location From Duct Bottom (cm)	Sampling Velocity (m/min)	Weight of Dust Collected (grams)	Sampling Time (min)	Dust Conc. (gr/m^3)
No. 1 30.5 cm Duct Building 1611	1.90	840	.0073	5.	0.093
	4.5	840	.0004	14.33	0.0020
	15.2(3)	857	.0017	12.	0.0089
No. 2 10.2 cm Duct Building 1611	1.6	619	0.3714	20.	1.61
	5.1(3)	686	0.146	14.	0.82
	5.1(3)	686	0.0317	1.38	0.65
	1.03	630	0.134	15.	0.76
No. 3 30.5 cm Duct Building 1611	4.5	933	.020	10.	0.115
	15.2(3)	948	.0081	10.	0.046
	26.0	948	.0076	10.	0.043
No. 5 5.1 cm Duct Building 1619	2.5(3)	2085	1.36	0.15	233.00
	2.5(3)	2085	3.29	0.30	282.00
	2.5(3)	2085	1.75	0.15	300.00
	2.5(3)	2085	3.83	0.30	330.00

(1) Sampling time corresponds to the time required to drill out one shell.

(2) Sampling time corresponds to the time required to drill out two shells.

(3) Sample taken at the duct centerline.

out described previously, and which is positioned on the bottom of the duct. Typical measurements are shown in the strip chart recordings of Figure 14. Each peak in Figure 14 corresponds to the dumping of the Composition B flake onto the shaker table and/or the operation of the shaker table. Notice that peaks in the electric field data correspond with similarly shaped peaks in the charge density data. There is a lag in the charge density-data which corresponds to the length of time required to transport the dust through the 30.5 m (100 ft) long sampling hose. Taking this time delay into account, one can see that the two instruments are in excellent agreement with respect to the arrival time, shape and duration of each pulse. The electric field data in Figure 14a (and the corresponding data for locations 2 and 3) together with the theoretical equations in Appendix B were used to obtain the charge density transfer function used throughout the remainder of the program. With the electric field levels indicated in Figure 14a, the maximum recorded charge density was -232 nC/m^3.

The electrostatic sampling at location 2 was performed in the cleanout which is below the 10.2 cm (4 in.) duct. Due to the small duct size, the electric fieldmeter could not be installed in this location without distorting the field measurements. Therefore, only the charge density instrument was used for the electrostatic measurements. However, the electric field sensor was left in place at sampling location 1 to provide a reference signal for monitoring the production line activities.

The results of these measurements are shown in Figure 15. The charge contained within the 10.2 cm (4 in.) diameter duct was positive in polarity which is a result of the processes occurring between sampling locations 1 and 2. When a box of Composition B material is initially dumped onto the sifting table, negatively charged dust is released (see Figure 15). This process leaves the bulk of the material falling into the hopper on the first floor charged in opposite polarity because of the absence of electrons created when the negatively charged dust is collected. In the data shown in Figure 15, there is a period where no activity occurred on the product on line while recording the data. When the product began to be dumped into the hopper, the peaks in the electric field data reflect the renewed activity on the production line. In the charge density data, this startup point is followed by a period of delay and then a gradual buildup of positive charge occurs in the 10.2 cm (4.0 in.) diameter duct. The peak variation in the electric field data at sampling location 1 is not present in the charge density data measured at location 2 because the screening and loading process is not continuous. The maximum charge density recorded at sampling location 2 was +184 nC/m^3.

The electrostatic measurements at sample location 3 were performed at the cleanout mounted on top of the duct. Both electric field and charge density measurements were performed at this location. Figure 16 shows typical measurements obtained at this location. As was the case at sample location 1, there is excellent agreement in the waveforms recorded by the two instruments. The high level negative pulses in the charge density data in Figure 16b are the result of initiating and

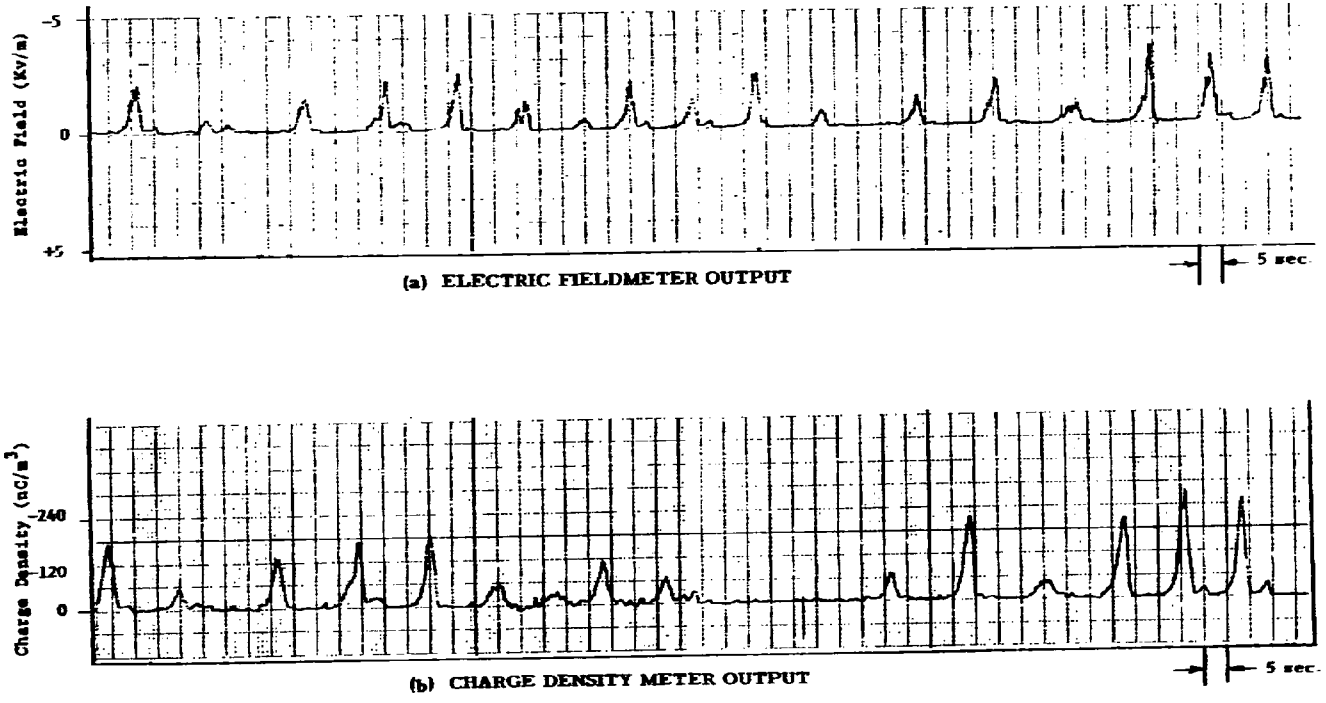

Figure 14. Electrostatic Measurements at Building 1611 in 30.5 cm Diameter Duct at Location 1

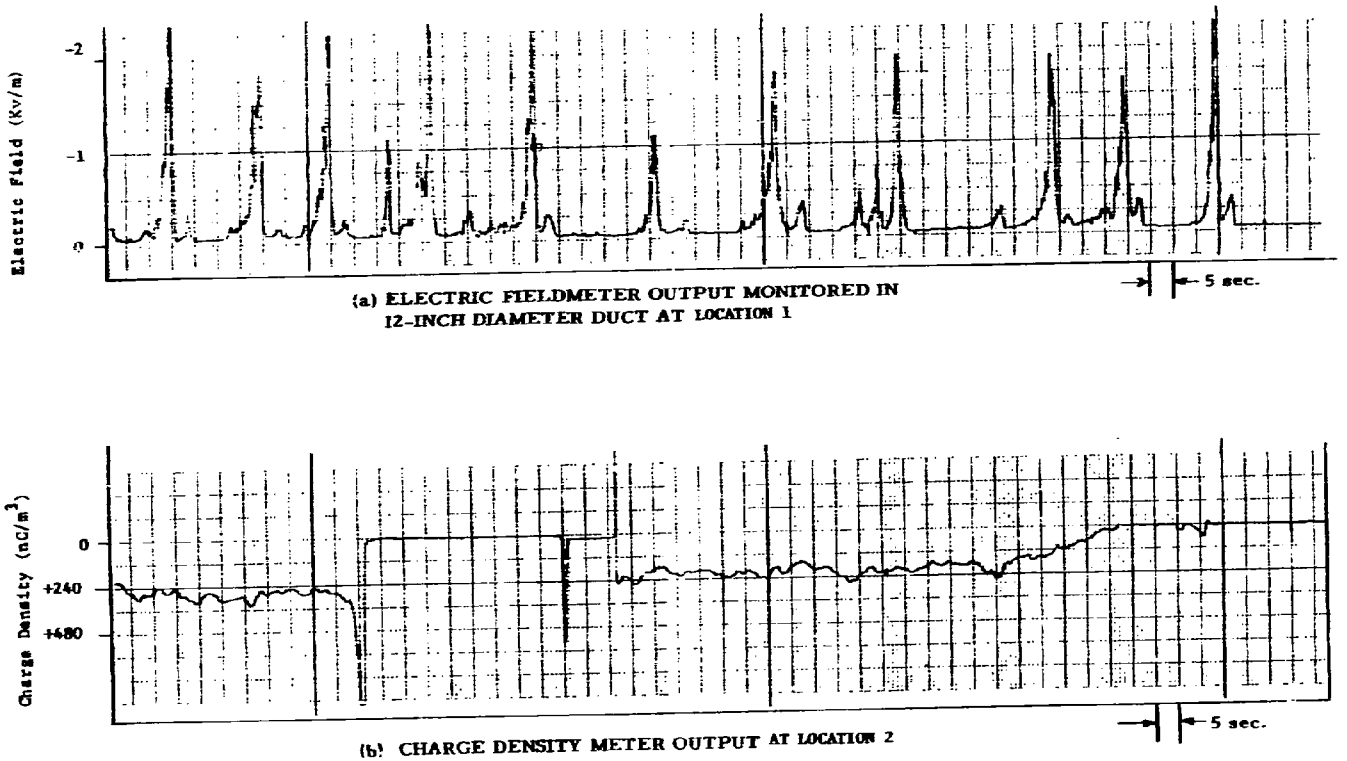

Figure 15. Charge Density Measurements at Building 1611 in 10.2 cm Diameter Duct at Location 2

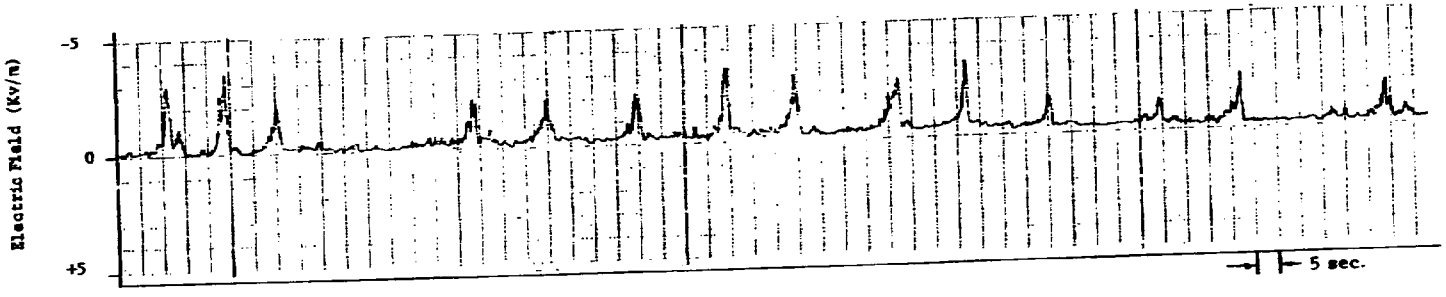

(a) ELECTRIC FIELDMETER OUTPUT

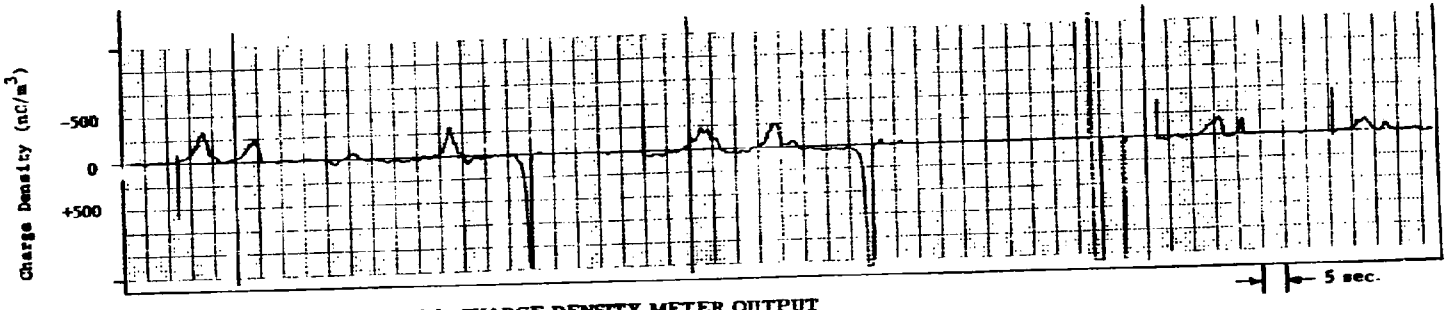

(b) CHARGE DENSITY METER OUTPUT

Figure 16. Electrostatic Measurements at Building 1611 in 30.5 cm Diameter Duct at Location 3

completing a measurement cycle and should not be confused with the actual charge density variations being monitored. The maximum charge density observed at location 3 was -287 nC/m^3. In comparison to results at the other two measurement locations, the charge density measured in the 10.2 cm (4.0 in.) duct is significant. However, in terms of the energy content and volume of charge moving through the system to sample location 3, the positive charge output of the smaller duct is entirely absorbed and neturalized by the negative charge in the larger duct with little or no observable effects in altering the levels of negative charge measured at location 3.

Building 1619.

The sampling performed at Building 1619 involved measuring the variations in the charge density occurring as a result of shallow and deep drilling operations on 155 mm artillery shells. The duct diameter was 5.1 cm (2.0 in.) so the instrumentation used was limited to the charge density meter.

A strip chart recording showing the charge density measurement for a typical deep drilling operation at sample location 4 is shown in Figure 17. The duration of the drilling operation and the amplitude and character of the charge density signal varies uniquely depending on the motions of the drill operator. However, it was observed that the charge density increases whenever the operator exerts a greater force on the drill. The polarity of the charge resulting from the drilling operation was always positive, and the maximum observed amplitude was +14,800 nC/m^3.

During shallow drilling, charge density measurements were made at sampling locations 4 and 5. No significant differences were found to exist in the magnitude of the charge at these locations. Figure 18 shows the output of the charge density meter (for location 5) over a portion of a typical shallow drilling operation involving 24 shells. No predictable characteristic can be seen in the charge density signal from one operation to another, since the charge generated is dependent on the force applied by the operator. With shallow drilling, the resulting dust concentrations are apparently less than the deep drilling operations as indicated by the reduced charge density ducts.

Charge and Energy Levels.

The energy which may be available for electrostatic discharge can be calculated from the electric field and charge density data using the equations in Appendix B. These energies and the maximum observed charge density levels are summarized in Table 3. Although the charge density levels observed in Building 1619 are two orders of magnitude greater than the corresponding levels in Building 1611, the energy levels are all approximately the same magnitude. This is due to the dependence of the energy of the duct diameter. In any case the calculated energies are many orders of magnitude smaller than the reported minimum ignition energies of explosives which are generally on the order of several hundred millijoules.

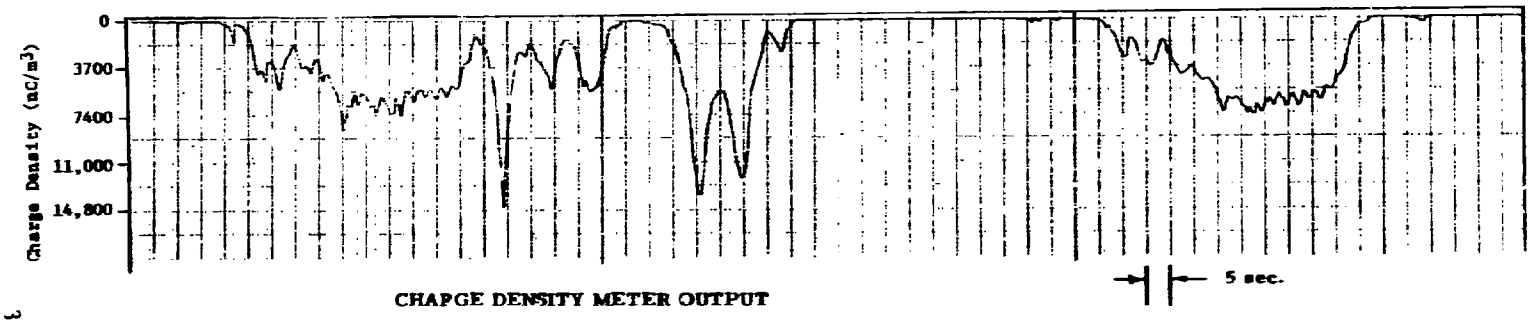

Figure 17. Charge Density Measurements at Location 4 During Deep Drilling Operations at Building 1619

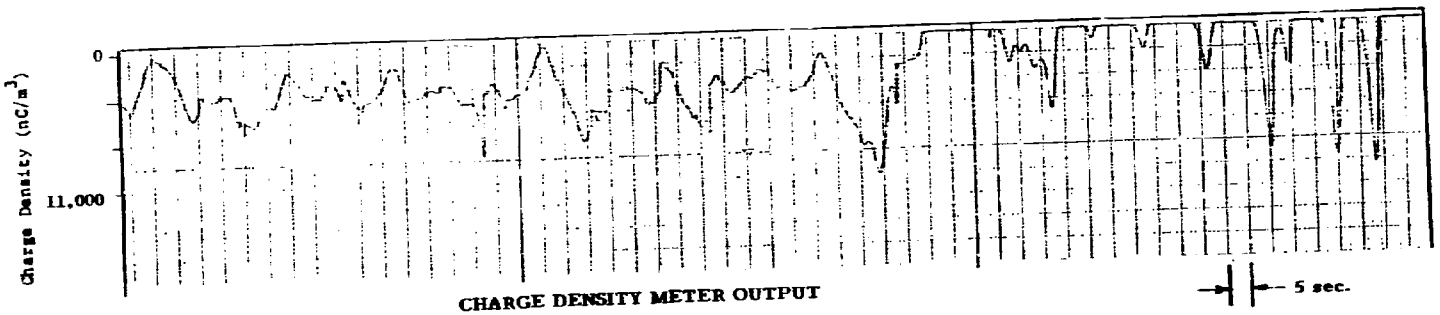

Figure 18. Charge Density Measurements at Location 5 During Shallow Drilling Operations at Building 1619

Table 3. Charge Density and Energy Levels Measured in Louisiana AAP

BUILDING	SAMPLE LOCATION AND OPERATION	DUCT DIAMETER (cm)	CHARGE DENSITY (nC/m^3)	ENERGY (μJ)
1611	1 - Screening	30.5	-232	2.43
1611	2 - Falling into Hopper	10.2	+184	0.005
1611	3 - Combination of 1 and 2	30.5	-287	3.00
1619	4 - Deep drilling	5.1	+14,800	1.02
1619	4,5 - Shallow Drilling	5.1	+11,100	0.57

Longhorn AAP

Both dust and electrostatic measurements were made in dust exhaust ducting of two very similar processes at the Longhorn AAP. Both processes involve the manufacture of illuminating flares. In Building B-7, one of the processes is the production of 4.2 "aluminum candles." The other process involves the manufacture of white signals flares and is housed in Building 34-Y. Both processes utilized 5.1 cm (2.0 in.) ducting.

Process Description and Sample Locations

Building B-7.

Building B-7 produces the 4.2 illuminate. The process consists of mixing the illuminate composition, weighing the illuminate, consolidation, removal of a cardboard plug, adding a primer stage and packaging. A schematic of the process sampled and the associated dust exhaust ducting is illustrated in Figure 19. A total of five inlets were available for dust pickup. Two inlets serve the three weighing stations, two pickups served the consolidation press, and one inlet served the cardboard disk removable area. All inlets except those on the consolidation press were used intermittently to vacuum dust generated during each process step. When not in use, the inlets were plugged to reduce the noise in the building. The only inlets not observed plugged during the entire sampling period were the two used on the consolidation press.

Two locations were sampled in Building B-7 by the SwRI sampling team. Sample location 7 investigated the dust flow and electrostatic conditions resulting from the disk removal and part of the consolidated press activities. Measurements taken at sample location 8 were concerned with the dust generated in the weighing operation in addition to the other two activities just mentioned. The probe attachment fixture used to interface the dust and electrostatic probes was similar in design to that described for Building 1619 of the Louisiana AAP.

Building 34-Y.

Building 34-Y produces a white signal flare (Aluminum Magnesium Illuminating Stars). The process consists of mixing the composition, weighing, consolidation, adding a primer stage and packaging. The portion of the process which was sampled is shown in Figure 20. The exhaust duct locations sampled were located in the 5.1 cm (2.0 in.) ducting that served identical weighing and consolidation bays. These were bays 103 and 104. The differences in the exhaust ducting serving these two bays were: a) the ducting serving bay 104 is longer than that serving bay 103; b) the ducting serving bay 104 had one extra inlet from bay 105; and c) the wet collector serving bay 104 was a 20 hp unit while the other bay was served by a 10 hp unit. During our visit, bay 105 was not in operation and the vacuum line for this bay remained plugged at all times.

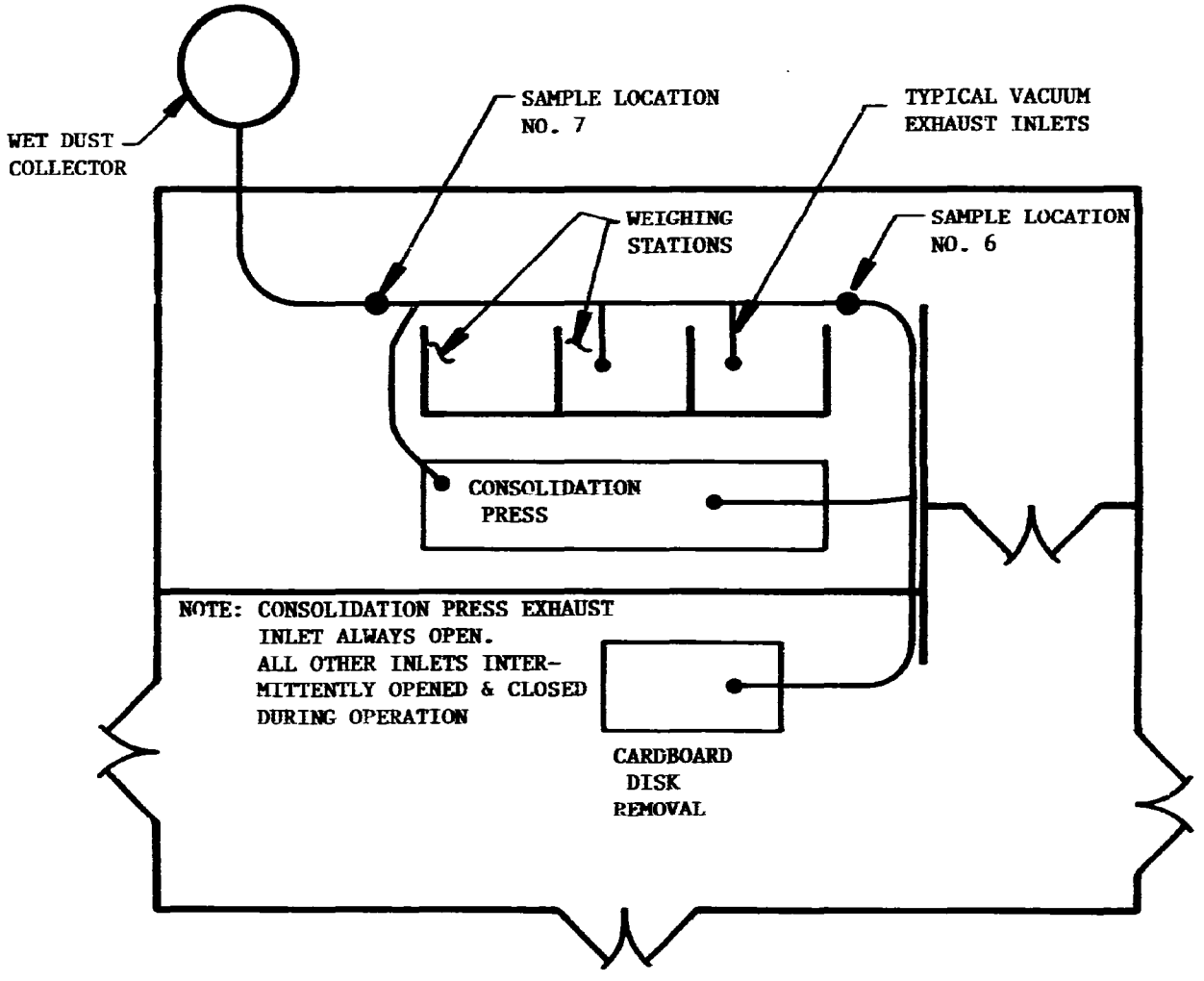

Figure 19. Dust and Electrostatic Sampling Locations in 4.2 Aluminum Candle Production Process in Building B-7, Longhorn AAP

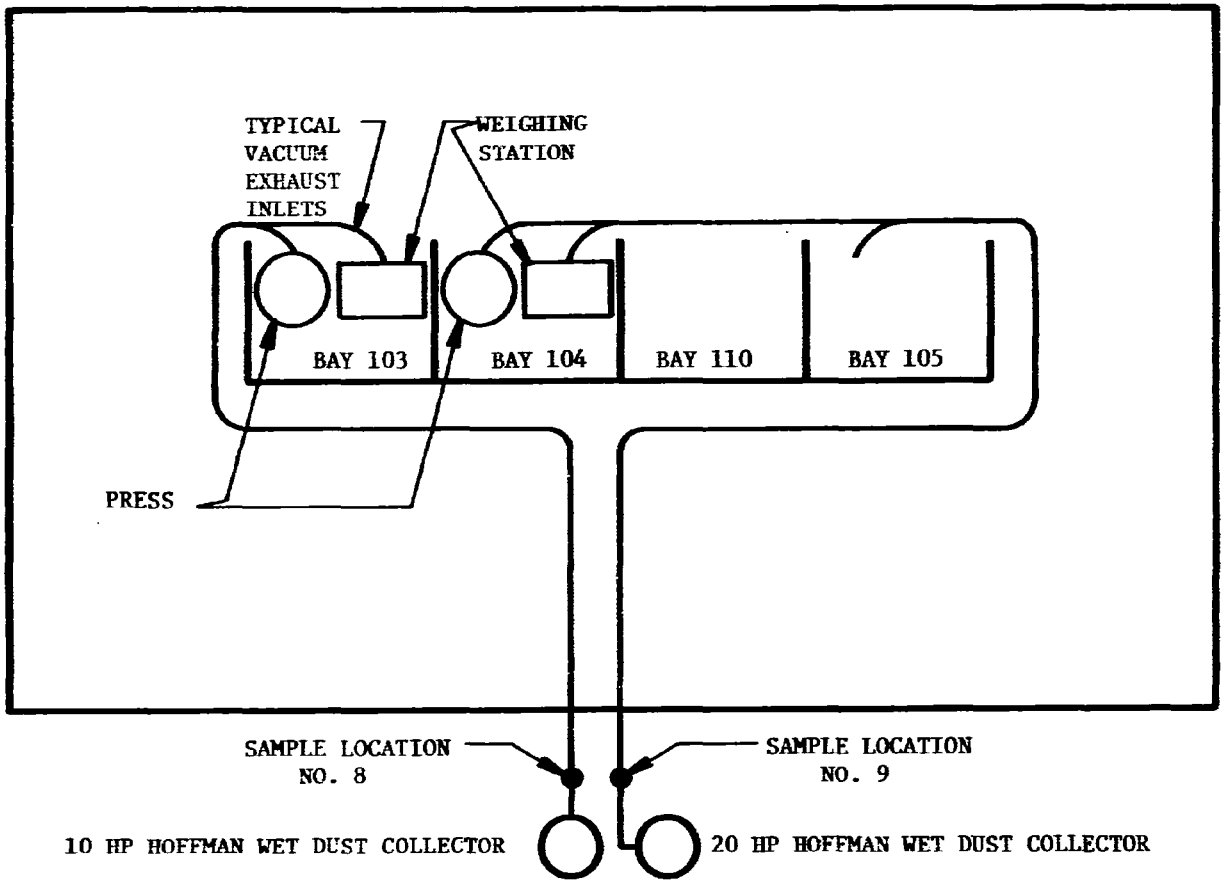

Figure 20. Dust and Electrostatic Sampling Locations in the Signal Flare Production Process in Building 34-Y, Longhorn AAP

The probe attachment fixtures used in 34-Y were similar to those used in Building 1619 at Louisiana AAP. Two such fixtures were used in 34-Y. Sample location 8 was in the ducting serving bay 103, and sample location 9 was connected to the ducting leading to bay 104.

Dust Concentration Measurements

Table 4 summarizes the duct velocity and flow rates obtained in Building B-7 at Longhorn AAP. The flow rate measured at location 6 was an order of magnitude lower than the flow rates measured at location 7, but this was because the only inlet was the constricted inlet which vacuumed up any dust on the rotating table of the consolidation press. The vacuum pressure measured at this location was the highest measured at any of the sample locations: 12.7 cm Hg. The flow conditions at location 7 were measured with the two inlets at the weighing station plugged (Column 2 of Table 4) and open (Column 3). When the weighing station pickups are plugged the velocity at location 7 is about an order of magnitude higher than the velocity recorded at location 6, and the static pressure is slightly lower. These higher readings are largely due to the second vacuum inlet on the consolidation press. When the weighing station dust pickups are open, the flow rate increases by about 30.5 m/min (1000 ft/min) and the static pressure is reduced by about 35 percent.

Table 5 summarizes the duct velocity and flow rates obtained in Building 34-Y in a very similar process as the one in B-7. The flow rate at location 8 was measured with the weighing station inlets open (Column 1 of Table 5) and closed (Column 2). As was the case in B-7, the velocities are about 30.5 m/min (1000 ft/min) higher with the inlets open, and the vacuum pressures are again about 35 percent lower. Sample location 9 is an independent vacuum system which has about twice the capacity of the vacuum system in which location 8 was installed. This is reflected in velocity flow rates which are nearly twice as great as the flow rates observed at location 8 under the same condition (weighing station inlets open). Vacuum pressures at location 9 were about 12 percent higher at location 9.

Table 6 summarizes the gravimetric dust sampling data obtained in B-7 and 34-Y. The consistency in the measured values appears to be rather poor; however, the processes being monitored are not continuous. Vacuuming at the weighing stations is performed intermittently, at the operators discretion. Vacuuming at these locations varied from 4 - 5 times per hour at the cardboard disk removal station in B-7 to about once every two minutes at the weighing stations at both B-7 and 34-Y. Only the inlets on the consolidation presses vacuum dust continuously, and by visual observation there appeared to be less dust on the consolidation presses than appears to be generated during the weighing operation.

Electrostatic Measurements

The dust collection systems studies at Longhorn AAP were confined to 5.1 cm (2.0 in.) diameter ducts located in Buildings B-7 and 34-Y.

Table 4. Duct Velocity and Flow Rate at Building B-7 at Longhorn AAP

VELOCITY TRAVERSE LOCATION FROM BOTTOM OF DUCT (cm)	SAMPLE LOCATION 6[1]		SAMPLE LOCATION 7[1]		SAMPLE LOCATION 7[2]	
	VELOCITY PRESSURE VP_i (mm Hg)	VELOCITY V_i (m/min)	VELOCITY PRESSURE VP_I (mm Hg)	VELOCITY V_i (m/min)	VELOCITY PRESSURE VP_I (mm Hg)	VELOCITY V_i (m/min)
4.7	0.056	235	3.175	1741	5.232	2171
2.5	0.075	271	5.613	2313	8.433	2752
0.89	0.037	191	4.876	2153	5.994	2321
	Humidity Measurement W_B/D_B = 53°F/88°F WH = 4 grains of water / lb dry air RH = 6% Duct Temperature T = 88°F Duct Static Pressure P = -127 mm Hg gage Duct Flow Rate Q = 0.47 m^3/min		Humidity Measurement W_B/D_B = 71°F/89°F WH = 87 grains of water / lb dry air RH = 42% Duct Temperature T = 89°F Duct Static Pressure P = -108 mm Hg gage Duct Flow Rate Q = 4.2 m^3/min		Humidity Measurement W_B/D_B = 71°F/89°F WH = 87 grains of water / lb dry air RH = 42% Duct Temperature T = 89°F Duct Static Pressure P = -70 mm Hg gage Duct Flow Rate Q = 4.9 m^3/min

NOTES: (1) Two duct inlets at weighing station plugged, Consolidation Press duct inlet open, inlet at Cardboard Disk Removal Station plugged.

(2) Two duct inlets at weighing station open, Consolidation Press duct inlet open, inlet at Cardboard Disk Removal Station plugged.

Table 5. Duct Velocity and Flow Rate Data at Building 34-Y at Longhorn AAP

VELOCITY TRAVERSE LOCATION FROM BOTTOM OF DUCT (cm)	SAMPLE LOCATION 8[1]		SAMPLE LOCATION 8[2]		SAMPLE LOCATION 9[2]	
	VELOCITY PRESSURE VP_i (mm Hg)	VELOCITY V_i (m/min)	VELOCITY PRESSURE VP_i (mm Hg)	VELOCITY V_i (m/min)	VELOCITY PRESSURE VP_i (mm Hg)	VELOCITY V_i (m/min)
4.7	2.245	1433	1.499	1170	4.293	1984
2.5	2.819	1602	2.060	1372	7.112	2550
0.89	2.060	1372	1.499	1170	3.175	1705
	Humidity Measurement W_B/D_B = 69°F/89°F WH = 75 grains of water / lb dry air RH = 36% Duct Temperature T = 89°F Duct Static Pressure P = -57.2 mm Hg gage Duct Flow Rate Q = 3.0 m^3/min		Humidity Measurement W_B/D_B = 69°F/89°F WH = 75 grains of water / lb dry air RH = 36% Duct Temperature T = 89°F Duct Static Pressure P = -88.9 mm Hg gage Duct Flow Rate Q = 2.5 m^3/min		Humidity Measurement W_B/D_B = 73°F/89°F WH = 102 grains of water / lb dry air RH = 50% Duct Temperature T = 89°F Duct Static Pressure P = -102 mm Hg gage Duct Flow Rate Q = 4.2 m^3/min	

NOTES: (1) Weighing station duct inlet open; press duct inlet open.

(2) Weighing station duct inlet closed; press duct inlet open.

Table 6. Dust Sampling Data in Building B-7 and B-34, Longhorn AAP

BUILDING NUMBER	DUCT SAMPLE LOCATION	TRAVERSE POINT LOCATION FROM BOTTOM OF DUCT (cm)	SAMPLING VELOCITY (m/min)	WEIGHT OF DUST COLLECTED (grams)	SAMPLING TIME (min)	DUST CONCENTRATION (gram/m^3) (4)
B-7	6	4.7	117	0.046	34.0	0.77
		2.5(3)	184	0.070	28.3	0.90
		2.5(3)	175	0.023	54.0	0.16
	7(1)	4.7	1643	5.126	40.4	5.2
		4.7	1143	2.837	26.2	6.3
		2.5(3)	1849	0.760	46.0	0.6
		2.5(3)	1849	0.422	21.6	0.7
34Y	8(2)	4.7	1187	2.23	15.0	8.4
		4.7	1187	5.49	28.0	11.0
		2.5(3)	1145	2.06	30.0	4.0
		2.5(3)	1355	3.74	30.0	6.1
		2.5(3)	1397	1.20	15.0	3.8
		0.89	1187	6.02	28.0	12.1
	9(2)	4.7	1335	0.107	17.0	0.31
		2.5(3)	1380	0.551	19.0	1.4
		2.5(3)	1467	0.145	13.0	0.51
		0.89	1423	0.235	15.0	0.73

NOTES: (1) Weighing station inlets plugged, Consolidation press inlet open for Building B-7, Cardboard disk removal station plugged.

(2) Weighing station inlet plugged, Consolidation press inlet open for Building 34Y.

(3) Sample taken at dust centerline.

(4) Gm/m^3 can be easily converted to the more familiar oz/ft^3 by dividing by 1000.

With these small diameter ducts, the instrumentation for the electrostatic studies was limited to the charge density meter. The locations of the sampling test points, and the processes and the materials involved are the same as those already described for the dust concentration measurements. The pyrotechnic materials used in the manufacturing processes at Longhorn AAP are different than the Composition B material used in the original calibration of the charge density meter. Therefore, in interpreting the data from the charge density meter, only relative charge levels can be inferred since the electric fieldmeter could not be used in the small ducts to calibrate the charge density meter for these different kinds of materials.

Overall, the tests revealed some relatively high charge levels, but due to the small diameter of the ducts, the energy levels contained in the dust transport systems are quite small. Positive and negative charge species were found to exist together. Negative charges result from the continuous vacuuming of the consolidation presses while the positive charges are the result of the intermittent vacuuming which occurs at the weighing stations.

Building B-7.

Sample location 6 monitored only dust from the constricted inlet on the consolication press and the vacuum inlet at the cardboard removal station. The greatest activity observed at this location occurred during vacuuming operations at the disk removal station. After a period of dust accumulation, the operator uses a flexible vacuum hose to clean the work area. Charge from this operation can either be positive or negative as seen by the typical charge density waveforms shown in Figure 21. The exact nature of the charge reversal is probably dependent on the manner in which the operator cleans the work surface. Typical polarity reversals of this nature can be explained by the phenomenon involved in the transfer of image charges. The maximum charge density recorded at location 6 was +7,750 nC/m^3; negative excursions as great as -4,430 nC/m^3 were observed.

Sample point 7 monitors the total dust collection activity in Building B-7. Typical data at this station are shown in Figure 22. Generally these data are characterized by the lack of electrostatic activity and there is no apparent pattern or repetition in the pulses since the dust collection occurs in a random manner determined by the line operators. Although the data shown in Figure 22 are for negative charge species, positive and irregular charge levels were also observed which can be attributed to the vacuuming operations occurring at sampling location 7. The maximum charge density recorded at this location was -11,100 nC/m^3.

Building 34-Y.

At Building 34-Y the sampling points were located near the wet collectors of two independent vacuum collection systems. The material collected in the dust cassettes was granular and larger in size

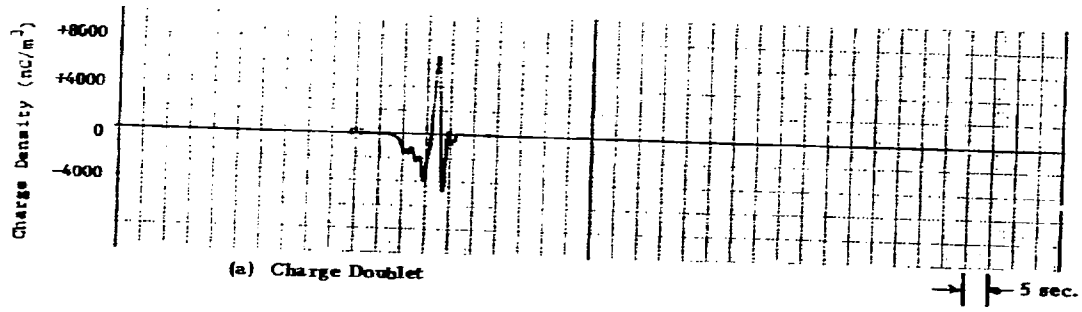

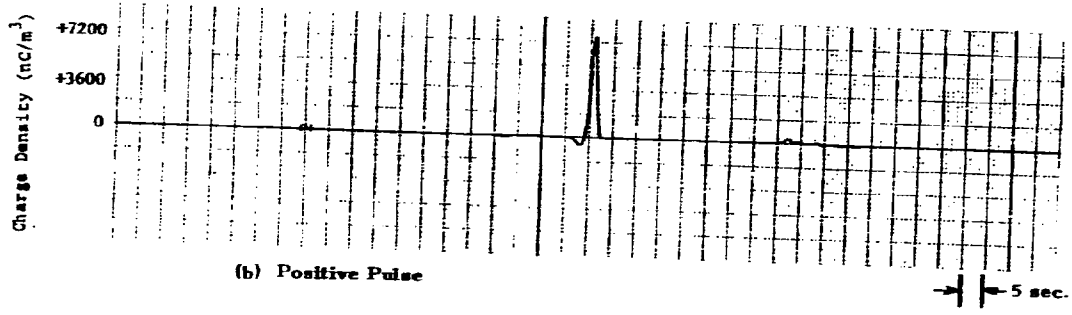

Figure 21. Charge Density Measurements at Building B-7 at Sample Location 6

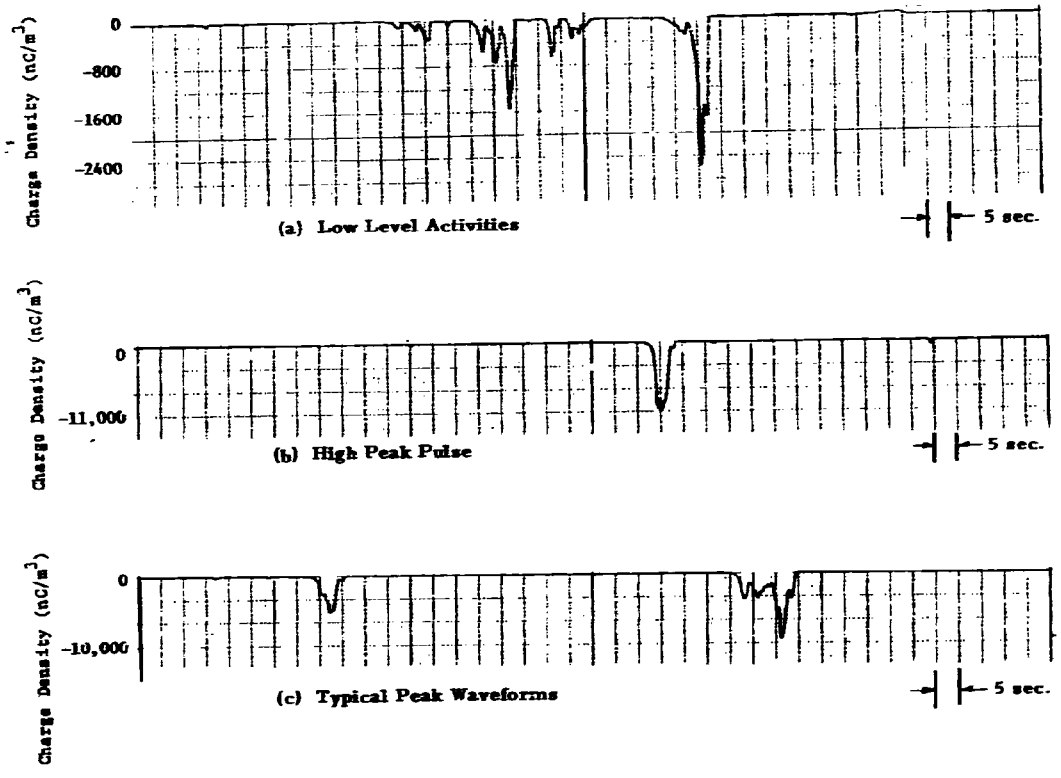

Figure 22. Charge Density Measurements at Building B-7 at Sample Location 7

than any of the powders collected at other sample locations in any of the plants. Apparently there is sufficient moisture or volatile content to allow the fine magnesium and aluminum particles to agglomerate to form relatively large particles by the time the dust arrives at the sample locations. Overall, the charge magnitudes were higher in the morning and then gradually decreased in the afternoon as the ambient temperature increased. As the temperature varied, moisture condensation formed on the duct surfaces around the test points where the dust was sampled. These moisture and temperature effects may also have contributed to the decreasing charge levels.

The dust sampling at location 8 consists of dust collected from both the weighing and pressing stations situated in Bay 103. Although the pressing operation is fully automatic, vacuuming around the press is solely determined by the press operator. In a similar manner, cleanup around the weighing station is done only as the operator deems it to be necessary. These random operations produce unpredictable charge output waveforms from the charge density meter as can be seen in Figure 23. Although a peak output is shown at a level of 3,500 nC/m^3, most of the peaks monitored at sampling location 8 were from 730 to 1,100 nC/m^3.

Two typical charge density waveforms measured at location 9 are shown in Figure 24. For the most part, the charge density magnitudes from the operations in Bay 104 were very low as shown in Figure 24a. The larger spikes in Figure 10b were probably due to a methodic vacuuming procedure being performed by the press operator as can be seen by the uniformity of the spacing of the pulses. During these tests, it was not possible to correlate fully the activities on the line with the output of the charge density meter since communications equipment could not be used within the plant for this purpose.

Charge and Energy Levels.

Table 7 lists the maximum charge density readings obtained at Longhorn AAP. As was the case at Building 1619, Louisiana AAP, the charge density levels are quite high. However, because of the small duct diameters and the dependence of the energy on the duct radius to the fifth power, the energy levels are quite low. The energy levels measured at 34-Y are about an order of magnitude lower than those observed at B-7. This is probably due to the agglomeration of the aluminate composition which occurred at 34-Y. The charge density readings and the energy levels reported in Table 7 were obtained using the transfer function for Composition B explosive. These numbers are presented for relative rather than quantitative comparison of results between sample locations.

Lone Star AAP

Dust and electrostatic sampling was performed in two different processes at Lone Star AAP. The first process sampled was a burster facing operation which was quite similar to the process in Building 1619

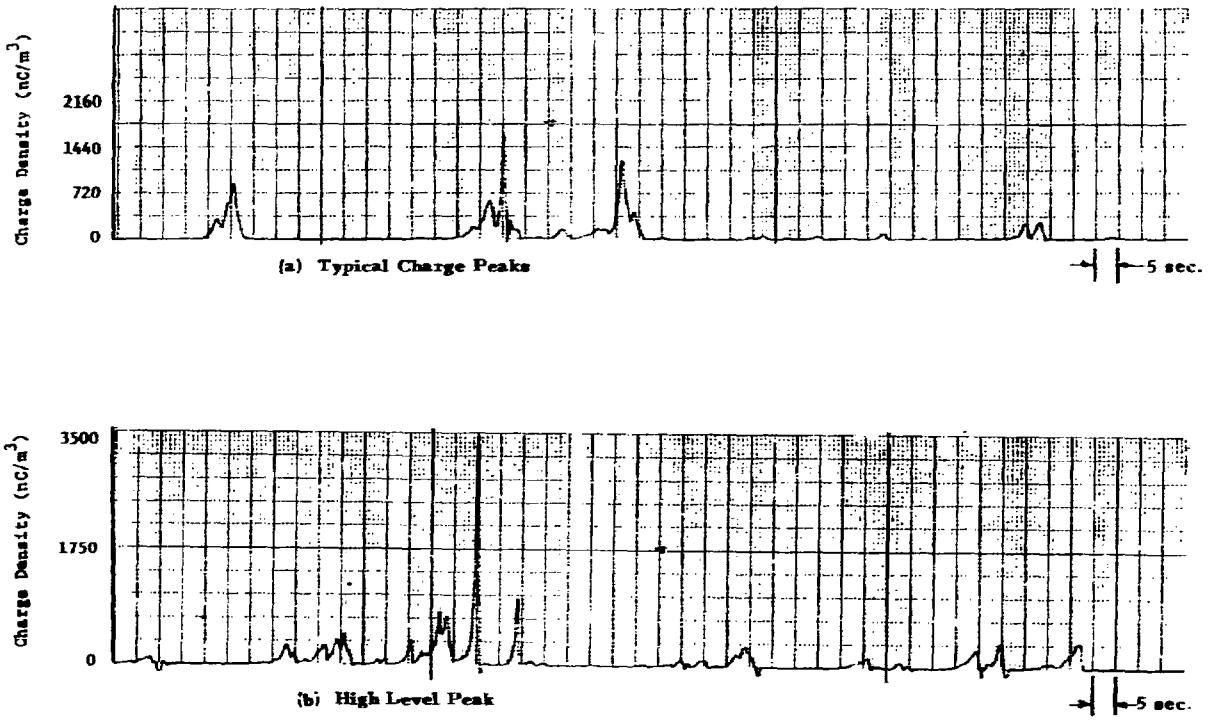

Figure 23. Charge Density Measurements at Building 34-Y at Sample Location 8

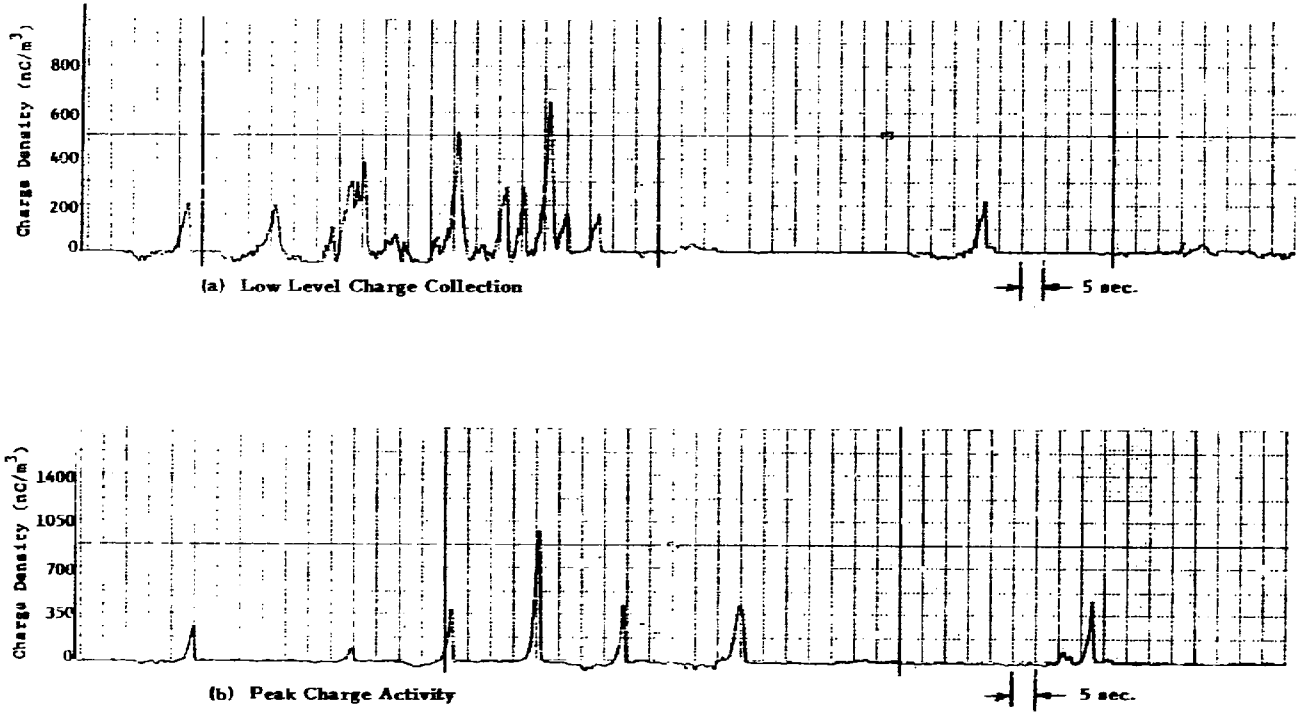

Figure 24. Charge Density Measurements at Building 34-Y at Sample Location 9

Table 7. Charge Density and Energy Levels Measured in Longhorn AAP

BUILDING	SAMPLE LOCATION	DUCT DIAMETER (cm)	CHARGE DENSITY (nC/m^3)	ENERGY (μJ)
B-7	6	5.1	+7,750	0.28
B-7	7	5.1	-11,100	0.57
34Y	8	5.1	+3,500	0.057
34Y	9	5.1	+1,030	0.005

at Louisiana AAP. The other process involved grenade production and included a pressing operation similar to the pressing operations at Longhorn AAP. The unique feature of the processes studied at Lone Star AAP was that both of these operations were fully automated.

Process Description and Sample Locations

Building 04-M-40.

Figure 25 shows a layout of the equipment and vacuum exhaust ducting of Building 04-M-40. The operation is comprised of two facing (shallow drilling) machines, a long thick-walled duct, and a primary and secondary dry dust collector. The facing machine in Bays 1 and 2 were operational during our sampling visit. Bursters filled with cast Composition B explosive were placed in a holder outside the facing bay and conveyed automatically to the facing machine. Once inside the facing machine, a drill head is lowered onto the burster and about 0.32 cm (0.125 in.) of Composition B explosive is drilled out. A drill head just prior to engagement on a burster is shown in Figure 26. The explosive dust created by the drilling operation is removed through the flexible rubber hose which is visible in the photograph. There are four drill heads on the facing machine and each drill head has its own dust exhaust line. One additional dust pickup vacuums fugitive dust on the facing table. All five rubber hoses branch into one 2.54 cm (1.0 in.) steel tube in which sample location 10 was installed. This line connects to a short length of 5.1 cm (2.0 in.) steel pipe just prior to exiting the building. Sample location 10 was located in this section. Sample location 11 was installed downstream of location 10 past the Y-connections from the ducting servicing Bays 3 and 4. The diameter of the ducting at location 11 was 7.62 cm (3.0 in.). The probe attachment fixtures used in 04-M-40 were similar to the ones used at Louisiana and Longhorn AAP's, with the exception that three dust sampling entry points were available to allow simultaneous dust collection at three different internal duct traverse points.

Building B-46.

Figure 27 shows a layout of the equipment and vacuum exhaust ducting of Building B-46. As seen in the figure, the process is composed of three separate operations. The sequence of operations is Consolidation, Demachining and Cone Swagging. A-5 explosive is pressed into a grenade casing at high pressure by the rotary press shown in Figure 28. Flexible rubber hoses, 5.1 cm (2.0 in.) are used to pick up dust generated by the pressing operation. The vacuum lines seen in the figure connect to stainless steel line which runs to the wet collectors located behind Building B-46. The two Y-junctions shown in the figure lead to sample locations 13 and 14. Sample location 14 is located in the exhaust ducting serving the press. Sample location 13 is in the exhaust line serving the conveyor leading from the press to the demachining area.

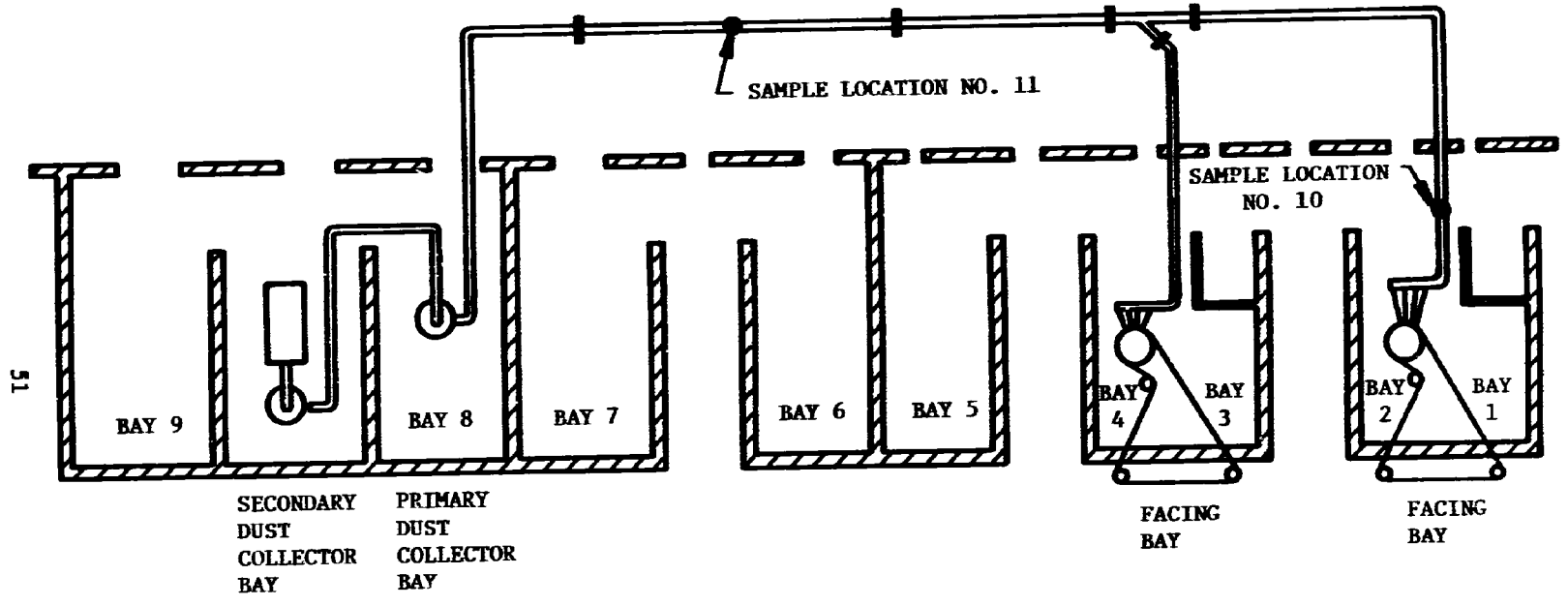

Figure 25. Vacuum Exhaust Ducting and Dust Collection System for Burster Facing Operation in Building 04-M-40

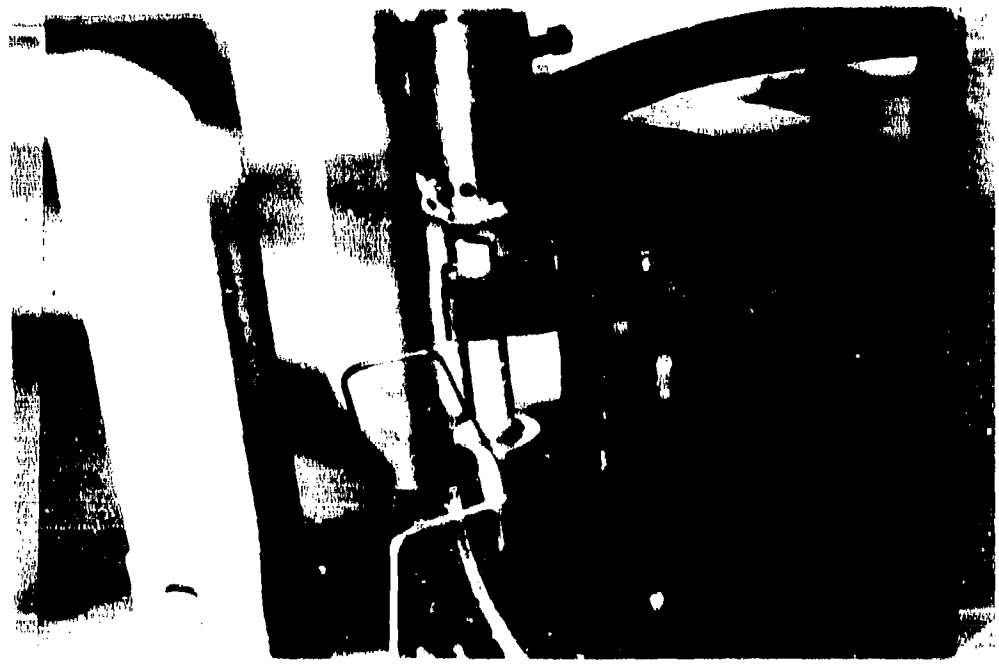

Figure 26. Dust Exhaust Line on Drill Head in 04-M-40

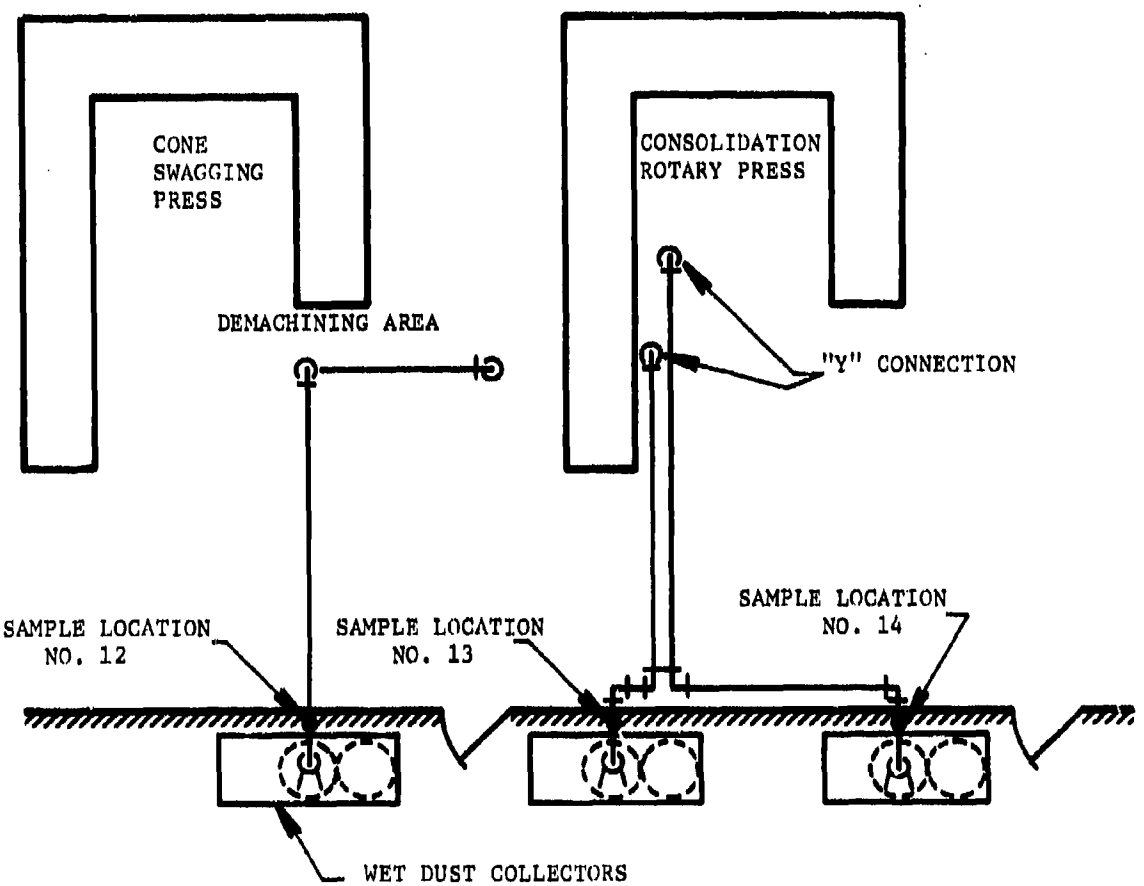

Figure 27. Vacuum Exhaust and Dust Collection System for Grenade Press Operation in Building B-46

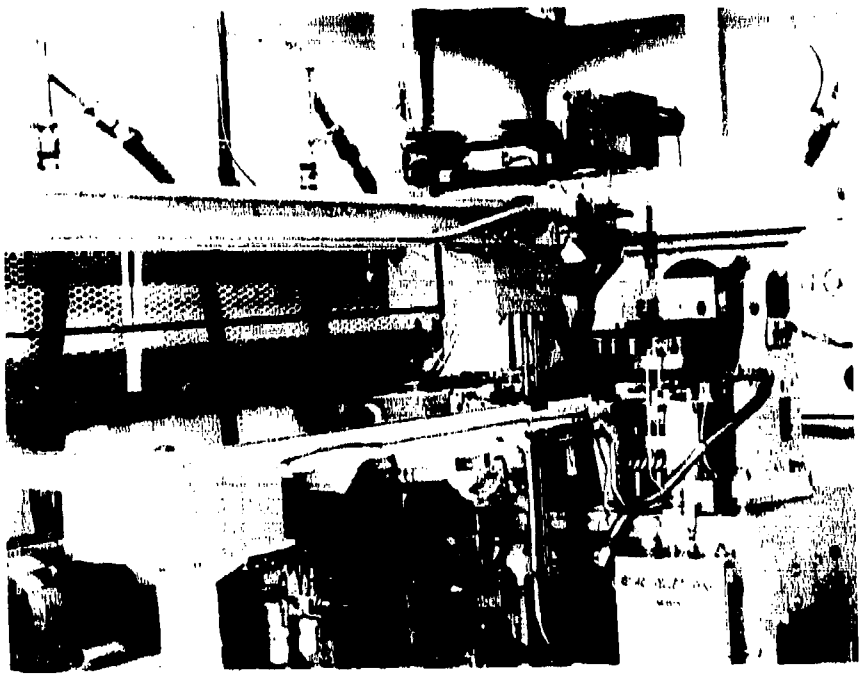

Figure 28. Rotary Pellet Press and Dust Collection Lines in Building B-46

After the pressing operation, the grenade is conveyed to the demachining area where the "nest," a fixture which supports the grenade housing during the pressing operation, is removed. Sample location 12 is located in the 2.0 in. (5.1 cm) dust exhaust line which serves the demachining operation. After demachining, the grenades are conveyed to the cone swagging press where the copper shaped-charge cones are forced into the grenade body. This last operation had no dust collection lines. The probe attachment fixtures used in Building B-46 were located outside the Building just prior to the wet dust collectors. Figure 29 shows one of the fixtures with two dust probes installed. The orientation of the dust probes, shown in Figure 29, was also used at Building 04-M-40.

Dust Concentration Measurements

Table 8 illustrates the duct velocity and flow rates measurements obtained in 04-M-40. The duct flow rate measured at location 11 is greater than at location 10 because the vacuum system draws air through the inoperative facing machine in Bays 3 and 4 as well as the operational unit in Bays 1 and 2. Table 9 summarizes the duct velocity and flow rates measured in B-46. As seen in the table, all three vacuum lines have the same static processes and the flow rates are all about the same. The velocity profiles across all five sample locations are blunt, indicating that the flow is turbulent in both processes at Lone Star AAP.

Table 10 summarizes the dust concentration data obtained at the Building 04-M-40 facing operation. The dust concentrations recorded at locations 10 and 11 were the highest recorded in any of the sample locations except the drilling operation in 1619 at Louisiana AAP. At location 10 the concentration appears highest at the bottom of the duct, while the top and centerline concentrations are fairly uniform. The concentrations at location 11 are somewhat lower, because of the larger duct diameter, and the concentration in the center of the duct is lower than at the top or the bottom of the duct.

Table 11 summarizes the dust concentration data obtained at Building B-46. The concentrations at these locations are similar, with the highest concentrations being generated at the demachining operation and the lowest concentrations generated by the rotary pellet press. The concentrations across the duct were fairly constant. This is attributed to the fact that the duct flow velocities were so high. High duct concentrations tend to disperse the dust evenly.

Electrostatic Measurements

The operations studied at Lone Star AAP were fully automated and the regularity of the operations is reflected in the wave forms recorded in the electrostatic measurements. Instrumentation for these tests was again limited to the charge density meter because of the small duct sizes 7.6 cm (3.0 in.) and 5.1 cm (2.0 in.) in diameter.

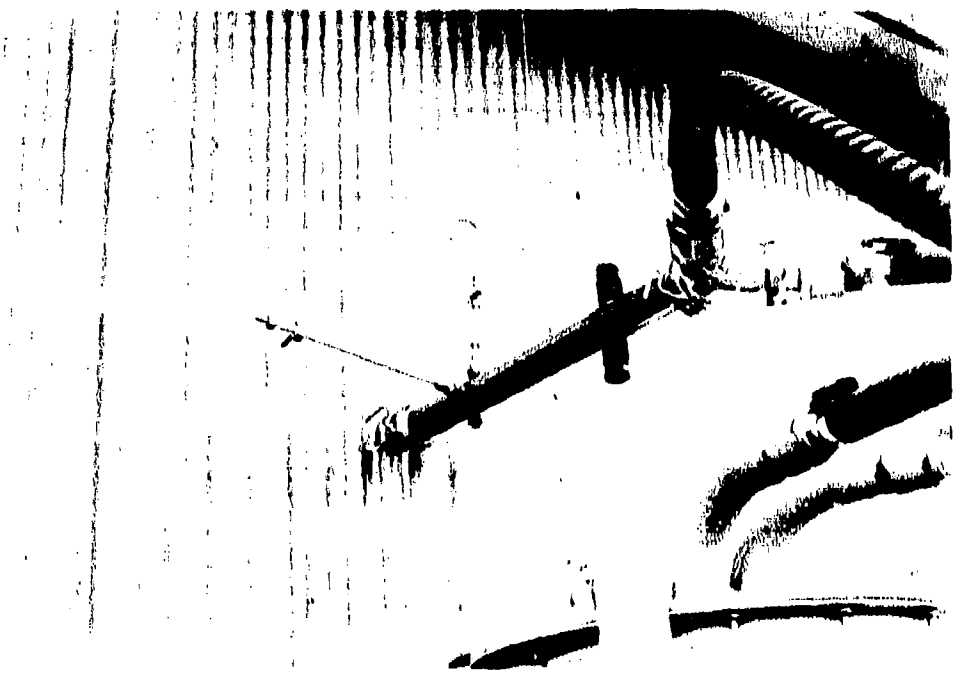

Figure 29. Probe Attachment Fixture Installed at Building B-46

Table 8. Duct Velocity and Flow Rate Data for Building 04-M-40 at Lone Star AAP

SAMPLE LOCATION NO. 10			SAMPLE LOCATION NO. 11		
Traverse Location From Bottom of Duct (cm)	Velocity Pressure VP_i (mm Hg)	Velocity V_i (m/min)	Traverse Location From Bottom of Duct (cm)	Velocity Pressure VP_i (mm Hg)	Velocity V_i (m/min)
0.32	3.175	1659	0.32	3.734	1833
0.76	3.556	1754	1.3	4.115	1920
1.4	3.378	1707	2.2	4.674	2049
2.5	3.378	1707	3.8	4.674	2049
3.6	2.616	1506	5.4	4.674	2050
4.3	2.616	1506	6.4	4.115	1920
4.8	NM	NM	7.3	NM	NM

Humidity Measurement

W_B/D_B = 71°F/79°F

WH = 102 grains of water/lb. dry air

RH = 67%

Duct Temperature

t = 79°F

Duct Static Pressure

P = -50.8 mm Hg

Duct Flow Rate

Q = 3.3 m^3/min

Humidity Measurement

W_B/D_B = 73°F/80.5°F

WH = 111 grains of water/lb. dry air

RH = 70%

Duct Temperature

t = 80.5°F

Duct Static Pressure

P = -76.2 mm Hg

Duct Flow Rate

Q = 9.0 m^3/min

NM = Not Measured

Table 9. Duct Velocity and Flow Rate for Building B-46 at Lone Star AAP

	Sample Location No. 12		Sample Location No. 13		Sample Location No. 14	
Traverse Location From Bottom of Duct (cm)	Velocity Pressure VP_i (mm Hg)	Velocity V_i (m/min)	Velocity Pressure VP_i (mm Hg)	Velocity V_i (m/min)	Velocity Pressure VP_i (mm Hg)	Velocity V_i (m/min)
0.32	4.674	2001	8.611	2714	8.230	2897
0.76	5.791	2228	9.347	2830	10.846	2968
1.4	6.553	2367	9.728	2886	11.608	3151
2.5	7.112	2467	9.931	2913	11.608	3151
3.6	6.375	2334	9.728	2886	12.725	3300
4.3	6.172	2299	9.728	2886	11.608	3151
4.8	NM	NM	NM	NM	NM	NM
	Humidity W_B/D_B = 71°F/75°F WH = 108 grains of water/lb. dry air RH = 82% Duct Temperature t = 75°F Duct Static Pressure P_D = - 50.8 mm Hg gage Duct Flow Rate Q = 4.7 m^3/min		Humidity $W_B D_B$ = 71°F/80.5°F WH = 98 grains of water/lb. dry air RH = 63% Duct Temperature t = 80.5°F Duct Static Pressure P = - 50.8 mm Hg gage Duct Flow Rate Q = 5.8 m^3/min		Humidity W_B/D_B = 71°F/80.5°F WH = 98 grains of water/lb. dry air RH = 63% Duct Temperature t = 80.5°F Duct Static Pressure P = - 50.8 mm Hg gage Duct Flow Rate Q = 6.3 m^3/min	

NM = Not Measured

Table 10. Dust Sampling Data at Building 04-M-40

SAMPLE LOCATION	TRAVERSE LOCATION FROM BOTTOM OF DUCT	SAMPLING VELOCITY (m/min)	WEIGHT OF DUST COLLECTED (gm)	SAMPLING TIME (min)	DUST CONCENTRATION (gm/m^3)
10	0.76	483	2.519	20	17.0
10	0.76	483	2.199	20	15.2
10	2.5	470	3.186	20	22.0
10	2.5	470	1.985	20	14.1
10	2.5	470	1.193	15	11.3
10	2.5	470	1.332	15	12.6
10	4.3	470	3.686	20	26.0
10	4.3	470	2.763	20	19.6
11	1.3	334	1.137	20	11.4
11	1.3	334	1.386	20	13.8
11	3.8	426	0.437	20	3.4
11	3.8	426	0.500	20	3.9
11	3.8	426	1.142	20	8.9
11	3.8	426	1.024	20	8.0
11	6.4	426	1.179	20	9.2
11	6.4	426	1.659	20	13.0

Table 11. Dust Sampling Data in Building B-46

SAMPLE LOCATION	TRAVERSE LOCATION FROM BOTTOM OF DUCT	SAMPLING VELOCITY (m/min)	WEIGHT OF DUST COLLECTED (gm)	SAMPLING TIME (min)	DUST CONCENTRATION (gm/m^3)
12	0.76	568	0.341	55	0.73
12	0.76	568	0.1832	31	0.70
12	2.5	667	0.414	55	0.75
12	2.5	667	0.1853	31	0.60
12	4.3	667	0.436	55	0.79
12	4.3	667	0.225	31	0.82
13	0.76	568	0.0533	17	0.37
13	0.76	568	0.1689	30	0.66
13	2.5	667	0.0690	17	0.41
13	2.5	667	0.1656	30	0.55
13	2.5	667	0.135	30	0.45
13	4.3	667	0.531	17	0.32
13	4.3	667	0.1589	30	0.54
14	0.76	568	0.047	30	0.18
14	2.5	667	0.0026	30	0.09
14	4.3	667	0.046	30	0.15

Building 04-M-40.

Charge levels measured at sampling location 10 on the dust collected from the rotary drill and facing machine were the highest of any charge levels measured in the entire testing program. The first tests at sampling location 10 produced charge levels that almost exceeded the measuring capabilities of the charge density meter. A short time after the initial start up of the line, it became apparent that the charge levels were steadily increasing and would exceed the measurement range of the charge density meter. At this point in the testing, the flow rate through the charge density meter was reduced to 7.1 ℓ/s (15 cfm) instead of the 9.4 ℓ/s (20 cfm) for which the instrument had been previously calibrated. To maintain the continuity of readings between the two flow rates, the peak measurements for the two flow rates were compared. With a flow rate of 7.1 ℓ/s (15 cfm) the charge density meter transfer function was found to be

$$\rho = 156.8 \left[\frac{100}{G}\right] V_o \ nC/m^3 \qquad (6)$$

After the initial start up of the process, the charge levels stabilized and typical waveforms observed from the drilling and facing operations are shown in Figure 30. Dust samples were withdrawn at the top and bottom of the duct by appropriate taps in the test fixture. Charge density levels were higher at the bottom than at the top which is reasonable considering the dust concentration profile of the duct. These data show that positive charges were generated and there is a charge peak for each time the drill penetrates a burster. The rotary facing machine contained four drill heads. One of the drill heads was not working which is evident by the data since the peaks generally occur in sets of three. Whenever less than three peaks appear, the operator failed to insert a burster on the conveyor belt for the drilling operation.

Further downstream in the same duct (location 1), electrostatic measurements were again repeated on dusts collected from the rotary drill and facing machine. As shown in Figure 31, the data are similar to the data observed at sampling location 10. What is noted, however, is that the charge density magnitudes decrease slightly due to the length of the duct. If the entire length of the duct could be sampled, there would be an exponential decrease in the charge being transported in the duct. Again, the sampling measurements were made at the top and bottom of the duct. As expected, the measurements at the top of the duct are slightly lower than at the bottom of the duct where the dust concentration is slightly higher.

Building B-46.

Electrostatic tests at Building B-46 on the A-5 explosive powders used in the grenade making process resulted in the most distinct and unusual waveforms observed in the electrostatic testing efforts. In the line operations, dust was collected and measured from two points on the consolidation rotary press and at a third sampling point in the

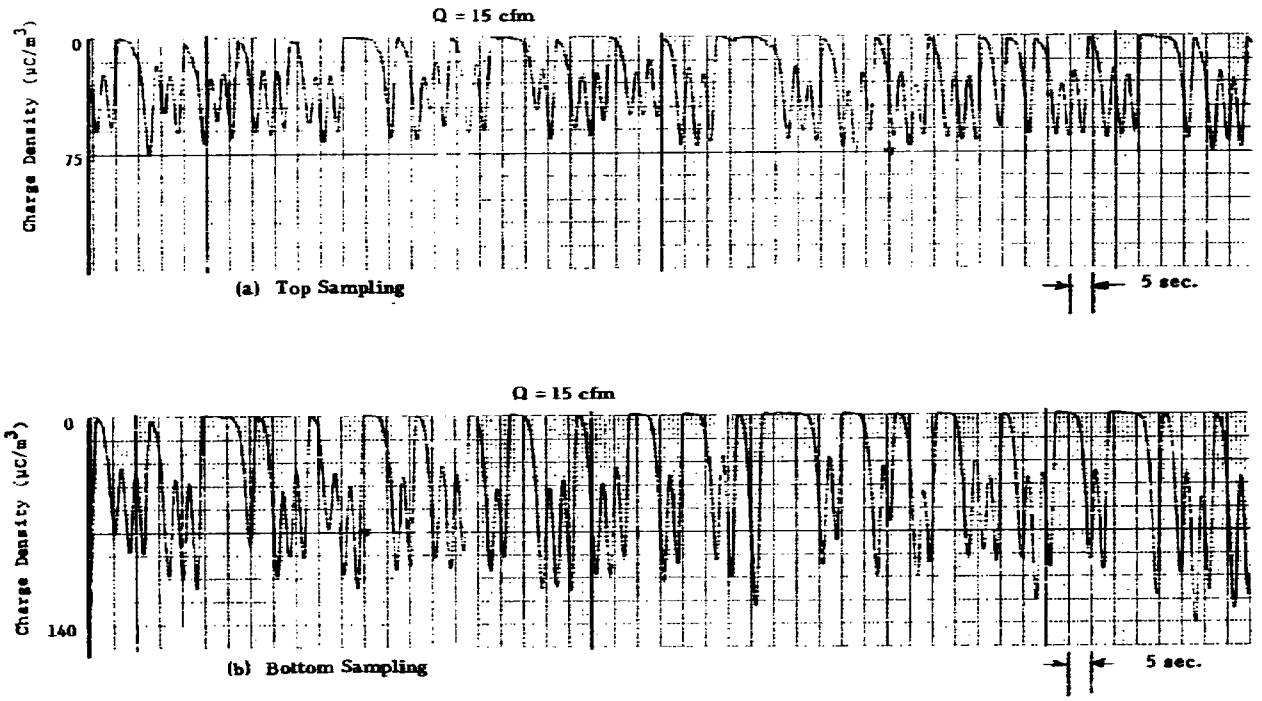

Figure 30. Charge Density Measurements at Building 04-M-40 at Sample Location 10

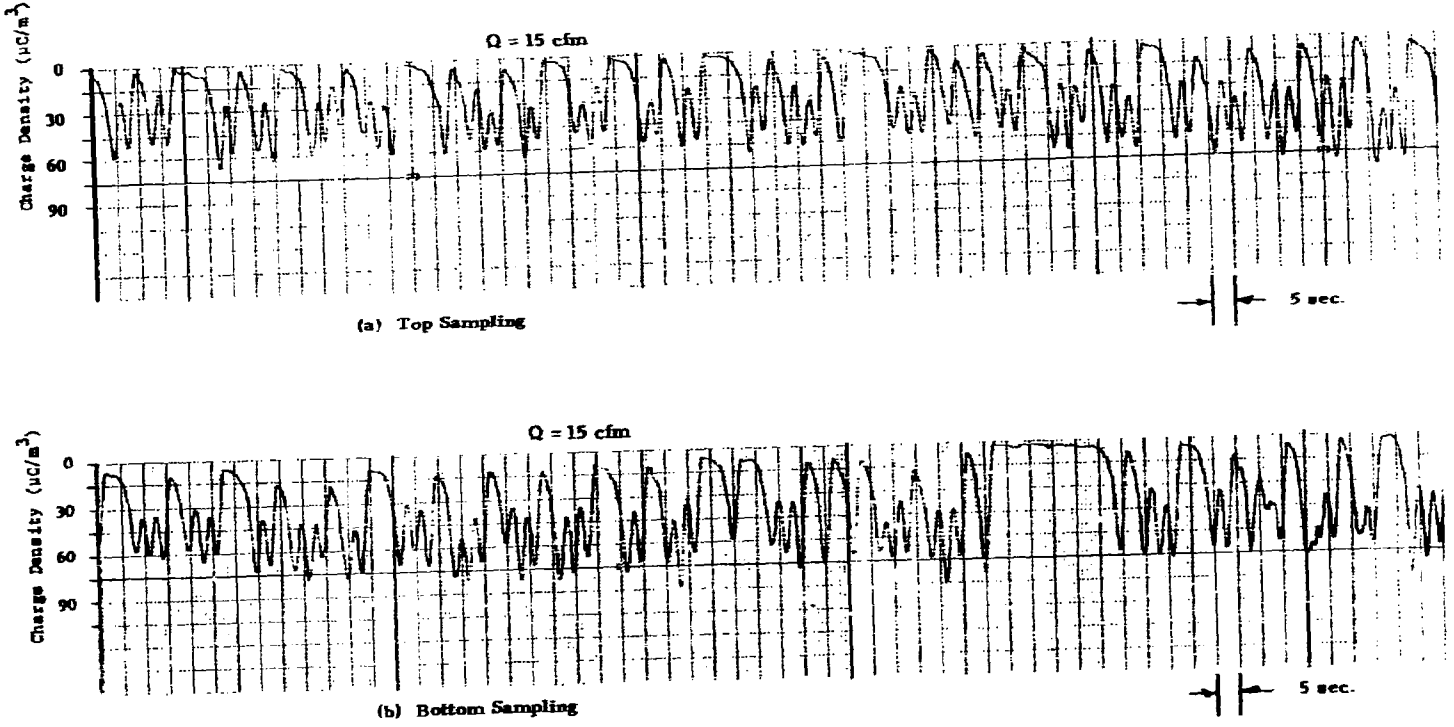

Figure 31. Charge Density Measurements at Building 04-M-40 at Sample Location 11

demachining area. Dust collected from the line operations is transported over short distances through 5.1 cm (2.0 in.) diameter ducts. While positive and negative charge species were found, the predominant charge was negative in polarity. Based upon the calibration factors of the charge density meter, the charge density levels were substantial.

The first electrostatic tests were conducted at sampling location 14. Dust from this sampling point is primarily collected at the hopper where the A-5 explosive material is dumped in powder form from a bucket into the rotary press. An additional pickup vacuums fugitive dust from the press itself. However, the electrostatic charge measured coincided exactly with the dumping of the A-5 powder into the press hopper visible in Figure 28.

Figure 32 shows the distinct charge doublets that result each time a bucket is emptied into the press hopper. As the bucket is dumped, the initial dust from the bucket is negative in polarity. With the deposition of the negative charge in the hopper, the opposite image charge is retained by the remaining powder in the bucket. As the bucket is emptied, the negative charge peaks and then begins to diminish in magnitude and reverses in polarity as can be seen in Figure 32. This phenomenon is completed as the image charge doublet of the opposite polarity is formed and returns to zero when the bucket is empty. From the data, the timing between each event when powder is dumped into the rotary press is three minutes. The data shown in Figure 32 were taken from a tap at the bottom of the duct.

In the operation of the rotary press, there are various vacuum hose inputs that collect dust from the press and a conveyor system that transports the grenades over to the demachining bay to the swagging operation. These various dust collection lines are connected to a common duct that transports the dust to sampling location 13 just before the dust enters the wet dust collector. In these line operations, the production of dust is continuous; therefore, as shown in Figure 33, there are no distinctive characteristics in the charge density meter waveforms that could be identified with any one manufacturing process on the line. Typical waveforms are shown in Figure 33 for the electrostatic measurements made at the top and bottom of the duct. In Figure 33a, the line operated for a short period of about four minutes. In Figure 33b, the data show another short-term operation period in which there were two minor interruptions between the start and shut-down points. The dust collected from the rotary press area was always negative in polarity.

The last point to be checked was at sampling location 12, which was representative of the dust collected from the demachining area. As the grenades moved along the conveyor, a continuous stream of dust was collected which resulted in the data shown in Figure 33c. In this strip chart presentation, the line was fully operational with no interruptions. These data were obtained by sampling at the bottom part of the test fixture and are virtually equivalent in magnitude as the charge measured at sampling location 13.

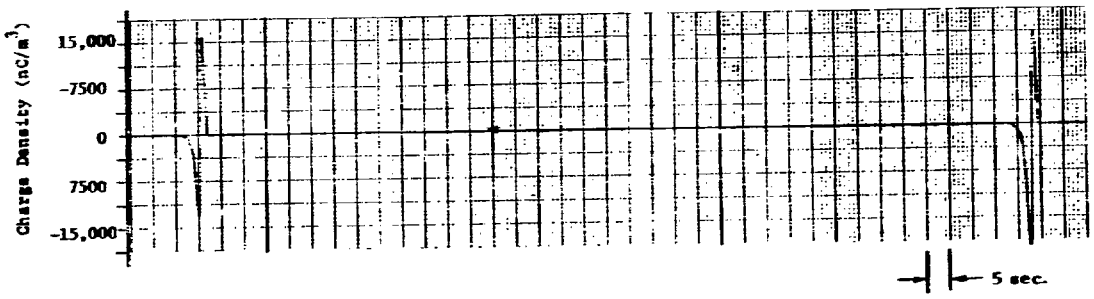

Figure 32. Charge Doublets Measured at Building B-46 at Sample Location 14

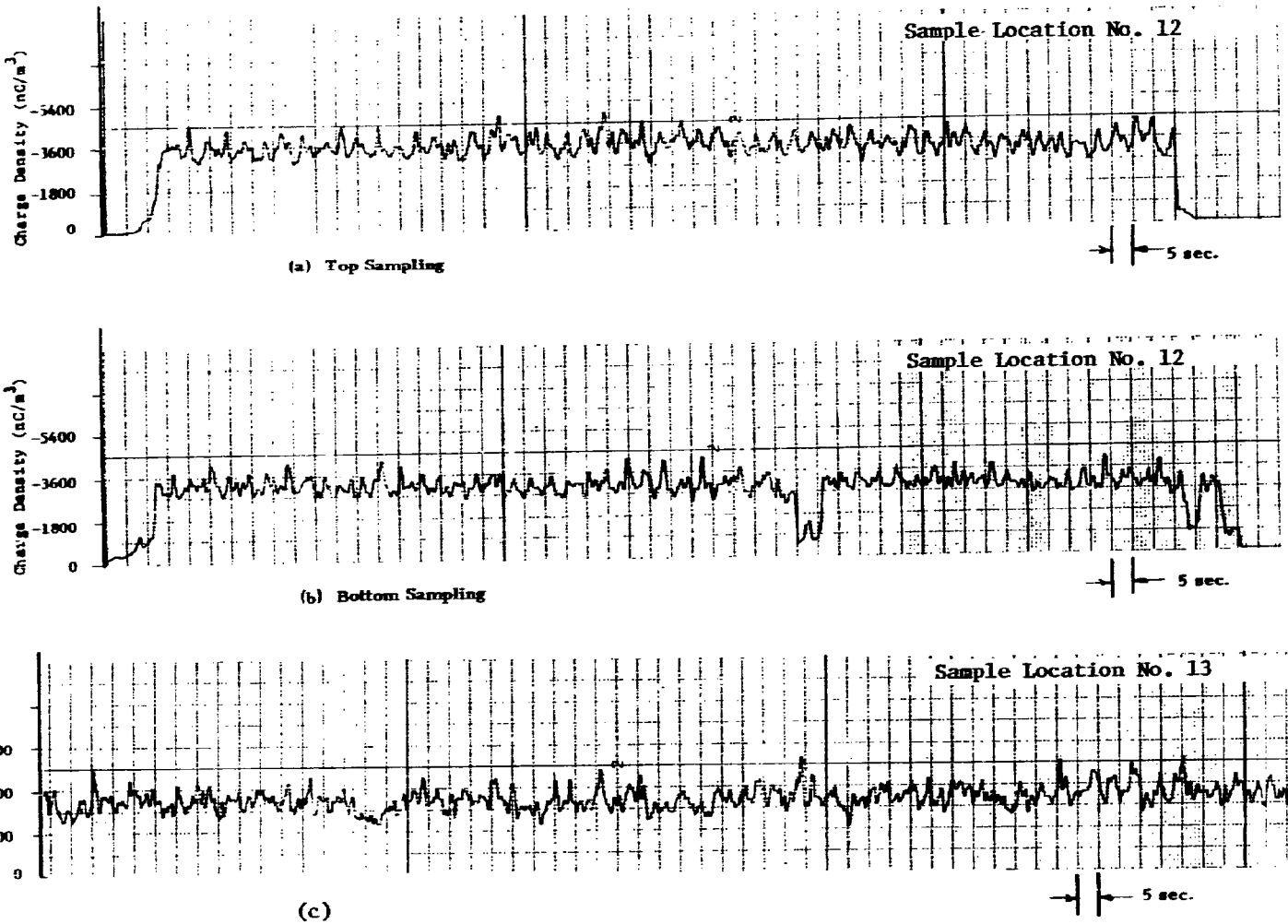

Figure 33. Charge Density Measurements at Building B-46

Charge and Energy Levels.

Table 12 lists maximum charge density measurements and the calculated energy levels. The charge density levels measured at 04-M-40 were the highest levels measured at any of the sample locations, and consequently the energy levels were the highest loads measured. At both 04-M-40 and B-46, charge density measurements were made with the exhaust line leading to the instrument drawing dust from the top and from the bottom of the duct. The largest readings were always obtained when the sample was withdrawn from the bottom of the duct.

Summary of Plant Sampling

Table 13 summarizes the data collected at the 14 sample locations in the three ammunition plants. In this table, we have listed the maximum values detected at each sample location. Although it is difficult to compare the results from such widely different processes, it is possible to draw some significant qualitative observations:

- Typically, sampling performed in small diameter vacuum system ducting resulted in:

  (a) higher vacuum pressures,
  (b) higher flow velocities,
  (c) higher dust concentrations,
  (d) lower flow rates, and
  (e) higher charge densities

- Processes involving drilling or facing of explosives generate significantly higher dust concentrations, charge densities and energy levels, than processes involving weighing, pouring, sifting or dropping of explosives.

- Flow velocities in the ducting were too low to achieve a uniform concentration across the ducting. Significantly higher dust concentrations and charge densities were generally measured below the duct centerline. This was also reflected in dust buildups in duct cleanouts and other duct penetrations placed below the duct centerline.

- All of the operations studied are batch operations, which means that the dust concentration is periodic with periods of high loading densities interspersed with periods of relatively low concentrations. The sampling technique employed on this program was gravimetric sampling which is dependent on the total mass of dust collected and the period of time

Table 12. Charge and Energy Levels Measured in Lone Star AAP

Building	Sample Location	Duct Diameter (cm)	Charge Density (nC/m^3)	Energy (μJ)
04-M-40	10	5.1	+140,000	0.698
04-M-40	11	7.6	+94,000	0.315
B-46	12	5.1	-4,890	0.112
B-46	13	5.1	-5,170	0.125
B-46	14	5.1	+19,600	1.79

Table 13. Summary of Measurements Taken During the Plant Sampling

Sampling Location		Material Sampled	Duct Diameter (cm)	Flow Rate (m^3/min)	Static Pressure (mm Hg)	Temp (°F)	Rel Humidity (%)	Dust Concentration (gm/m^3)	Charge Density (nC/m^3)	Energy (μJ)
Louisiana AAP:										
Building 1611:	1	Composition B	30.5	63	-2.29	62	41	0.093	-232	2.43
	2	Composition B	10.2	4.9	-2.29	63	50	1.61	+184	0.005
	3	Composition B	30.5	68	-2.29	72	36	0.115	-287	3.00
Building 1619:	4	Composition B	5.1	-	-	-	-	-	+14,800	1.02
	5	Composition B	5.1	3.8	-152.4	75	35	330.0	+11,100	0.57
Longhorn AAP:										
Building B-7:	6	Aluminate	5.1	0.47	-127.0	88	6	0.90	+7,750	0.28
	7	Aluminate	5.1	4.9	-108.0	89	42	6.3	-11,100	0.57
Building 34-Y:	8	Aluminate	5.1	3.0	-88.9	89	36	12.1	+3,500	0.057
	9	Aluminate	5.1	4.2	-101.6	89	50	1.4	+1,030	0.005
Lonestar AAP:										
Building 04-M-40:	10	Composition B	5.1	3.3	-50.8	79	67	26.0	140,000	698.0
	11	Composition B	7.6	8.9	-76.2	80	70	13.8	94,000	315.0
Building B-46:	12	A-5	5.1	4.7	-50.8	75	82	0.82	-4,890	0.112
	13	A-5	5.1	5.8	-50.8	80	63	0.66	-5,170	0.125
	14	A-5	5.1	6.3	-50.8	80	63	0.18	+19,600	1.79

over which the sample was taken. This means that the concentrations listed in the tables of this section of the report are average concentrations. Instantaneous duct concentrations may be significantly higher. Minimum explosive concentrations of explosive and pyrotechnic dusts have been reported (Ref 4) in the range of 40 to 1000 gm/m^3 (.04 to 1 oz/ft^3). The maximum average concentrations listed in Table 13 are all below this range with the exception of location 5 at Building 1619 at Louisiana AAP.

- Minimum ignition energies have been reported (Ref. 4) in the range of 0.2 to 8.0 J for explosive and pyrotechnic dusts. The energies calculated from the charge density measurements are all very low with the maximum energy level being 700μJ. This reading was unusually high, the maximum energy level measured at locations other than Building 04-M-40 (Lonestar AAP) was 3.0μJ at Building 1611 in Louisiana AAP.

- The charge density appears to be roughly proportional to the peak mass flow rate (duct flow rate, Q times the maximum dust concentration) in the duct. This correlation is shown in Figure 34. The correlation appears good for Composition B and the aluminate composition. The Composition A-5 data points fall somewhat below the other points, which may reflect differences in the explosive properties. The correlation is surprisingly good, since the measurements of the charge density and the dust concentration were not measured simultaneously at any one location. Instead these two parameters were measured at different times to prevent distortion of the charge density by the metal dust probe.

  The consistency of the data in this type of presentation would probably be improved by the simultaneous measurement of instantaneous concentrations, flow rate and charge density. This should be explored in future plant sampling endeavors.

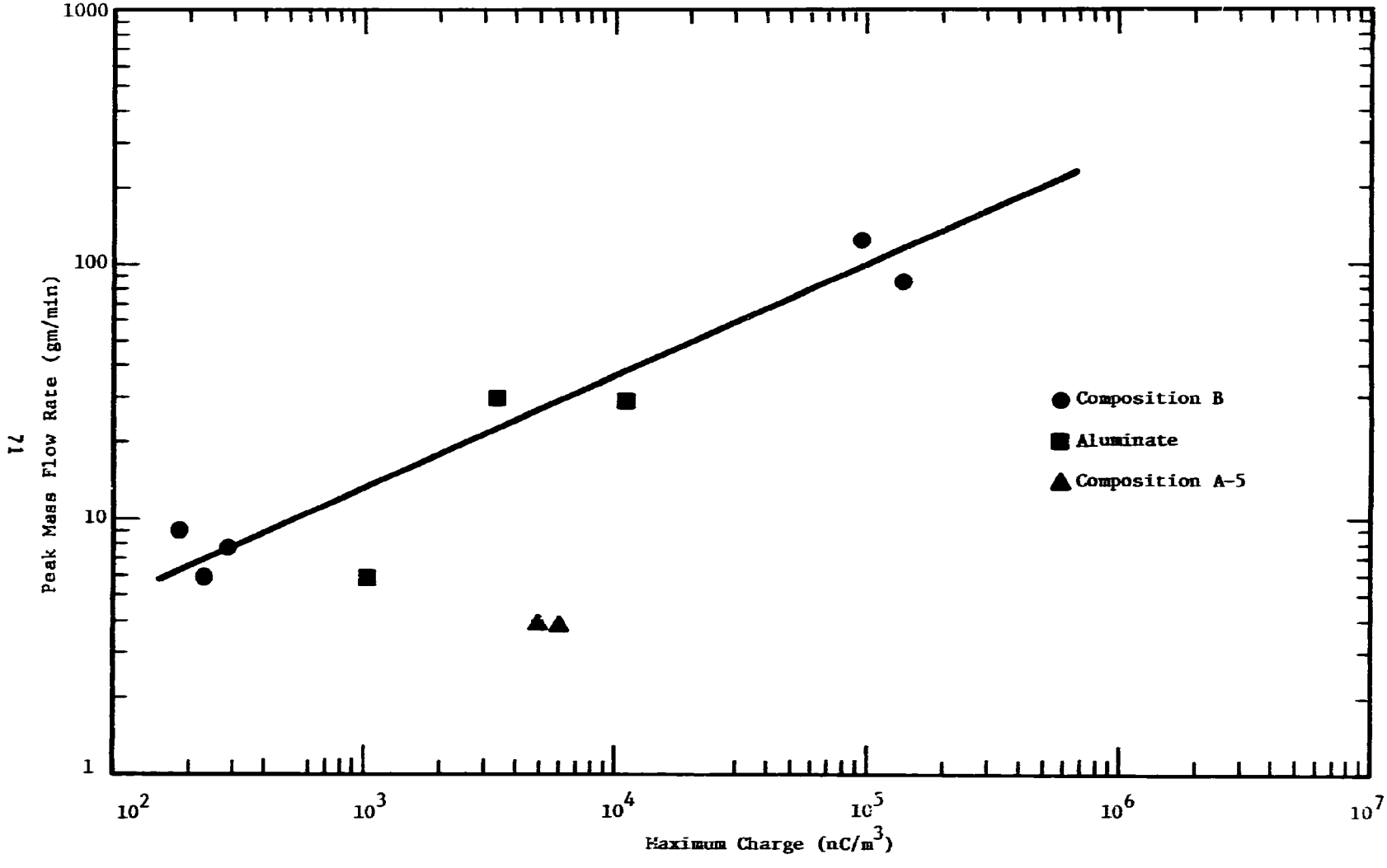

Figure 34. Charge Density Dependence on Mass Flow Rate Through the Duct

SELECTION OF DUST DETECTION EQUIPMENT

Survey

An extensive survey of off-the-shelf dust detection equipment was performed to identify commercially available equipment capable of detecting hazardous dust concentrations. The survey was initiated by contacting by letter over 200 corporations which manufacture scientific equipment. The corporations were identified through the Thomas Register (Ref. 5) and the "Guide to Scientific Instruments 1980-1981," (Ref. 6). The letter solicited descriptions of any products which the manufacturer produced which may be used for the stated purpose. Eighty manufacturers responded to our request for information; however, the bulk of the responses were not applicable to dust concentration measurement.

In general two classes of dust concentration measurement instrumentation were identified. One category of instrumentation is intended for monitoring respirable dust concentrations in a room or other large volume. This type of instrument cannot measure large particles [>100μm (>2.73 x 10^{-5} in.)] and cannot injest dust at the high velocities required for isokinetic sampling. Another general class of instruments is used for particular emission from stacks. These devices have probes which are often 0.9 m (3.0 ft) long which could cause mounting problems in the small ducts generally in use in the Army Ammunition Plants. Although these instruments can measure particles up to 100μm (2.73 x 10^{-5} in.) they still suffer from the inability to inject the dust particles at high flow rates. Table 14 summarizes the specifications of the more promising instruments identified during the instrument survey. Appendix C presents the instrument data sheets for the instruments listed in Table 14.

Later another dust concentration instrument became available (Ref. 7). This instrument was developed by GCA Corporation, Bedford, MA, under contract to the Bureau of Mines. Operation of the dust concentration monitor is based on the attenuation of beta rays by the dust. The unit is said to be capable of measuring dust levels in the range of 20 to 500 gm/m^3 (0.020 to 0.5 oz/ft^3) with a sample rate of one sample per 10 seconds. In its current configuration, the entire unit must be mounted so that the probe located on top of the unit penetrates the duct. This means the duct must support the concentration sensor. The present unit would not be suitable for measurement of concentration in the small ducts encountered in most of the sample locations described in Section III.

Evaluation of a Dust Sensor

After a review of the data presented in Table 14, the Omni-Wave Continuous Particulate Monitor was selected for evaluation. This

Table 14. Dust Detection Equipment

DUST DETECTOR TYPE	PARTICLE SIZE RANGE	CONCENTRATION RANGE	SAMPLE FLOW RATE	RESPONSE/SAMPLE TIME	OPERATING PRINCIPLE	COMMENTS
Met One Inc Model 200–	0.5, 1, 2, 5, 10 μm and larger	Main frame–$3x10^5$ p/m^3 Digital Display – 5 Digits Analog display $3x10^2$–$3x10^5$ p/m^3	0.005 ℓ/sec (Probe for 50.8 cm/sec air flow is optional)	1 min	—	• Analog display has alarm • Room monitor
Met One Inc Model 209–	0.5 μm and larger	5 Digit display or printer	0.47 ℓ/sec Sample mode .0028, 0.023 0.28m^3 (Probe for 100 ft/min)	0.1 min	—	• Audible alarm • Room monitor
HIAC/Royco Inc Model 220	0.5 μm and larger	$3x10^4$ p/m^3 is Max	0.047 ℓ/sec	—	Optical – Right Angle Scatter	• Alarm optional • Room monitor • Display continuously updated
HIAC/Royco Inc Model 245/507	0.5 μm and larger (size ranges are selectable with incremental features)	8500p/m^3	0.47 ℓ/sec (Sampling probe optional)	1 min	Optical – Near Forward Scatter	• Alarm optional • Room monitor • Samples for 1 and 10 minutes
HIAC/Royco Inc Model 225/518	0.5 μm and larger (with incremental selection over full dynamic range (dynamic range: 40:1)	$3x10^6$ p/m^3 is Max Display–6 Digit	0.047 or 0.0047 ℓ/sec	1 min	Optical – Near Forward Scatter	• Samples for 1 and 10 minutes, or manual
HIAC/Royco Inc Model 245/518	0.5 μm and larger (same as 225/518)	8500p/m^3	0.47 ℓ/sec	1 min	Optical – Near Forward Scatter	• Samples for 1 or 10 minutes or manual

Table 14. (CONT)

DUST DETECTOR TYPE	PARTICLE SIZE RANGE	CONCENTRATION RANGE	SAMPLE FLOW RATE	RESPONSE/SAMPLE TIME	OPERATING PRINCIPLE	COMMENTS
ONMI-Wave Model 207	0.1 -100 μm	23 -0.00023gm/m^3 (Mass flow range)	—	—	Charge Transfer	• Portable • Isokinetic sampler
ONMI-Wave Model 2710	0.1 -100 μm	230 -0.000023gm/m^3	—	0.5 sec	Charge Transfer	• In-stack sampling • Isokinetic sampler
Environmental Systems Corp (ESC)-P-5A	0.1 -10 μm	.001 -10gm/m^3	Independent of gas velocity	—	Optics - Backscatter	• Mounts in std. ducts 10.2 cm or larger
Model P-5G	0.1 -20 μm					
Horiba Model APDA-200E	System contains two cut impacters 10 μm and 7.07 μm	0 -0.5mg/m^3	—	3-15 min	Optics - Light Scatter	• Alarm available • 3 minute response time
FPM	5-50 μm	200gm/m^3	—			

instrumentation consists of an electrically conductive sensing element and a high gain amplifier. The sensing element is mounted in the sampling stream. When particulates impact the sensing element, changes on the particulates are transferred and a small current is produced. The current is amplified and converted into a voltage proportional to the particulate mass flow. The amount of amplification can be varied to obtain concentration measurements in the range of 2.28×10^{-4} to 22.8 gm/m^3 (2.28×10^{-2} to 0.0228 oz/ft^3). A special probe is available to extend the concentration measurements to 228 gm/m^3 (0.228 oz/ft^3).

To evaluate this sensing system, the probe was mounted in the duct simulator described in Appendix B. The 0.914 m (3.0 ft) probe was cut off at 20.3 cm (8.0 in.) and mounted in the ducting 6.1 m (20.0 ft) from the exhaust fan. The screw feeder used to meter the dust was eliminated since these experiments were to utilize Composition B explosive dust. Instead, measured quantities of the dust were placed in the bottom of the duct and the turbulent air flow was used to suspend the dust. In these tests the duct flow velocity was about 28.3 m^3/min (1000 ft^3/in.). This flow velocity was sufficient to suspend and totally exhaust 454 gm (1 lb) of Composition B dust in two minutes. The dust concentration developed in this manner was initially very heavy but tapered off continuously during the two minutes of air flow.

During repeated tests, the sensor output saturated at all gain levels indicating that the dust concentration was about the measurable range of the instrument. During these experiments it was noticed that the instrument response reached a saturated condition in 0.5 sec, which corresponds to the manufacturers stated system response time.

After discussion with the manufacturer, it was learned that the amplifier could be modified to reduce the overall sensitivity. The modification consisted of replacing some precision resistors in the amplifier. The sensor was then installed in the 1m^3 explosion chamber which will be described in the next section. In a series of experiments using Composition B dust with concentrations of 120 to 380 gm/m^3 (0.12 to 0.380 oz/ft^3) the modified instrument responded by saturating again. After further discussions with the manufacturer it was learned that the sensing probe had been damaged and since no funds were available for leasing the instrument for a longer period of time, the sensor evaluation was terminated.

CHARACTERIZATION OF EXPLOSIVE DUSTS

Overview

The manufacture of propellants and explosives produces a large amount of dust, particularly in the dryers. Realizing the serious hazards of the energetic dusts, the ammunition manufacturing plants have installed dry dust collection systems to remove dust particulates from the process line. These systems, while removing the hazard of finely divided dust from the process line, have introduced a new potential for catastrophic explosion. This is because frictional forces on the energetic particulates flowing through a duct or through collision with other particulates create substantial accumulations of static electric charges. Although grounding devices have been universally accepted as the appropriate method for dissipating electrostatic charge accumulations of static electric charges, dust explosions still occur.

Present data on the detonation characteristics of explosive or pyrotechnic dusts are incomplete. The available data are limited largely to Composition B, M-1, M-30, HMX and RDX (Refs. 4, 8, 9) for which the minimum explosive energy, minimum explosive concentration and minimum ignition energy have been measured. These measurements were performed in the small scale chambers developed by the Bureau of Mines, which until recently had been widely accepted. During this present effort the data base for the explosibility of energetic dusts was extended for Composition B, sodium nitrate and A-5 and TNT materials. Besides conducting the tests in the small scale chambers, tests were also conducted in 40 liter and $1m^3$ chambers.

In order for a dust cloud to explode the following basic criteria must be satisfied:

a) the dust must be suspended in the proper concentration range,
b) the dust must be combustible,
c) the cloud must engulf an ignition source of sufficient strength,
d) there must be sufficient oxygen within the cloud to support combustion, and
e) there must be some degree of confinement.

If one element in the chain is broken, there can be no explosion. Most of the time all of the above conditions are not met; however, catastrophic results often occur when all of the conditions are satisfied. Many parameters influence the explosibility of dusts both in terms of the

ability to ignite the cloud, and the strength of the reaction which develops after ignition. These parameters include:

- concentration
- particle size
- moisture content
- bulk material properties (volatile content, heat of combustion)
- atmospheric composition (humidity, presence of solvents)
- ignition souce strength and duration
- turbulence.

The effect of each of these parameters on the explosibility of dusts has been described by a number of authors (Refs 10, 11, 12) and will not be repeated here. The discussions are centered around commercial dusts, but are applicable as well to explosive and pyrotechnic dusts.

Methods for Determining the Explosibility of Dusts

The most common dust explosion test methods and test equipment are described in the section. Table 15 summarizes the characteristics of the various dust explosion vessels which are reported in the literature. Common features for all the test equipment include: a) means of achieving a dust suspension, b) an ignition source and c) some degree of confinement (completely enclosed or one side provided with a rupture diaphragm). Note in the table that most of the test vessels use a short burst of air to disperse the dust. Using this technique, care must be taken to attempt ignition when the dust is optimumly dispersed. Two dust explosion systems listed in the table use different techniques for dust dispersion. The Tohoku University system uses vessel rotation to suspend the dust. According to Reference 13, this vessel should not be used for dust concentrations below about 300 gm/m^3 (0.3 oz/ft^3). In the Cargill system the dust is placed on a fan blade in the bottom of the vessel. When the fan is started, the dust is thrown outward and upward. Ignition is attempted at an optimum time as determined from previous experiments.

The procedures generally used for dust explosibility testing in this country were originally developed and standardized by the U.S. Bureau of Mines (Ref. 14). The measure for explosibility which has evolved is a highly qualitative one and consists of rating the sample dust against Pittsburgh Seam coal dust (Ref. 14). This index is defined as:

$$\left.\begin{array}{l}\text{Index of Explosibility} = \text{Ignition Sensitivity} \times \text{Explosion Severity} \\ \text{where} \\ \text{Ignition Sensitivity} = (\text{minimum ignition temperature} \times \text{minimum ignition energy} \times \text{minimum explosive concentration})^{-1} \\ \text{and} \\ \text{Explosion Severity} = (\text{maximum explosion pressure} \times \text{maximum rate of pressure rise})\end{array}\right\} \quad (7)$$

Table 15. Comparison of Dust Explosion Test Vessels

TYPE	PARAMETER MEASURED	VOLUME (m^3)	SHAPE	DISPERSION SYSTEM	IGNITION SOURCE
Hartmann Tube	Min. Explosive Concentration	0.0012	Cylinder	Air Burst	Constant AC Arc
	Min. Ignition Energy	0.0012	Cylinder	Air Burst	Capacitive Discharge
Far-Mar-Co	Min. Explosive Concentration Min. Ignition Energy	0.04	Rectangular	Air Burst	Capacitive Discharge
Cargill	Min. Explosive Concentration Min. Ignition Energy	0.317	Rectangular	Fan	Capacitive Discharge
Hartmann Bomb	Maximum Pressure and Maximum Pressure Rise Rate	0.0012	Cylinder	Air Burst	Constant AC Arc
Bartknecht 20ℓ Vessel	Maximum Pressure and Maximum Pressure Rise Rate	0.02	Spherical	Air Burst	Capacitive Discharge
Bartknecht $1m^3$ Vessel	Maximum Pressure and Maximum Pressure Rise Rate	1.0	Cylindrical	Air Burst	Pyrotechnic Squibb
Tohoku University	Maximum Pressure and Maximum Pressure Rise Rate	0.01	Cylindrical	Vessel Rotation	Capacitive Discharge
Factory Mutual	Maximum Pressure and Maximum Pressure Rise Rate	0.004	Spherical	Air Burst	Capacitive Spark
Godbert-Greenwaldt Furnace	Minimum Ignition Temperature	0.00015	Cylindrical	Air Burst	Heating Element

All of the above quantities are relative to Pittsburgh Seam coal dust which has an Index of Explosibility of 1. By definition "weak," "moderate," "strong," and "severe" explosion hazards have an Index of Explosibility in the range of less than 0.1, between 0.1 and 1.0, between 1.0 and 10 and more than 10, respectively.

Ignition

Minimum Explosive Concentration

The minimum explosive concentration of a dust cloud is determined using the Hartmann Tube. SwRI's Hartmann Chamber is shown in Figure 35. This apparatus consists of a 0.0012 m^3 (75 in^3) Lucite cylindrical chamber, 0.3 m (1 ft) high mounted on a precision-machined base, which acts as the sample holder. Varying amounts of sample dust are caused to form uniform clouds by injection of a burst of air from a 1310 cm^3 (80 in^3) reservoir at 70 kPa (10 psi). The injection creates a momentary overpressure of approximately 3.4 kPa (0.5 psi) in the chamber. As the dust rises in the chamber, it passes through an AC arc from an 11 kilovolt transformer. The criterion for explosion is the rupture of a paper diaphragm which forms the top of the tube; appearance of flame or flashes is not considered a positive test. Development of 15 to 20 kPa (2.0 to 30.0 psi) within the tube is required to rupture the paper diaphragm. The mass of sample is reduced until the lowest mass permitting an explosion to propagate is established to $\pm$ 5 x 10^{-3} gm (1.1 x 10^{-5} lb). The minimum concentration for explosion is defined as that concentration at which a positive result is obtained on one out of four trials.

Minimum Ignition Energy

Determination of the minimum amount of electrical energy required to ignite a dust cloud is also performed in the Hartmann tube. The experimental procedure is essentially the same as for the minimum explosive concentration with the following variances. The concentration of the dust used is kept constant at 5 to 10 times the minimum explosive concentration. The ignition source is a capacitive discharge which must be timed with the dust dispersion. The spark energy can be varied from 50 to 800 mJ using a variable capacitor bank. The minimum ignition energy is the lowest level used in which a positive result is obtained in one of at least four trials.

Minimum Ignition Temperature

The minimum ignition temperature for a dust cloud is determined using the Godbert-Greenwald Furnace. The furnace consists of a thermostatically controlled vertical alundum core, would with heating wire so as to provide uniform temperature throughout its length. The top of the furnace is connected through a brass dust chamber to a 500 cm^3 (30.5 in^3) air reservoir. A burst of air from the reservoir propels the 0.10 gm (0.0035 oz) sample downward through the furnace. Appearance of flame or sparks at the bottom of the furnace is the criterion for a positive trial. The ignition

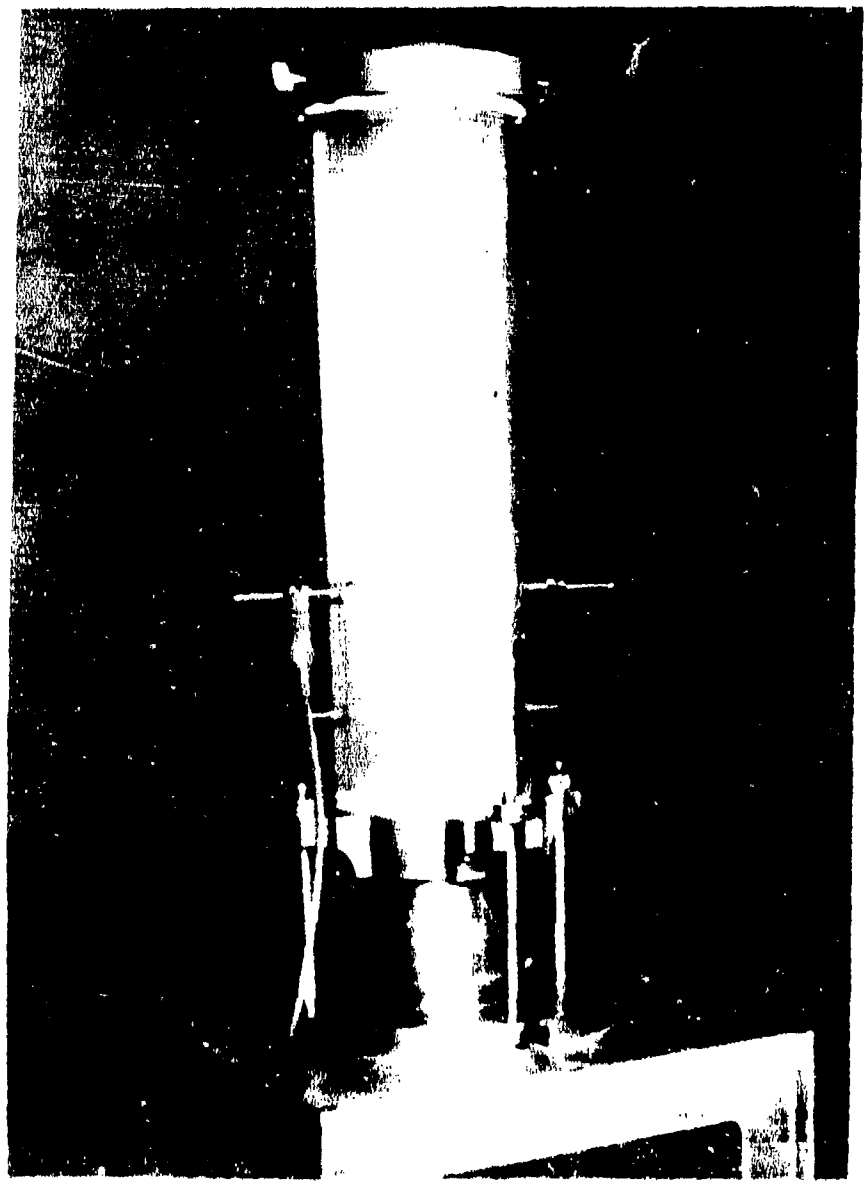

Figure 35. Minimum Ignition Energy Tests Using the SwRI Lucite Hartmann Apparatus

temperature is the minimum furnace temperature at which a positive result is obtained in one or more trials in a group of four. The increment of temperature variation is 10°C; the highest temperature attainable in the furnace is 800°C.

Explosion Severity Tests

Dust explosion severity determinations are performed using the Hartmann Bomb. This apparatus is a steel version of the Lucite Hartmann tube shown in Figure 36. A burst of air from a 1310 cm^3 (80 in^3) reservoir at 70 kPa (10 psi) is injected into the chamber. As the sample is dispersed, it flows through an 11 kilovolt AC arc across electrodes 10 cm (4 in.) from the bottom of the tube. The resulting pressure-time history is recorded on direct writing oscillograph equipment. If an ignition occurs, the resulting pressure record is analyzed to determine the maximum pressure and the maximum rate of pressure rise for that particular event. This experiment is repeated at dust concentrations of 0.1, 0.2, 0.5, 1.0 and 2.0 gm/m^3 (.0001, .0002, .0005, .001 and .002 oz/ft^3) in order to determine the concentration for which the most severe reaction develops.

Explosibility Test Results

During this effort, explosibility tests were performed on a variety of energetic materials. The materials investigated were Composition B, sodium nitrate, Composition A-5 and TNT. The test conducted included: a) minimum explosive concentration, b) minimum ignition energy, c) minimum ignition temperature, d) volume resistivity, and e) explosion severity. Many of the tests were conducted using the standard small scale dust explosion chambers (Hartmann and Godbert-Greenwaldt) described in the previous section. These small scale tests were conducted by Hazards Research Corporation, and their results are summarized in their report which is included as Appendix D. In addition, SwRI conducted a series of experiments in the 40ℓ and $1m^3$ chambers in which the maximum pressure and maximum pressure rise rate developed in Composition B and A-5 dust explosions were monitored. These tests investigated the effects of particle size, ignition source type and delay to ignition.

The Composition B dust used in the experiments was collected from the dry dust collection system in Building 04-M-40 at Louisiana AAP. The sodium nitrate was obtained from Longhorn AAP and the Composition A-5 was obtained from Lonestar AAP. The latter two materials arrived at SwRI in a granular form and had to be ground to a fine particle size to produce dust. This task was accomplished with a Molinex coffee grinder which was controlled remotely. In the various tests described below, the dust suspended and passed either a -40 mesh (<425 μm or 0.0165 in.) or a -100 mesh sieve (<150 μm or 0.0059 in.). Unless otherwise stated, the dust tested was dried to a <1% moisture content.

The 40 liter chamber consists of a 30.5 cm (12.0 in.) diameter, 61 cm (24.0 in.) long cylinder with 5.08 cm (2.0 in.) thick concrete walls lined with 0.762 mm (0.03 in.) sheet metal. This chamber is shown in Figure 37. The dust suspension system consists of an air reservoir, a dust container

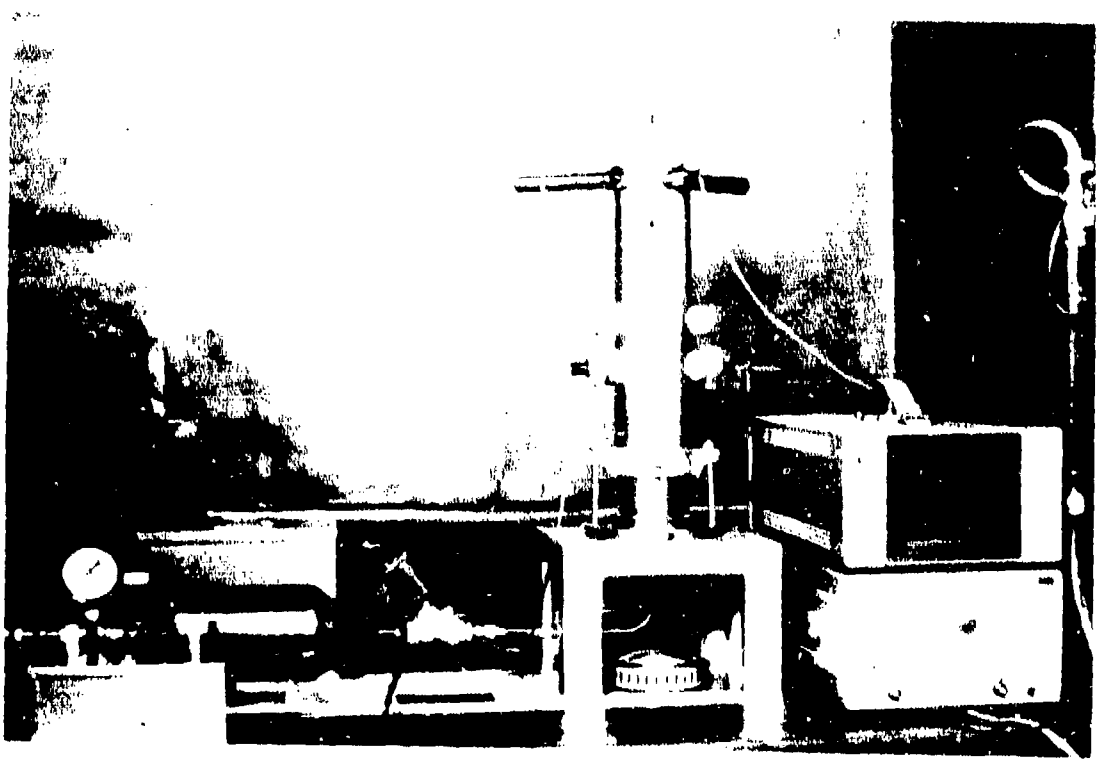

Figure 36. Hartmann Bomb Apparatus

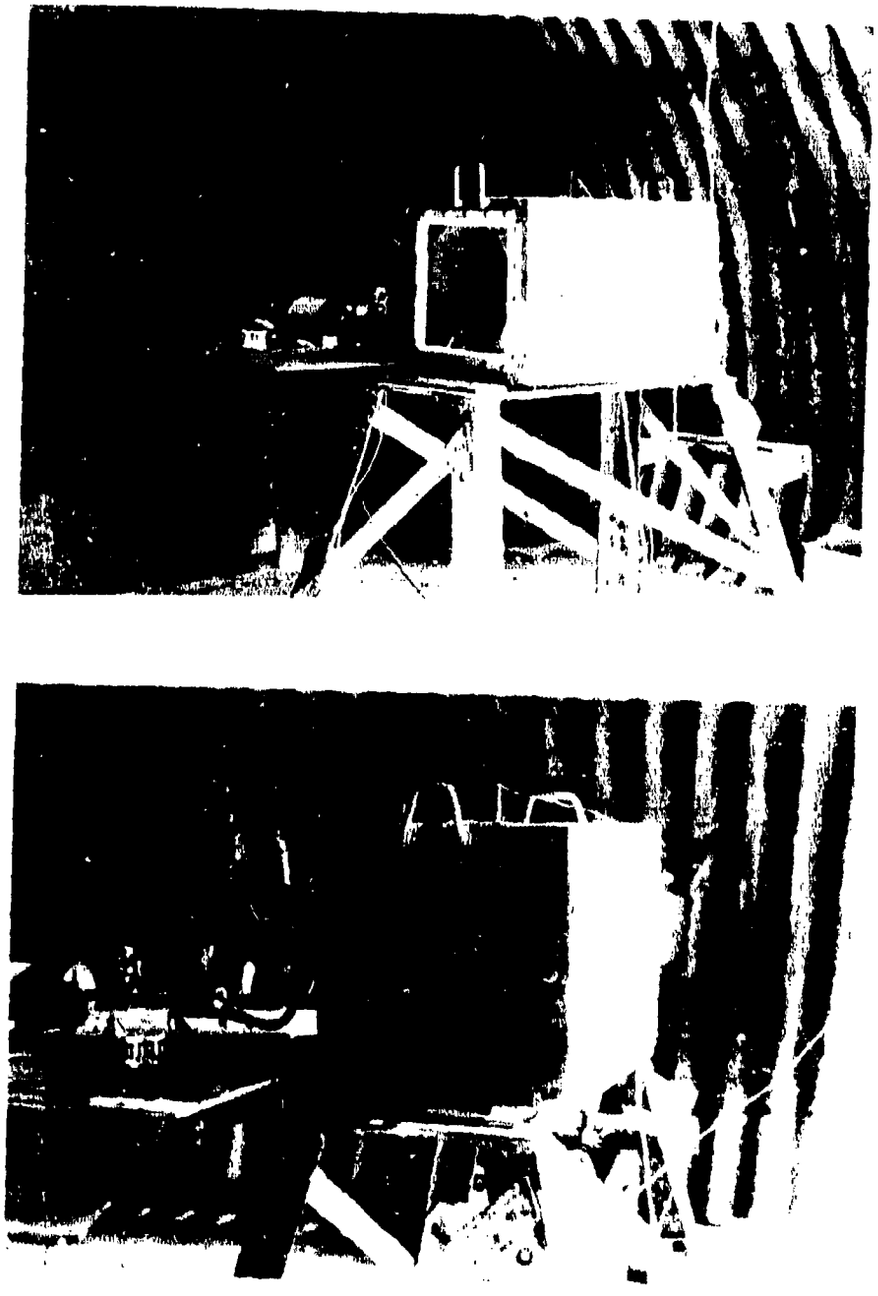

Figure 37. 40-Liter Explosion Chamber

and a nozzle into the chamber. In practice, a measured quantity of dust is placed in the dust container, and the air reservoir, filled to 3.3 bars, is dumped. The resulting air flow entrains the dust and carries it through the nozzle and into the chamber. In tests conducted with a transparent cover over one end of the cylinder, we have found that this system delivers a relatively uniform distribution of dust within the chamber.

The ignitors used in these experiments were either an AC Arc or a Boosted Electric Match (BEM). The AC Arc ignitor was exactly the same ignition system used in the Explosion Severity experiments in the Hartmann steel bomb. The BEM consisted of an Atlas Powder Company Electric Match (Number 250), boosted with 2 gm of FFF black powder. Since the suspension of the dust achieved in the 40-liter chamber is momentary, attempts at ignition must be timed with the release of the dust. In most cases, we have found that a 0.5 second delay between the opening of the solenoid valve and the firing of the ignitor was optimum. In the tests with Composition A-5 we found that a 0.25-second delay was optimum for this material. With the electric arc, the delay to ignitor is not a problem since the arc is struck prior to the onset of suspension, and maintained throughout the experiment.

BEM ignitor produces a detectible pressure rise when fired alone in the 40-liter chamber. This pressure rise was determined to be 0.8 bar. Thus all of the maximum pressures produced by the BEM and listed in this report were reduced by 0.8 bar. No compensation to the pressure rise rate data was attempted.

Appendix E presents a comprehensive summary of the experiments conducted in the 40-liter chamber. Typical pressure wave forms obtained in the chamber are provided in Figure 38. Note that the reactions shown at the top of the figure are relatively mild reactions characterized by low maximum pressures and pressure rise rates. More severe reactions are found in the center of the figure, and a severe reaction in which the 40-liter chamber failed is given at the bottom of the figure. The 40-liter chamber data are summarized graphically in Figures 39 to 41. Figure 39 presents the explosion severity data for Composition B dust ignited by the AC arc. These data are characterized by a very steep rise in maximum pressure and pressure rise rate between 260 and 300 gm/m^3, and a slight tapering above this range. When Composition B dust is ignited by the BEM, as seen in Figure 40, reactions are obtained at concentrations (100 gm/m^3 and up) and the pressure increases less dramatically than with the AC arc. Also in Figure 40, the effect of moisture content is seen to be a substantial reduction in pressure development with wet dust (10% by weight) as compared to dry material (<1%). In the case of the maximum pressure data, the presence of the material reduces the maximum pressure by 1.3 bar over the entire concentration range tested. Figure 41 presents the data accumulated in the 40-liter chamber using the BEM to ignite Composition A-5. As stated earlier, we have generally used a 0.5-second delay to ignition for most dusts in this chamber. However, in determining the optimum time delay, we found that

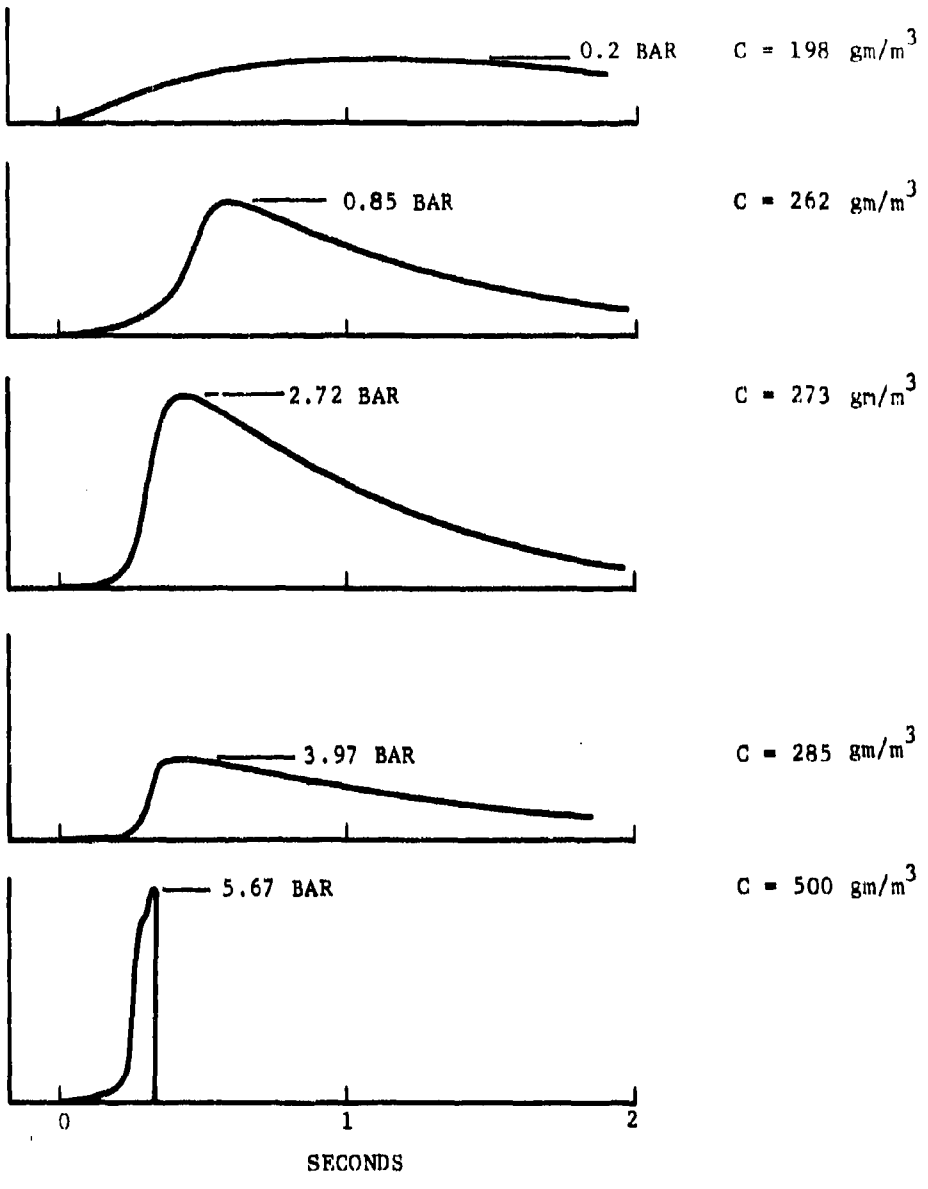

Figure 38. Pressure Wave Forms Obtained in Composition B Explosives Ignited by the AC Arc in the 40-Liter Chamber

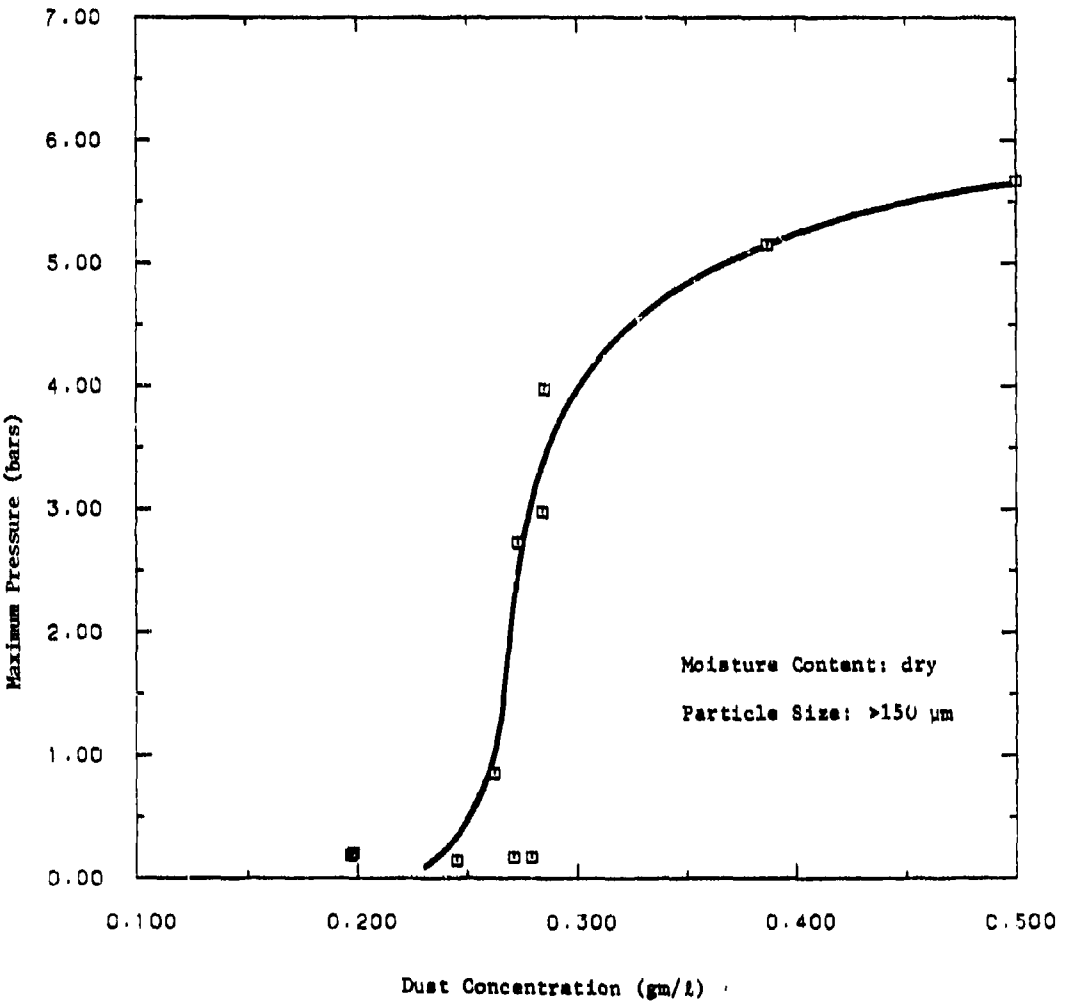

Figure 39a. Maximum Pressure in Composition B Explosions Ignited by the AC Arc in the 40-Liter Chamber

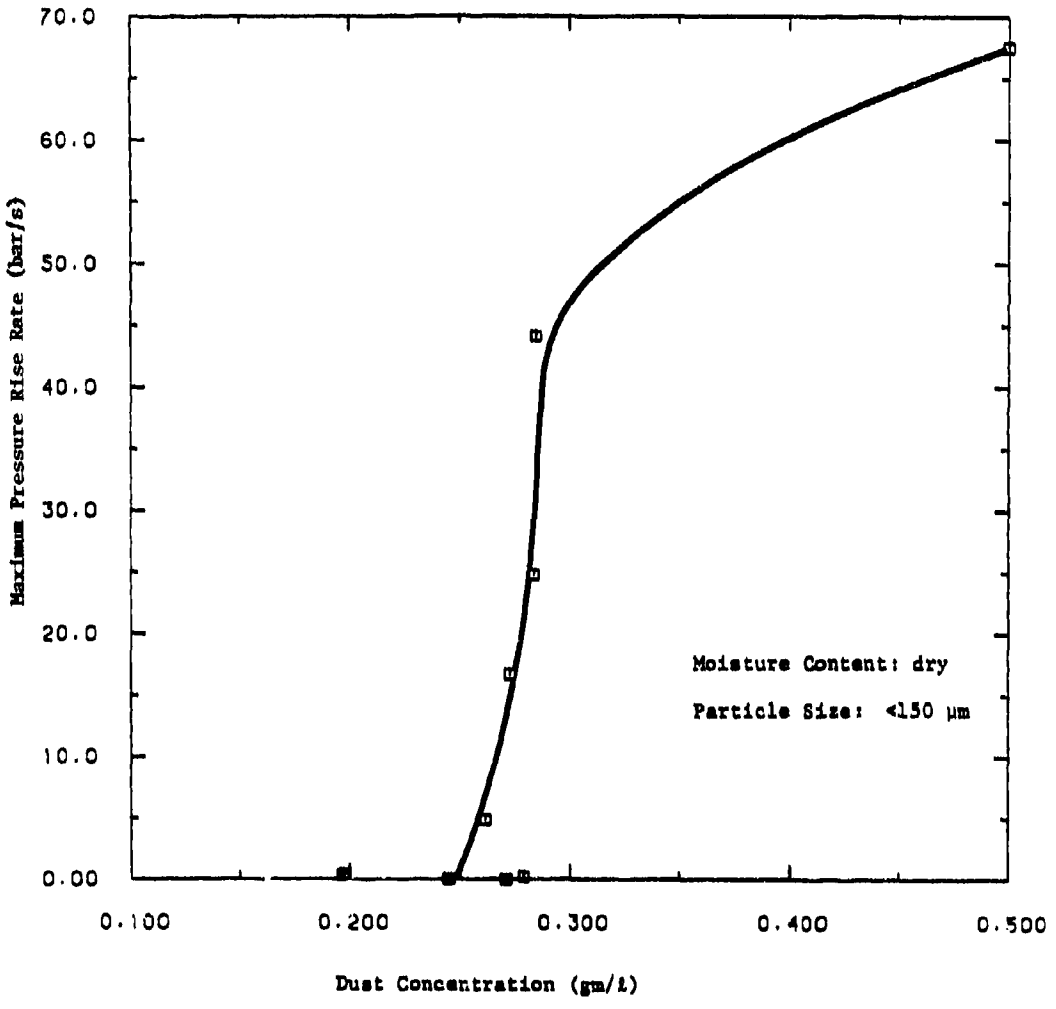

Figure 39b. Pressure Rise Rate in Composition B Explosions Ignited by the AC Arc in the 40-Liter Chamber

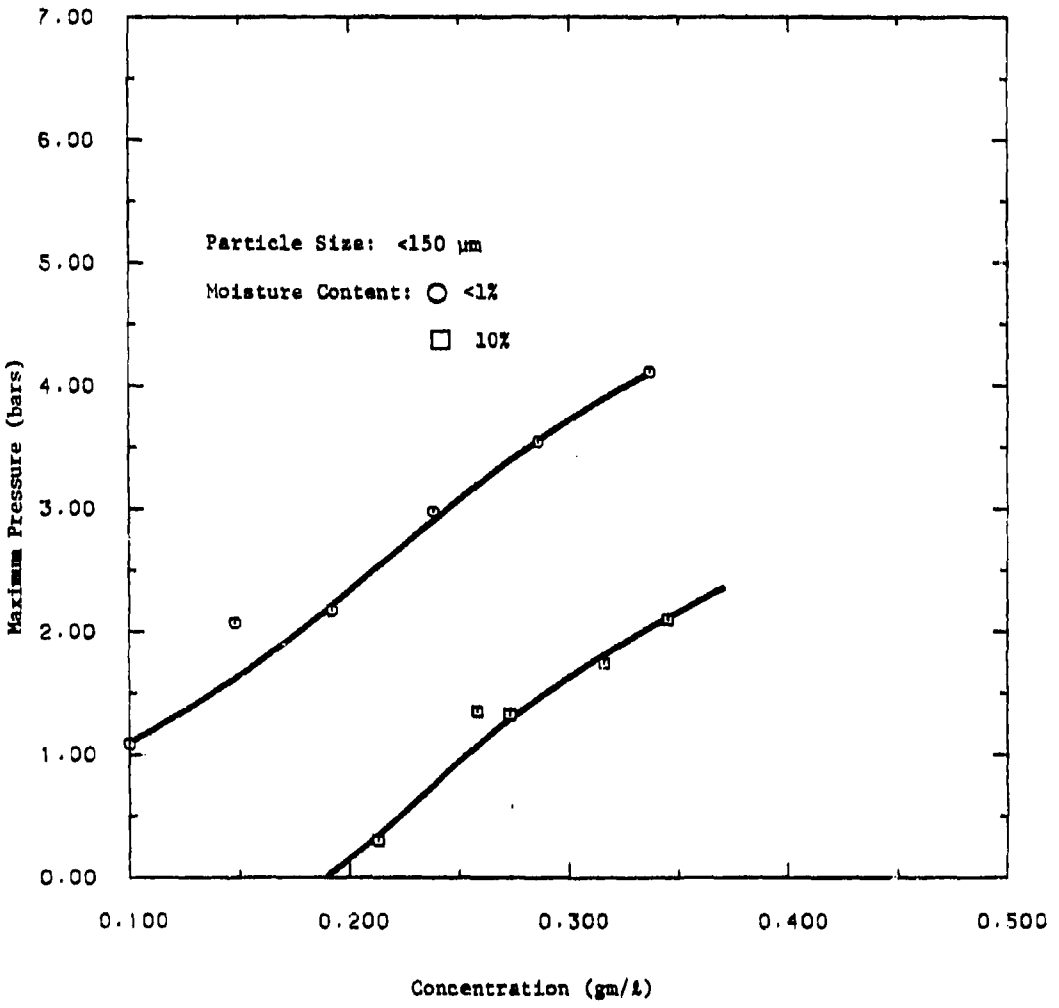

Figure 40a. Maximum Pressure in Composition B Explosions Initiated by the BEM in the 40-Liter Chamber

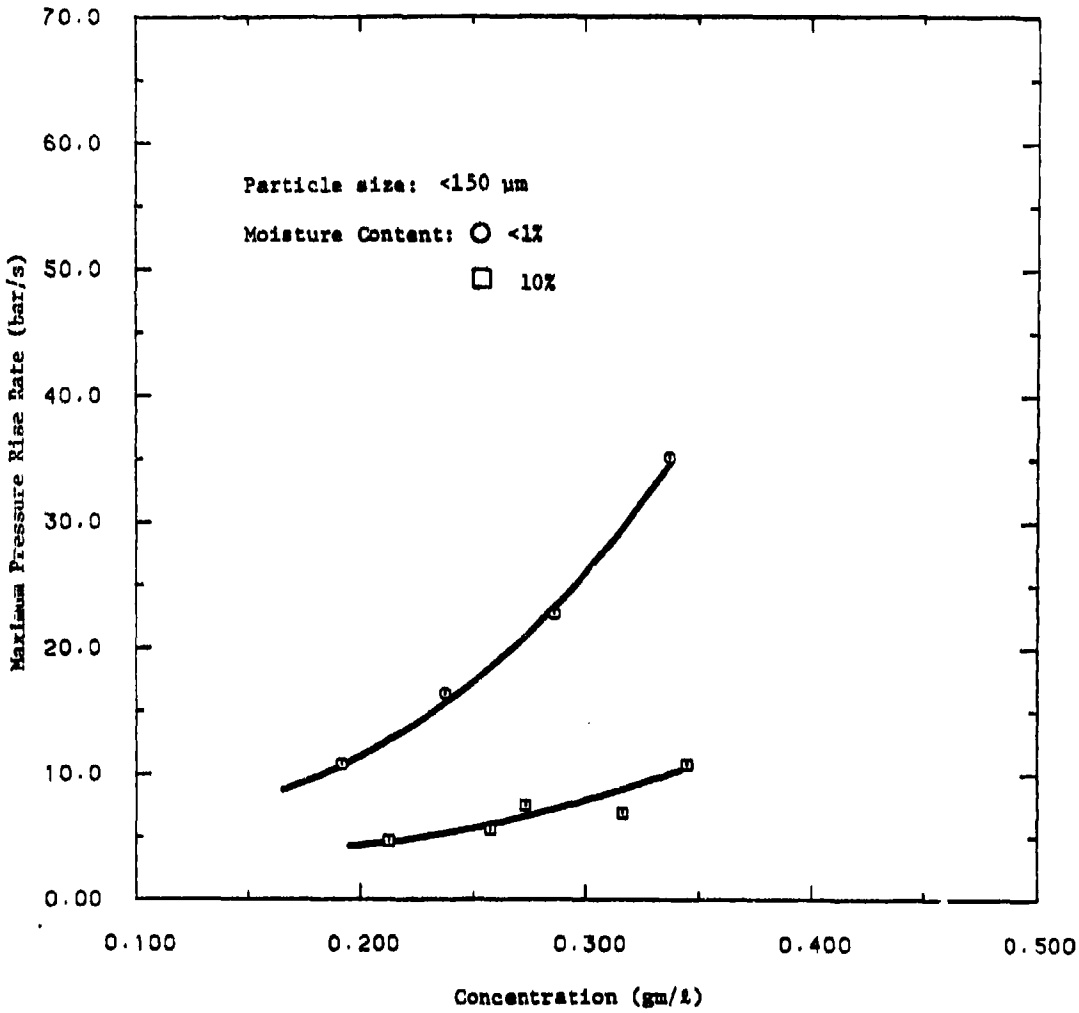

Figure 40b, Pressure Rise Rate in Composition B Explosions Ignited by the BEM in the 40-Liter Chamber

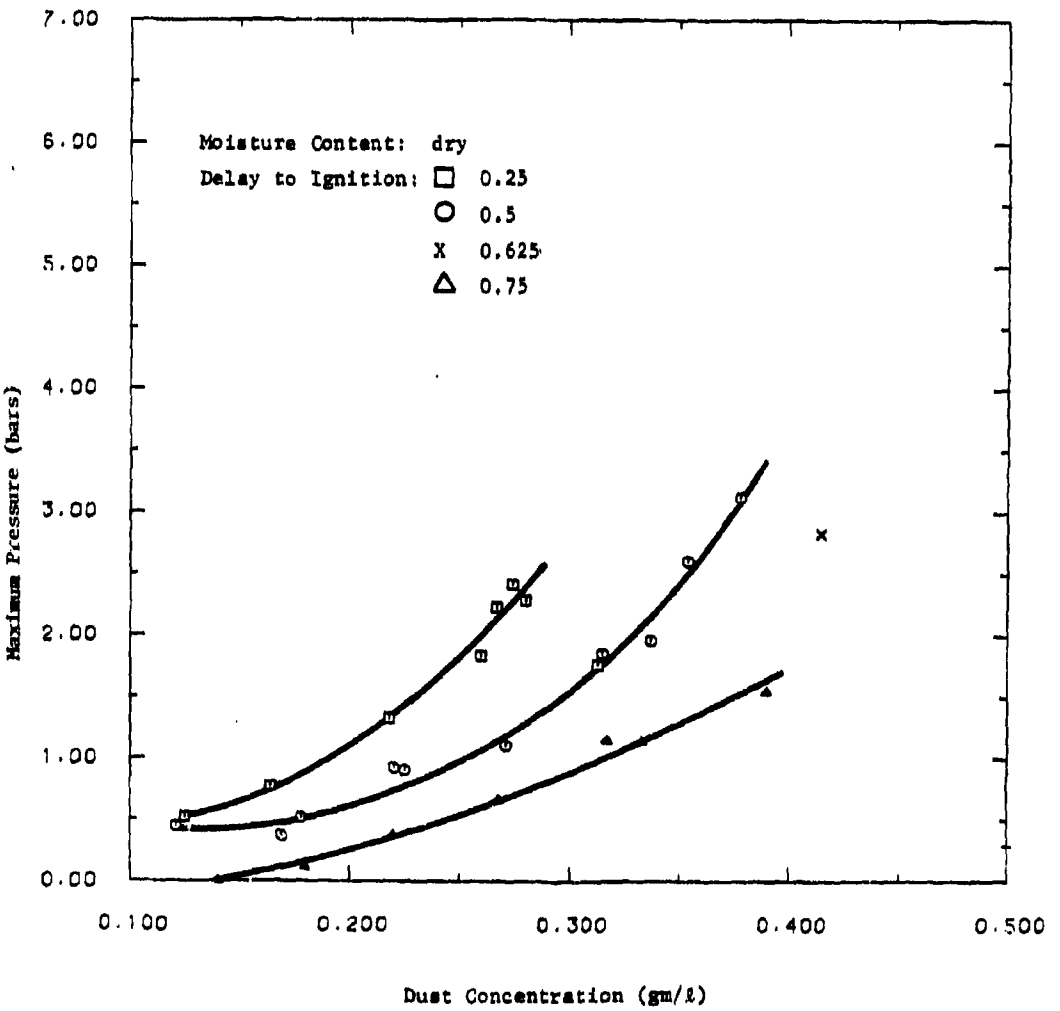

Figure 41a. Maximum Pressure in Composition A-5 Explosions Ignited by the BEM in the 40-Liter Chamber

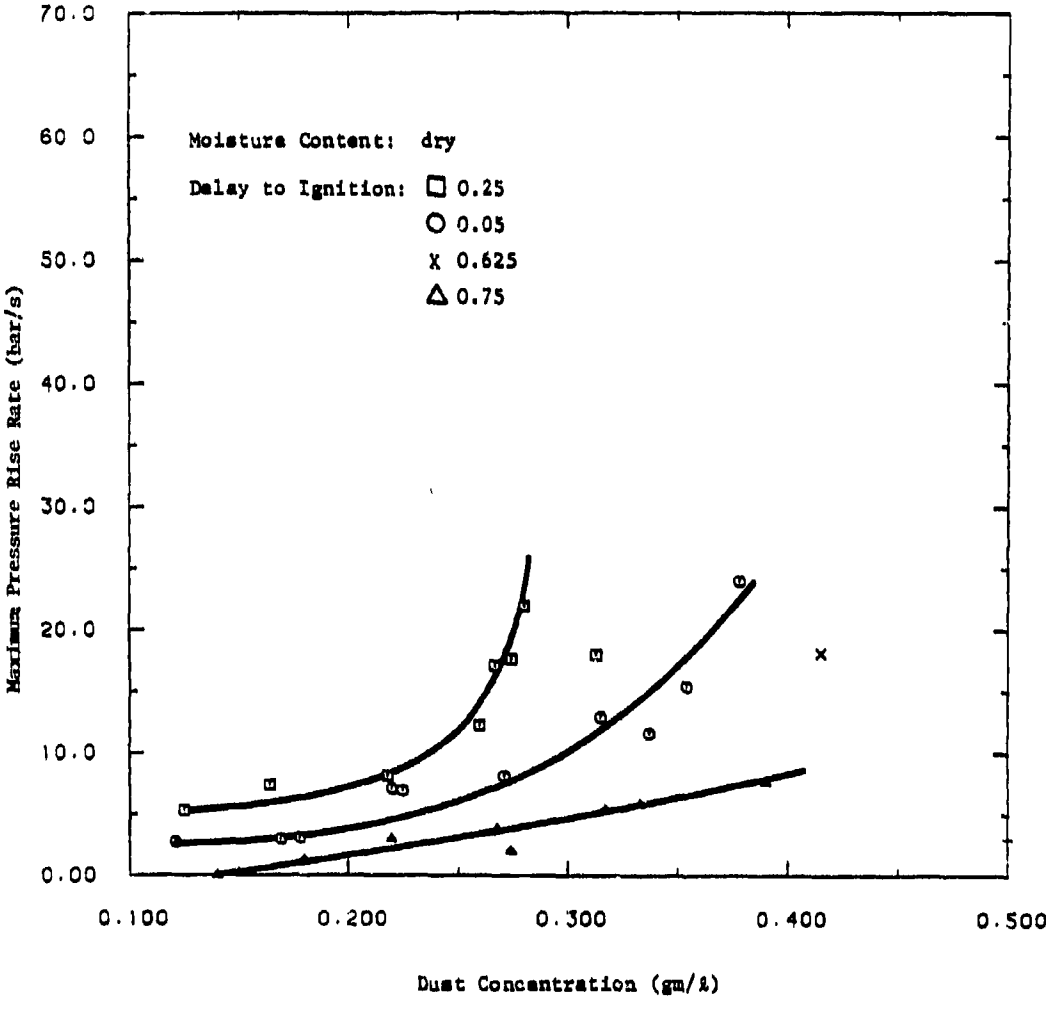

Figure 41b. Pressure Rise Rate in Composition A-5 Explosions Ignited by the BEM in the 40-Liter Chamber

for A-5 the optimum delay time was 0.25 seconds. Figure 41 clearly shows the effect of delay to ignition on the pressure development. Each delay time investigated can be represented by a curve which parallels the other delay time curves.

Test Results in the $1m^3$ Chamber

The $1m^3$ chamber consists of a thick-walled chamber with a length equal to the diameter of 1.08 m (42.5 in.). Thus the interior volume is 1.0 m^3 (35.3 ft^3). The chamber has 2.54 cm (1.0 in.) thick walls and has been pressure tested to 40 bars. This chamber is shown in Figure 42. The dust suspension system is similar in principle to that used in the 40-liter chamber, but is more elaborate. The dust system again consists of an air reservoir, a dust container and a dispersing tube. In practice weighed dust is placed in the dust container and sealed. The air reservoir is pressurized to 6.7 bar and on command the two solenoid valves open simultaneously to initiate dust flow into the chamber. One solenoid valve is between the air reservoir and the dust container, and this valve is used to release the air which is used to drive the dust into the vessel. The other valve is a pneumatic full port (2.54 cm (1.0 in.) diameter) valve located between the dust container and the $1m^3$ vessel. Its function is to seal off the dust vessel just prior to ignition to contain the reaction within the $1m^3$ vessel. The dust dispersion ring seen in Figure 43 has about a hundred small diameter holes strategically located to optimize dust suspension. The dust driven from the dust container flows through dispersion rings and into the dust vessel through these many small nozzles. The dust disbribution throughout the large interior volume chamber was monitored with a video camera in some preliminary experiments and was found to be quite uniform. The ignitor used in these experiments was the same AC arc used in the Hartmann and 40-liter experiments.

Five experiments were conducted in the $1m^3$ chamber with dry Composition B dust. The test data are tabulated in Appendix E along with the 40-liter chamber data. Figure 43 presents the pressure time curves obtained in the four experiments in which reactions were measured. The shape of these traces is similar to the ones presented in Figure 38 (40 liter data, except the time scale is slightly longer because of the larger chamber volume). Figure 44 presents the maximum pressure and pressure rise rate measured in the $1m^3$, 40ℓ and Hartmann tube. These data utilized in this comparison were for explosions of dry Composition B explosive ignited by the AC arc ignitor. The highest pressures were measured in the $1m^3$ vessel, intermediate pressures were obtained in the 40ℓ chamber and the lowest pressures were measured in the Hartmann Bomb. A similar trend was observed for the pressure rise data, except the Hartmann bomb and 40ℓ data are of the same magnitude. These tests indicate that the design of plant facilities and equipment should be based on $1m^3$ chamber results.

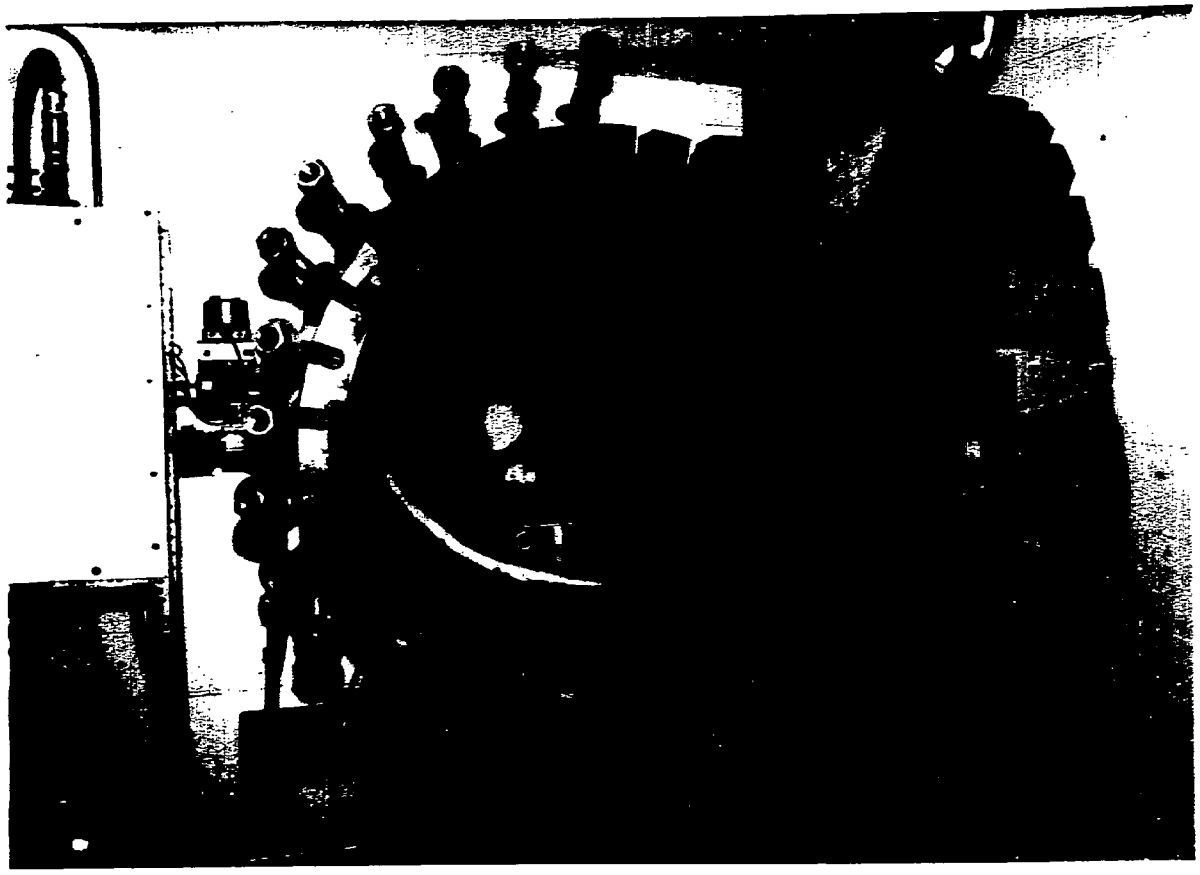

Figure 42. Picture of $1m^3$ Vessel

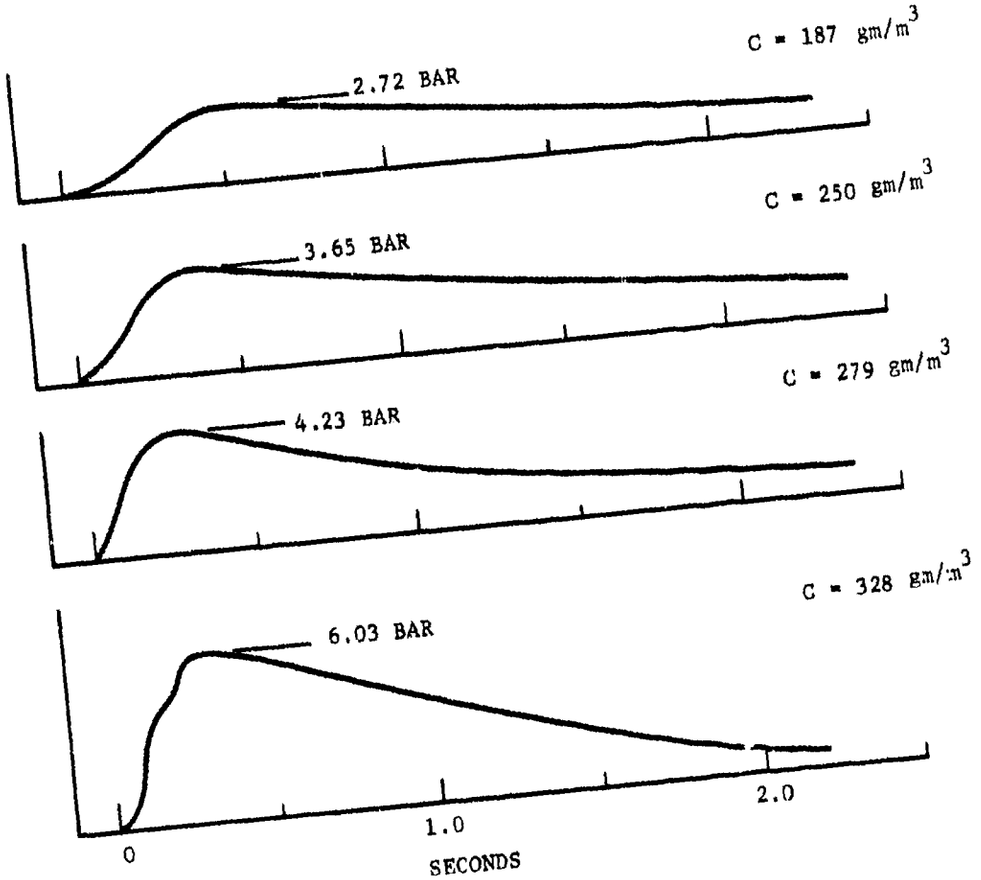

Figure 43. Pressure Wave Forms Obtained in Composition B Explosives Ignited by the AC Arc in the $1m^3$ Vessel

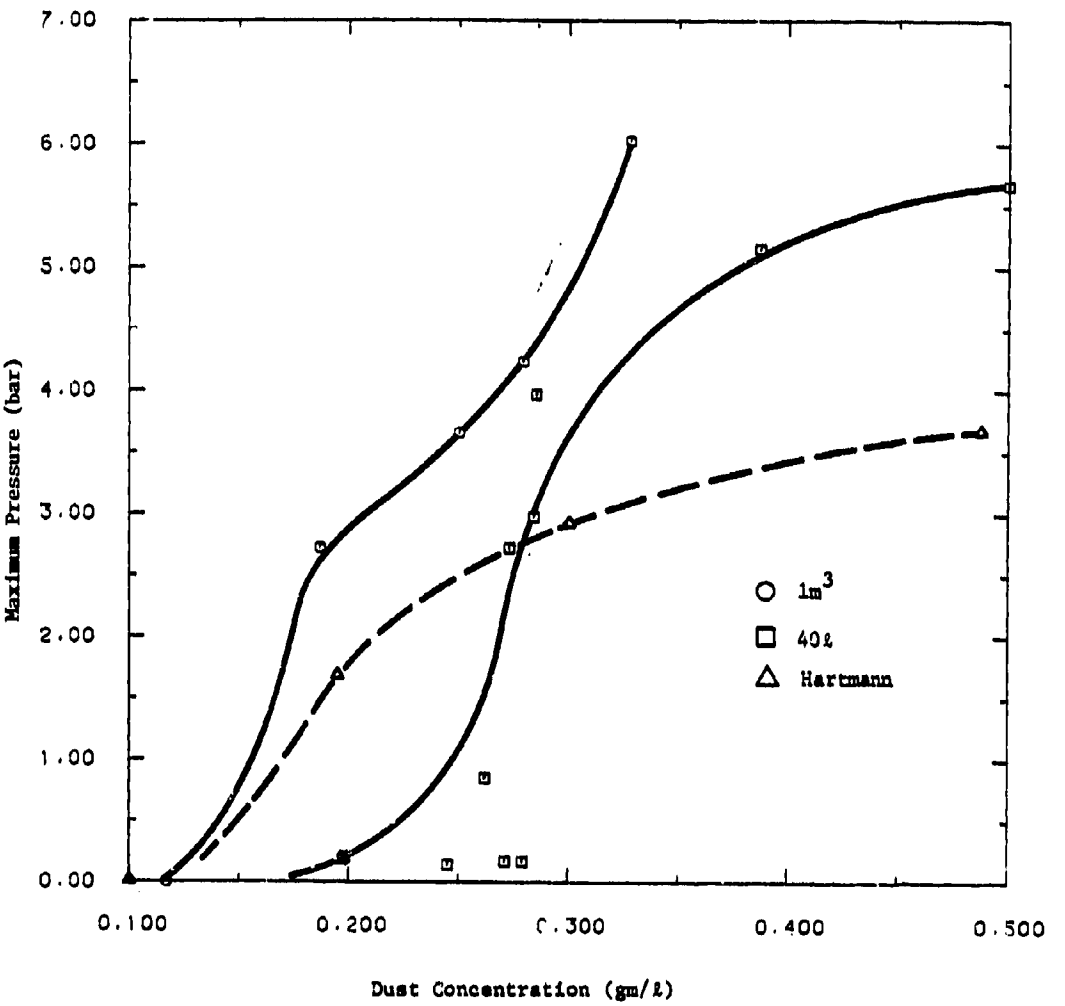

Figure 44a. Comparison of Maximum Pressures Obtained in Composition B Explosives and Vessels of Different Volumes

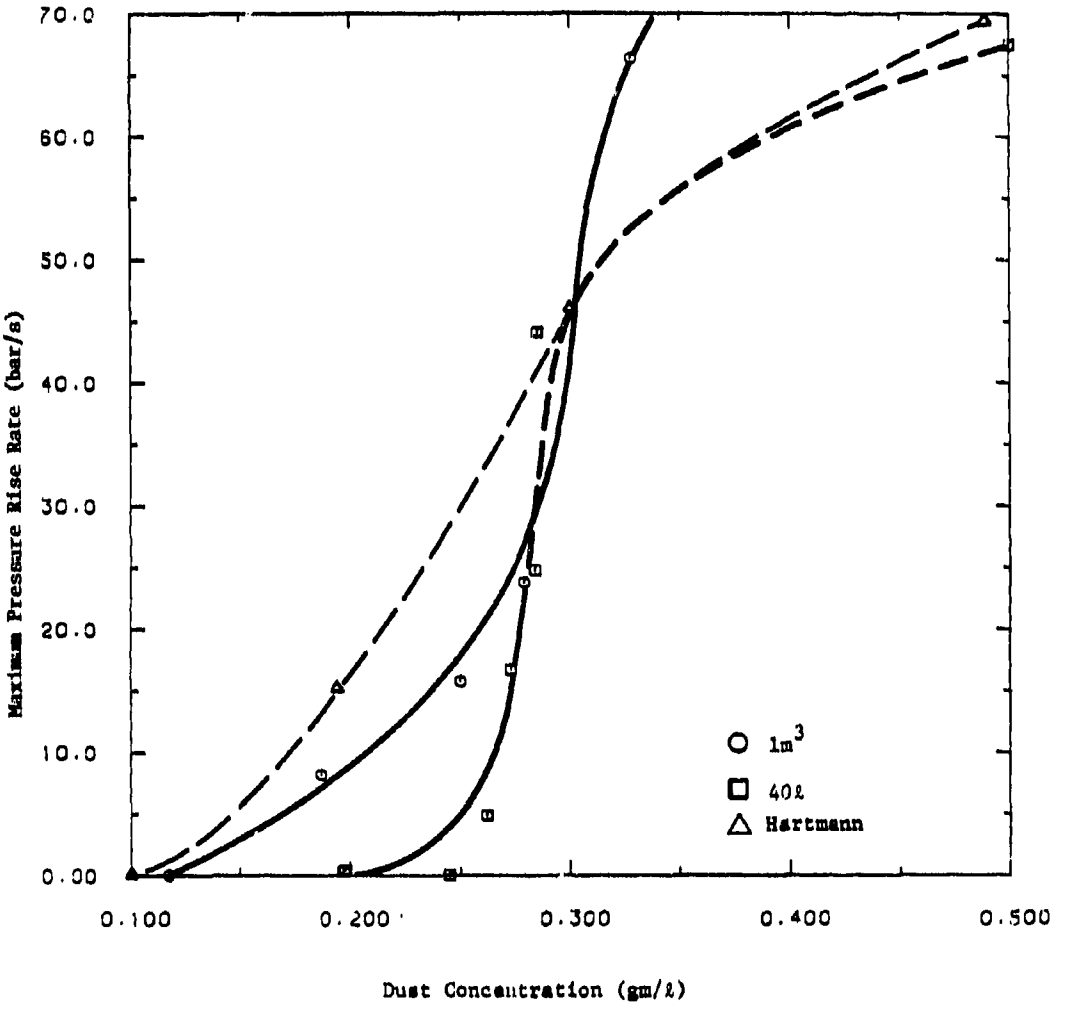

Figure 44b. Comparison of Pressure Rise Rates Obtained in Composition B Explosions in Vessels of Different Volumes

CONCLUSIONS

Based on the work performed the following conclusions are drawn:

Plant Sampling

- Processes involving drilling or facing of explosives generate significantly higher dust concentrations, charge densities and energy levels, than processes involving weighing, pouring, sifting or dropping of explosives.

- Flow velocities in the ducting were too low to achieve a uniform concentration across the ducting. Significantly higher dust concentrations and charge densities were generally measured below the duct centerline. This was also reflected in dust buildups in duct cleanouts and other duct penetrations placed below the duct centerline.

- Minimum explosive concentrations of explosive and pyrotechnic dusts are generally in the range of 40 to 1000 gm/m^3 (0.04 + 0.1 oz/ft^3). The maximum average concentrations measured in the plant sampling were all below this range with the exception of location 5 at Building 1619 at Louisiana AAP.

- Minimum ignition energies are generally in the range of 0.2 to 8.0 J for explosive and pyrotechnic dusts. The energies calculated from the charge density measurements are all very low with the maximum energy level being 700μJ.

- The charge density appears to be roughly proportional to the peak mass flow rate.

Survey of Concentration Equipment Measurement:

- Although several dust concentration sensors on the market show promise for use in Army Ammunition Plants, none appear suitable because:

    1. The range of detectable particle sizes is too narrow, and is biased to smaller particles.

    2. Those instruments using exhaustive techniques do not extract dust at high enough velocities

    3. The sensors are not compact enough to be practical for penetrating the small diameter ducts common in the Ammunition Plants.

    4. The instruments have too narrow a concentration range, biased to low concentrations.

Explosion Tests

- The moisture content of the dust has a significant effect on the pressure generated in a dust explosion. In tests with Composition B dust in the 40 liter vessel, the maximum pressure developed with dry dust was two bars higher than explosions with dust containing 10 percent moisture content. The same effect was noted for pressure rise rate, except the pressure rise rate increases more dramatically for dry dust, especially at high concentrations.

- Relative humidity of the atmosphere also plays an important role in the ignitability and pressure development of a dust explosion. We were not able to ignite the A-5 dust with the electric arc. These tests were conducted during a week with nearly 100 percent humidity. The tests are setup so that the dust is exposed to the atmosphere for about five minutes prior to ignition. This allows sufficient time for the dried dust to absorb moisture from the atmosphere. Thus the particles were harder to ignite both because of the increased moisture content, and because of the tendency of Composition A-5 particles to agglomerate. By contrast, the Composition A-5 in the Hartmann tests performed by Hazards Research was ignited fairly easily in the controlled laboratory atmosphere.

- Composition B, Composition A-5 and TNT are all significant dust explosion hazards. When dispersed into a dust cloud these materials can be ignited by electrical or thermal ignition sources. Once ignited, Composition B and A-5 generates pressure at about the same rate TNT generates pressure at a slower rate.

- Sodium nitrate is not a significant dust explosion hazard. No explosions were produced in any test with this material.

- Composition A-5 is a significant explosion hazard based on its ability to generate and store static electricity for up to 80 seconds low ignition energy and rapid pressure rise rate. (See Appendix D.)

- It was observed that higher explosion severities were obtained in the Hartmann tests using high delivery pressures then when using lower delivery pressures. This is probably due to a greater amount of oxygen at higher pressures and increased turbulence in the apparatus. (See Appendix D.)

- Explosion pressures were the highest for tests in the $1m^3$ vessel, intermediate for the 40ℓ chamber and lowest in the Hartmann bomb.

- Based on these last two observations, the design of plant facilities and equipment should be based on test results in the $1m^3$ vessel. Utilization of peak pressures or pressure rise rates observed in the Hartmann bomb will result in a nonconservative estimate of the full scale pressures.

RECOMMENDATIONS

Although much information is available for explosive and propellant dust explosions in small chambers or volumes, little information which can be extrapolated to full scale problems is available. Thus, the design of new plant facilities or evaluation of the safety of existing facilities which handle explosive and propellant dusts should be based on dust explosion tests conducted in the $1m^3$ chamber.

The explosion properties of explosive and pyrotechnic dust flowing through exhaust ducting should be thoroughly examined in other plants. These tests should investigate electrostatic charge buildup, ignition thresholds and pressure development as a function of the particle size, dust moisture content, flow velocity and dust diameter.

Explosion mitigation concepts should be formulated and tests conducted in a simulated exhaust duct to establish the lower and upper explosive limits for various types of dust.

Based upon the information obtained at Louisiana AAP, additional tests should be conducted to establish the hazard potential of rectangular ducts for use in transporting dust.

It is recommended that Louisiana AAP locate their clean-out ports in top of the ducts to prevent dust accumulations from increasing the potential of a dust explosion.

To improve the Hartman test data reliability a correction function should be established from the cubic meter test results.

Tests with air and bar ionizers to reduce static charges in ducts transporting explosive propellant and pyrotechnic dusts should be investigated in the Longhorn, Lone Star and Louisiana AAP in-process operations to determine their effectiveness.

Additional work efforts arerequired to secure a sensor that can monitor dust concentrations under dynamic flow in two and four inch diameter ducts.

Where possible, moisture should be added to the air stream transporting dusts through ducts as a method to desensitizing ignition by electrostatic charges. Simulated dusttests with controlled moisture additions should be made to establish the degree of desensitizing the dust to explosive ignition by electrostatic charges.

REFERENCES

1. Tranbarger, O., Owen, T.E., "Bulk Carrier Operations Safety Enhancement Project Phase III Final Report - Volume II, Electrostatics Full Scale Measurements and Model Correlations," Report No. MA-RD-920-80087, July 1980.

2. Owen, T. E., "Method and Apparatus for Measuring Electrostatic Charge Density," U.S. Patent No. 4,249,131, Feb 1981.

3. Tranbarger, O., Duff, B.M., Owen, T.E., "Helicopter Model Studies for On-Board Electrostatic Sensor," Report No. AVRADCOM TR-81-D-26, Sept 1981.

4. Petino, G. Jr., Gehring, G. W., Friesenhahn, G. J., Moore, W. T., Lu, P., Roorda, S., Fishburn, B., Slagg, N., Rindner, R.M., and Seals, W. O., "Explosibility of Energetic Material Dusts," Contractor Report No. ARLCD-CR-80042, U. S. Army Research and Development Command, Jan 1981.

5. Thomas Register of American Manufacturers, Thomas Publishing Company, New York, 1980.

6. Guide to Scientific Instruments 1980-1981, published by the American Association for the Advancement of Science, Washington, DC.

7. "New Monitor Detects Explosive Levels of Cloud or Grain Dust," Department of the Interior Press Release, Dec 20, 1981.

8. Petino, G. Jr., and Seals, W. O., "Dust Explosion Sensitivity Test on M-1, M-30 Composition B and HMX, Contractor Report No. ARLCD-CR-79011, U.S. Army Armament Research and Development Command, Jun 1979.

9. Moore, W. T., Lu, P., Roorda, S., Fishburn, B., Slagg, N., "Explosibility of Explosive and Propellant Dusts," Technical Report No. ARLCD-TR-79045, U.S. Army Armament Research and Development Command, Jul 1980.

10. Palmer, K.M., Dust Explosion and Fires, Chapman and Hall, London, 1973.

11. Bartknecht, W., Explosions, Springer-Verlag Berlin, 1981.

12. Field, P., Dust Explosions, Elsevier Scientific Publishing Company, Amsterdam, 1982.

13. "Explosion Characteristics of Agricultural Dust Clouds," H. Enimoto, Proceedings of the International Symposium on Grain Dust Explosions, Sponsored by the Grain Elevator and Processing Society, Kansas City, Missouri, Oct 4-6, 1977, p. 143-170.

REFERENCES

14. "Laboratory Equipment and Test Procedures for Evaluating Explosibility of Dusts," Dorsette, H.G., Jacobson, M., Nagy, J. and Williams, J. P., Bureau of Mines Report of Investigation 5624, 1960.

APPENDIX A

Calculation of Duct Velocity

Calculation of Duct Velocity at the ith Traverse Point

$$V_i = 1096\sqrt{\frac{VP_i}{\rho}} \qquad (1)$$

V_i = Duct velocity at i^{th} traverse point

VP_i = Duct velocity pressure measured by pitot static tube (in. H_2O)

ρ = Density of the gas stream flowing in duct (lb/ft^3)

$$\rho = \frac{MW_{mix}\ P}{R\ T}$$

MW_{mix} = Effect of humidity or moisture in air

$$MW_{mix} = X_H \times 18 + (1-X_H)29 \quad \left(\frac{\text{lbs mix } (H_2O + \text{air})}{\text{lb mole}}\right)$$

X_H = Mole fraction of water in air

X_H is obtained from WB & DB Temperature

For a WB & DB, obtain W_H $\left(\frac{\text{grains moisture}}{\text{lb dry air}}\right)$ from psychometric chart

Then

$$X_H = \frac{\frac{W_H}{126108}}{\frac{W_H}{126108} + .034483}$$

P = Duct static pressure (in. H_2O)

P = 406.9 + p, p = gage pressure (in. H_2O)

R = Universal gas constant 297.22 $\frac{\text{in. } H_2O\ ft^3}{\text{lb mole } °R}$

T = Duct Temperature (°R)

T = (460 + t), t = °F

$$V_i = 18{,}805\sqrt{\frac{VP_i(460 + t°)}{[X_H 18 + 29(1-X_H)][406.9 + p]}}\ \frac{ft}{min}$$

APPENDIX B

- Derivation of Electrostatic Energy Contained in a Dust-Filled Duct
- Electrostatic Instrument Calibration
- Development of Sampling Procedures

Electrostatic Energy Contained in a Dust-Filled Duct

Electrostatic sampling in the field tests was performed in all cases within circular cross-section ducts. For this geometry, the electrostatic field intensity within the duct can be determined from Poisson's equation using the cylindrical coordinate system shown in Figure 1. In this analysis, assume that (a) the space charge density, ρ, contained within the duct is uniform, and (b) the cylinder is sufficiently long that end effects are not factors in the solution. The general form of Poisson's equation in cylindrical coordinates is:

$$\nabla^2\phi = \frac{1}{r}\frac{\partial}{\partial r}\left[r\frac{\partial\phi}{\partial r}\right] + \frac{1}{r^2}\left[\frac{\partial^2\phi}{\partial\phi^2}\right] + \frac{\partial^2\phi}{\partial Z^2} = -\frac{\rho}{\varepsilon} \qquad (1)$$

where:

ϕ = space potential in volts;

ρ = space charge density in coulombs/m^3;

ε = permittivity of medium in farads/m; and

(r,ϕ,Z) = coordinates of point P.

Also from Figure 1,

a = radius of the duct in meters, and

ℓ = length of a finite section of the duct in meters.

With the assumptions mentioned earlier, the last two terms in Equation 1 are zero; thus, Equation 1 can be reduced to the integral form:

$$\int \frac{\partial}{\partial r}\left[r\frac{\partial\phi}{\partial r}\right] dr = -\frac{\rho}{\varepsilon}\int r\,dr \qquad (2)$$

By completing the two step integration process an expression for the space potential can be found:

$$\frac{\partial\phi}{\partial r} = -\frac{\rho}{\varepsilon}\left[\frac{r}{2}\right] + \frac{C_1}{r} \qquad (3)$$

and

$$\phi = -\frac{\rho}{\varepsilon}\left[\frac{r^2}{4}\right] + C_1 \ln r + C_2 \qquad (4)$$

where C_1 and C_2 are integration constants.

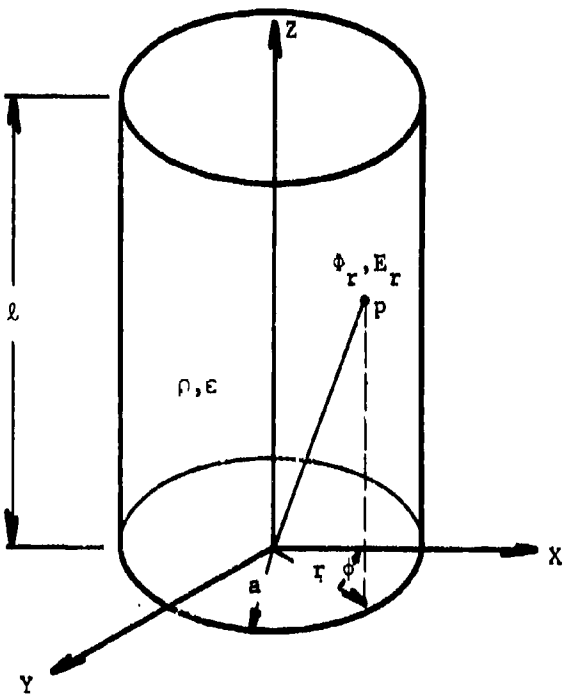

Figure 1. Coordinate System Used in the Solution of Poisson's Equation

Since the electric field intensity is the negative of the rate of change of the space potential, Equation 3 yields:

$$E = -\frac{\partial \phi}{\partial r} = \frac{\rho r}{2\varepsilon} - \frac{C_1}{r} \tag{5}$$

For a duct fabricated of electrically conductive material, the electric field at the center of the duct is zero, as is the space potential on the duct's inner surface:

$$E\ (r = 0) = 0 \tag{6}$$

$$\Phi\ (r = a) = 0 \tag{7}$$

From these boundary conditions, the integration constants can be evaluated as:

$$C_1 = 0 \tag{8}$$

and

$$C_2 = \frac{\rho a^2}{4\varepsilon} \quad \text{volts.} \tag{9}$$

Substituting the above constants into Equations 4 and 5, the complete solutions for the space potential and the electric field are:

$$\phi = \frac{\rho}{4\varepsilon}\left[a^2 - r^2\right] \quad \text{volts} \tag{10}$$

and

$$E = \frac{\partial \phi}{\partial r} = \frac{\rho r}{2\varepsilon} \quad \text{volts/m.} \tag{11}$$

Equations 10 and 11 show that the space potential and the electric field intensity at any point can be determined by measuring only the space charge density. Also the charge density can be determined by measuring the electric field intensity at the inner wall of the duct. Although Equation 10 for the space potential is somewhat limited for the present application, Equation 11 is particularly useful as a means of interrelating the electric field and the charge density within the duct. There are some cases where it is more practical and expedient to measure only charge density instead of the electric field because of the relative size of the electric field sensors and the duct diameter.

Another important consideration is the amount of energy that can be stored by the electric field within the duct. The energy contained within a section of duct with a volume, V, is:

$$W = \frac{1}{2}\,\varepsilon \int_V E^2 dV \quad \text{joules} \tag{12}$$

In terms of the charge density, the energy contained in the electric field for a cylinder of length ℓ, is:

$$W = \frac{\rho^2}{8\varepsilon} \int_0^{\ell} \int_0^{2\pi} \int_0^{a} r^3 dr d\phi z \tag{13}$$

$$= \frac{\pi \rho^2 a^4 \ell}{16\varepsilon} \quad \text{joules.} \tag{14}$$

As the length of the duct becomes infinite, the amount of stored energy becomes infinite. At some critical duct length, the amount of stored energy will exceed the ignition energy of the explosive or pyrotechnic material being transported in the duct. Not all of the energy contained in the duct is ever available at one discharge point. On this basis it is reasonable to limit the length of duct to 10 diameters to establish the energy available for discharge in the design or evaluation of munitions plant ductwork for an ℓ/d ratio of 10, the total energy stored in the duct by a charge density of ρ, and which may be available for discharge is:

$$W = \frac{5\pi \rho^2 a^5}{4\varepsilon} \quad \text{joules.} \tag{15}$$

Electrostatic Instrument Calibration.

The procedures required for calibrating the Monroe Electric Fieldmeter involve the use of a voltage standard and a large parallel plate capacitor. The electric field between the two parallel plates can be calculated with precision as a function of the voltage across the plates. The calculated electric field is then used to determine the calibration constants of the Monroe Electric Fieldmeter.

To calibrate the charge density meter, simultaneous electrostatic measurements must be made using the charge density meter and the electric fieldmeter in a standard geometry configuration in which the electrostatic field conditions are known. By comparing the simultaneous measurements under a uniform space charge condition, the electric fieldmeter was used as a standard for determining the transfer function for the charge density meter. This transfer function accounts for the effects of the medium being measured, the flow conditions through the instrument, and the characteristics of the sampling hose. Calibration

measurements were possible during the sampling performed in the 30.5 cm (12 in.) diameter ducting at Building 1611 at Louisiana AAP. From these tests the instrument transfer function was determined using Equation 11 and the simultaneous measurements of the electric field and the charge density. The transfer function is based on Composition B explosive dust flowing through 30.5 m (100 ft) of 2.54 cm (1 in.) diameter conductive hose at 9.4 ℓ/s (20 cfm):

$$\rho = 36.9 \left[\frac{100}{G}\right] V_o \quad nC/m^3 \ * \tag{16}$$

where:

G = gain of the charge density instrument

and

V_o = output voltage of the charge density instrument.

Since the electric field could not be measured in the small diameter ducts, Equation 16 was used to estimate the charge density at these sample locations.

As part of the preparation for the plant sampling, SwRI designed and fabricated a test fixture which was used to simulate dust flow in a duct. This fixture was built primarily to test our sampling procedures, and to determine if any modifications were required to our sampling equipment. The duct simulator is shown in Figure 2. This fixture consists of three major parts: a) the dust suspension system, b) the duct, and c) the dust collector. The suspension system is shown in Figure 3 and consists of a centrifugal blower to achieve the dust flow, and a screw feeder to meter accurately the amount of dust injected into the flow. The duct consists of 4.6 m (15 feet) of 20.3 cm (8 inch) diameter duct and 4.6 m (15 feet) of 30.5 cm (12 inch) diameter duct. The duct and expansion joints are made from standard galvanized air conditioning ducting. The dust collector, shown in Figure 4 consists of two 55 gallon barrels housing a water spray nozzle for dust removal. In the tests, little or no dust was seen to escape from the top of the barrels, which indicates that the collector was reasonably efficient. The duct simulator in the present configuration is capable of generating airflows of 26.9 m^3/min (950 ft^3/min) and dust concentrations of 4 gm/m^3 (0.004 oz/ft^3).

The duct simulator was used to trouble shoot our air sampling procedures. In these tests we used concrete dust as the test material to avoid explosion problems. During these tests two equipment problems were indicated. The charge density meter accumulated so much dust that its ability to injest and measure the charge density was impaired. The stainless steel wool in the filter was replaced by a series of steel

* $1nC/m^3 = 1.0 \times 10^{-9}$ coulombs

screens to avoid this problem. In a series of trials the optimum number of screens and screen placement was determined. The modified charge density meter performed very well in the actual sampling. The other problem had to do with dust concentration measurement. The dust concentration was to be measured with millipore filter casettes as seen in Figure 5. These casettes were intended for personnel sampling applications, in which low airflow rates are used to transport the dust to the filter. In order to get dust samples representative of duct conditions, the samples must be withdrawn from the duct isokinetically. This means that the sampling velocity must be the same as the velocity in the duct. In the tests that were performed at SwRI, the filter paper in the casettes was damaged at the high flow rates representative of plant conditions. To correct this problem, the standard cassette inlet was enlarged to reduce the impact velocity on the filter paper. The modified casette proved to be satisfactory in the actual sampling.

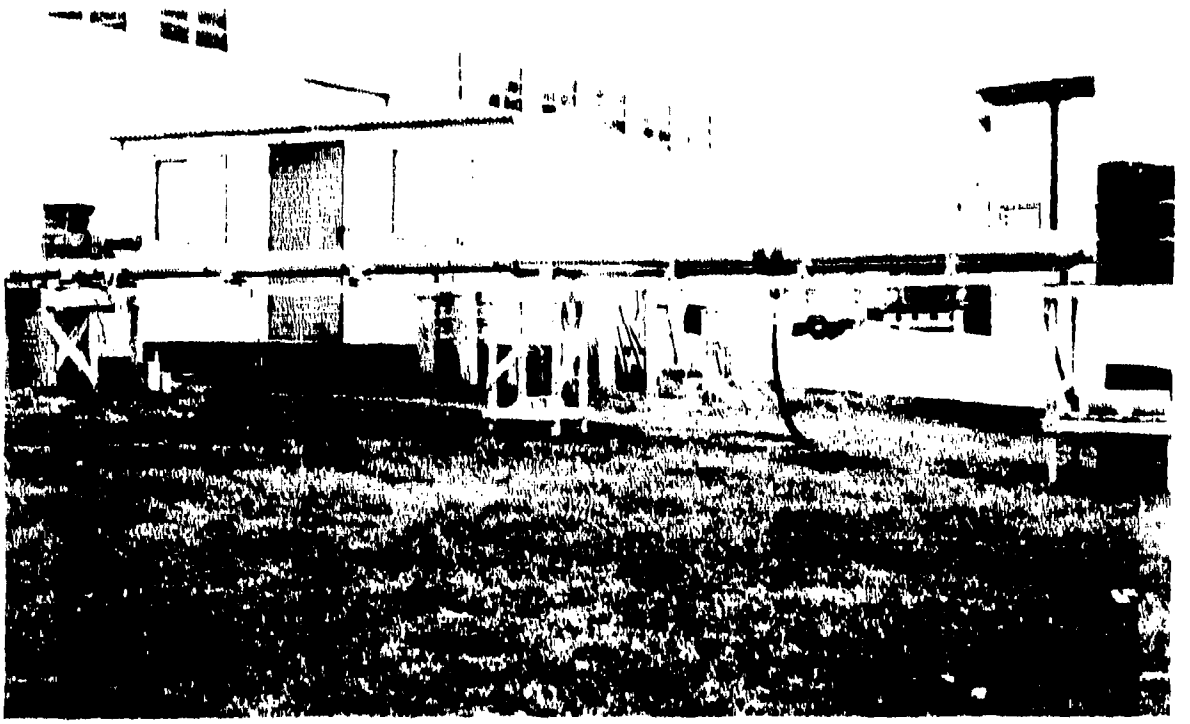

Figure 2. Overview of the Duct Simulator

Figure 3. The Dust Suspension System

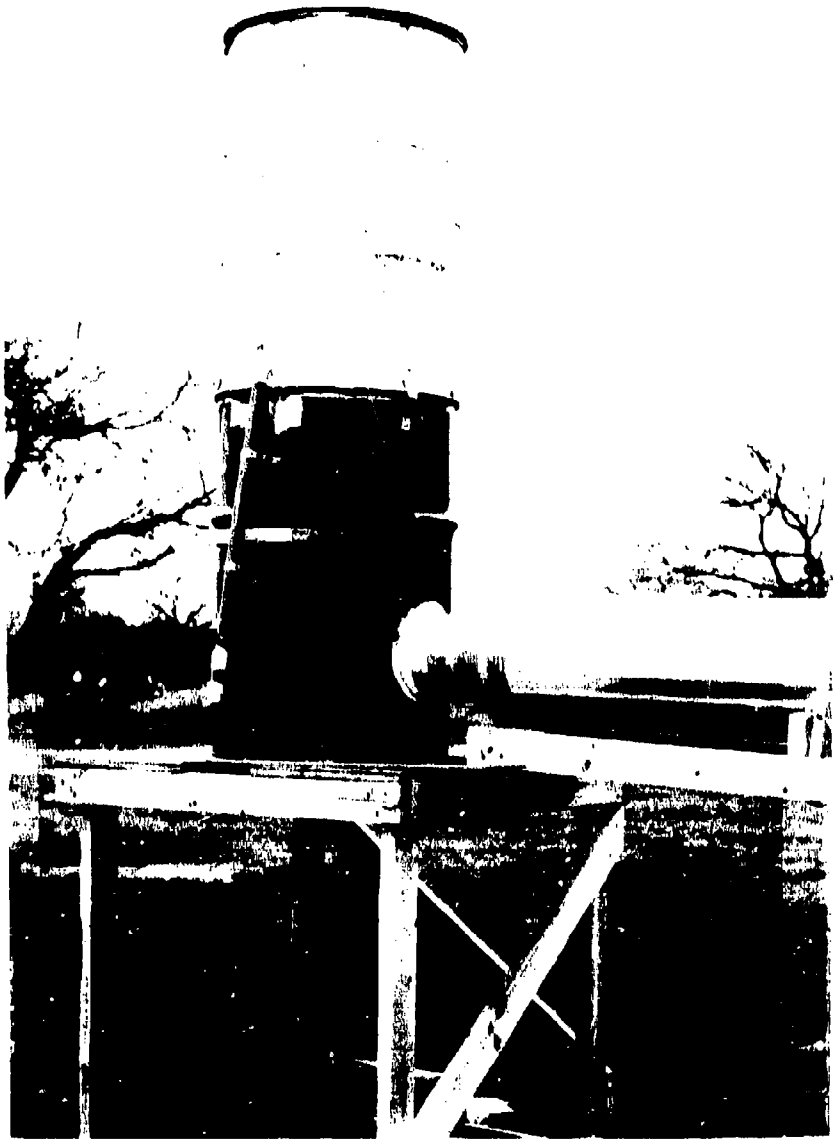

Figure 4. The Wet Dust Collector

Figure 5. Millipore Filter Casette Used to Collect Dust Concentration Data

APPENDIX C

Dust Detection Instrumentation Data Sheets

The specifications of the more promising instruments identified during the instrument survey are presented in the instrument data sheets which are available from the following manufacturers:

Model 200 Aerosol Dust Monitor Model 209 Particle Counter	Net One 154 San Lazaro Avenue Sunnyvale, CA 94086
Model 220 Multi-Range Particle Counter Model 245/507 Particle Counter Model 225/518 Particle Counter Model 245/518 Particle Counter	Royco Instruments, Inc. 141 Jefferson Drive Menlo Park, CA 94025
Model 2710 In-Stock Continuous Particulate Monitor	OMNI-WAVE Electronics Corporation Blackburn Industrial Park Gloucester, MA 01930
Model P-5A Particulate Monitor	Environmental Systems Corporation 1212 Pierce Parkway Knoxville, TN 37921
Model APDA-200E Indoor Dust Monitor	Horiba, Ltd. Miyanohigashi, Kisshoin, Minami-Ku, Kyoto, Japan

APPENDIX D

Dust Explosion Characteristics of Composition A-5, TNT and Sodium Nitrate

by

George Petino

Hazards Research Corporation

(Subcontractor)

This report summarizes the results of a series of experiments performed by Hazards Research Corporation, Rockaway, New Jersey, for Southwest Research Institute of San Antonio, Texas, under Standing Order No. 2383. Contact with Southwest Research Institute was maintained through Mr. Jim Hokanson.

The purposes of this program were to determine the following for Composition A-5, TNT and sodium nitrate:

(1) Minimum Explosive Concentration of a Dust Cloud

(2) Minimum Spark Ignition Energy of a Dust Cloud

(3) Dust Explosion Severity

(4) Volume Resistivity of a Dust Layer

An additional experimental series was performed on sodium nitrate to determine its minimum dust cloud ignition temperature.

MATERIALS

HRC performed a volatiles content analysis on the three samples supplied by the client. Results of this analysis are presented in the following table:

Sample	Volatiles Content
TNT	0.25%
Composition A-5	0.10%
Sodium Nitrate	0.20%

All three materials were impact ground in a mill then dried to 0% volatiles. Only dry material that passed through a 100 mesh sieve was used for the experiments.

DESCRIPTION OF EXPERIMENTS

All experiments were performed at an ambient temperature of 21°C ± 2°C and a relative humidity of 40% ± 5%. In order to evaluate the effects of dust dispersion pressure on the experimental results, two sets of dispersion apparatus were used on this program for the minimum explosive concentration, minimum ignition energy and explosion severity experiments. The apparatus have been designated the "1 bar" and "6.9 bar" dispersion systems respectively. Ordinarily, the standard procedure at HRC is to use the "1 bar system" for the minimum concentration and ignition energy experiments and the "6.9 bar system" for the explosion severity experiments. The differences between these two systems are detailed in the tasks that follow.

Task 1. Minimum Explosive Concentration of a Dust Cloud

The minimum explosive concentration or the lower explosive limit of a dust sample is determined in the Hartmann apparatus. A weighed amount of dust is spread in a thin layer in the dispersion cup. The top of the Hartmann tube (Lucite) is covered with a filter paper diaphragm held in place by a locking ring. A 0.16 cm hole is made in the center of the filter paper to prevent pressure build-up in the tube from the dispersing air and the tungsten electrodes are adjusted to a gap length of 0.48 cm. The dust cloud is formed in the Lucite tube by releasing air from a 1.31

liter reservoir through the full-port solenoid valve; optimum air pressure is 1 bar. This combination of the 1.31 liter air reservoir and 1 bar air pressure is the "1 bar system".

Following ignition of the dust, sufficient pressure must develop to burst the filter paper diaphragm; appearance of flame in the tube is not considered propagation. The pressure required to burst the paper diaphragm is about 0.2 bar, depending on the rate of pressure rise. If propagation occurs for a given weight of dust, the weight is reduced by a five-milligram increment and another trial made until a quantity is obtained which fails to propagate flame in any of four successive trials. The lowest weight at which flame propagates is used in calculating the minimum concentration. Tests are made with the electrodes 10 cm from the bottom of the tube.

Task 2. Minimum Spark Ignition Energy of a Dust Cloud

The minimum electrical energy required to ignite a dust cloud is determined in the Hartmann apparatus. It consists of a vertically mounted, seven cm diameter combustion tube 30.5 cm long and auxiliary equipment for producing the dust dispersion. The tube, made of Lucite, is attached to a cylindrical metal base (dispersion cup) by four brass bolts. The top of the tube is covered with a filter paper diaphragm held in place by a locking ring. The total free volume of

the test chamber is 1.23 liters. Dispersion is accomplished by a single blast of air from a 1.31 liter reservoir. Air pressure in the reservoir is 1 bar. The quantity of dust dispersed is five times the minimum explosive concentration or a maximum of 2 gm/liter. Concentrations greater than 2 gm/liter cannot be dispersed in this apparatus.

The igniting spark passes between two pointed, 20 gauge tungsten electrodes that are separated by a 0.64 cm air gap. These electrodes are mounted 10 cm above the base of the tube. Electrical energy for the spark ignition is obtained from the discharge of condensers at 100 or 400 volts. The bank of ten condensers has a capacitance range of 2 to 100 microfarads. This combination of voltage and capacitance allows energy levels to be varied from 50 to 500 millijoules in 50 millijoule increments (at 100 volts) and from 800 to 8000 millijoules in 800 millijoule increments (at 400 volts).

The energy of the spark (in joules) is calculated as $0.5\ CV^2$ where C is the capacitance of the condensers in farads, and V is the charging potential in volts. Dust cloud minimum ignition energy is the least amount of energy required to produce flame propagation of 10 cm or longer in the tube. Four trials are made at each condenser setting; however, if the dust ignites in initial trials, lower energy is tried until a minimum is obtained.

Task 3. Dust Explosion Severity Determination

Dust explosion severity determinations are performed using the Hartmann Dust Explosibility Bomb designed at the U. S. Bureau of Mines (Bruceton Station). The system consists of a 1.23 liter stainless steel cylindrical chamber, 30 cm. high, mounted on a precision-machined base, which acts as the sample holder. A burst of air from a 0.049 liter reservoir at 6.9 bar is injected into the base to disperse the sample uniformly throughout the chamber. This combination of the 0.049 liter air reservoir and 6.9 bar air pressure is the "6.9 bar system".

The quantity of air used to disperse the dust brings the pressure in the chamber to effectively 0.2 bar. When the sample is dispersed, an induction arc from an 11 kilovolt transformer is struck between tungsten electrodes 10 cm. from the base. If ignition occurs, maximum pressure and rate of pressure rise are monitored on high speed recording equipment.

Experiments are performed as a function of dust concentration at levels of 0.1, 0.2, 0.5, 1.0 and 2.0 gm/liter so that the concentration for maximum burning rate is determined.

Explosion severity is defined as follows:

$$\text{Explosion Severity} = \frac{\text{Max.Press. x Max.Press.Rise Rate (Sample)}}{\text{Max.Press. x Max.Press.Rise Rate (Pittsburgh Coal)}}$$

Task 4. Volume Resistivity of Dust Layer

The volume resistivity is measured in an apparatus which contains three basic components: (1) a high voltage (D.C.) power supply, (2) a test cell designed specifically for particulate materials and (3) an electrometer capable of measuring currents of the order of 10^{-14} amperes. Figure 1 is a schematic of the test apparatus.

In performing an experiment, the current through the standard sample geometry is measured as a function of applied voltage. The volume resistivity is given by the following relationship:

$$\rho = \frac{EA}{IL} \text{ ohm-cm}$$

where:

ρ = Volume Resistivity, ohm-cm

E = Applied Potential, volts

A = Cross-sectional area of disc electrode, sq.cm.

I = Current measured at the electrometer, amperes

L = Thickness of sample layer between electrodes, cm.

For the test apparatus used on this program, the following values are constant in the above equation:

E = 1,000 volts A = 5.06 sq.cm. L = 0.50 cm.

Ten measurements are made at each test condition. Volume resistivity is calculated for each reading and the results of the ten readings are averaged.

Task 5. Minimum Ignition Temperature of a Dust Cloud

The minimum ignition temperature for a moving dust cloud is determined using the Godbert-Greenwald Furnace developed at the U.S. Bureau of Mines (Bruceton Station). The furnace consists of a thermostatically controlled vertical alundum core (23 cm. long by 3.7 cm. i.d.) wound with heating wire so as to provide uniform temperature throughout its length. The top of the furnace is connected by glass tubing through a brass dust chamber to a 500 cc air reservoir at 0.2 bar. A burst of air from the reservoir propels the sample (0.10 gm) downward through the furnace. Appearance of flame or sparks at the bottom of the furnace is the criterion for a positive trial. The ignition temperature is the minimum furnace temperature at which a positive result is obtained in one or more trials in a group of four. The increment of temperature variation is 5°C; the highest temperature attainable in the furnace is 800°C.

EXPERIMENTAL RESULTS

The results of this test program are summarized in Tables 1 through 10. Plots of maximum pressure and maximum rate of pressure rise as a function of concentration are presented in Figures 2 through 5. Pressure vs. time traces of the oscillograph records are presented in Figures 6 through 9.

DISCUSSION OF RESULTS

Minimum Explosive Concentration

Tables 1 and 2 present the results of the minimum concentration for explosion tests. It is seen that, in the "1 bar system", the TNT ignited at the lowest value 0.075 gm/l, Composition A-5 ignited at 0.120 gm/l and sodium nitrate did not explode.

Results presented in Table 2 for the "6.9 bar system" reveal that both materials ignited at higher concentrations using the high pressure dispersion system. TNT ignited at 0.110 gm/l and Composition A-5 ignited at 0.135 gm/l. In both dispersion systems, TNT ignited at a lower concentration than the Composition A-5.

It is worthwhile noting that most combustible dusts ignite at about a 0.05 gm/l concentration. A man standing in a room containing a uniformly dispersed dust cloud at a 0.05 gm/l concentration will not be able to see his outstretched hand.

Minimum Spark Ignition Energy for Dust Clouds

Minimum spark ignition energy results for both dispersion systems are presented in Tables 3 and 4. In Table 3, it is noted that TNT ignited at 0.20 joules while Composition A-7 ignited at 0.15 joules. Sodium nitrate did not ignite at the 8 joules maximum capacity of the test apparatus. There was no change in results for the TNT in the "6.9 bar system",

however, the Composition A-7 ignited at a higher value (0.30 joules) in this system.

The significance of this data is that it is possible for ungrounded processing equipment to store and discharge the energy levels that have been shown to ignite the TNT and Composition A-5. Therefore, electrical grounding and bonding of all conductive elements that contact these materials is strongly recommended. In addition, non-conductive materials should not be used in systems handling TNT or Composition A-5 powder.

Explosion Severity

Results of the explosion severity experiments are presented in Tables 5 and 6. Calculated values of explosion severity are found in Table 9.

The relative explosion hazard of a dust is classified by the Bureau of Mines by ratings of weak, moderate, strong or severe. The ratings are correlated with the empirical index as follows:

Relative Explosion Hazard Rating	Explosion Severity
Weak	<0.5
Moderate	0.5 - 1.0
Strong	1.0 - 2.0
Severe	>2.0

Based on the index given above, it is seen that TNT and Composition A-5 both qualify for a "severe" explosion severity rating regardless of the dispersion system used. Sodium nitrate did not propagate a dust explosion in the Hartmann apparatus.

Upon studying the results presented in Table 9, it is seen that the dispersion system has a significant effect on the explosion severity. It is clear that the "6.9 bar system" results in a much more energetic dust explosion. TNT explosion severity values were 4.4 and 10.8 for the "1 bar system" and "6.9 bar systems" respectively. Similarly, Composition A-5 values were 21.4 and 39.2.

Electrostatic Charge Leakage Rate and Volume Resistivity

The charge leakage rate from a sample is dependent solely on the parameter known as relaxation time, t_r. Relaxation time depends on the volume resistivity (ρ), and the dielectric constant (K) of the material. Mathematically,

$$t_r = 8.85 \times 10^{-14} K \rho$$

Where:

ρ = volume resistivity, ohm-cm

K = 4.5, the average dielectric constant of TNT and Composition A-5

In general, the value of the relaxation time is determined by what leakage paths are available to the charge generated. The leakage path through air depends on the presence of ions

and the possible presence of ionizing material. The leakage path through powders involves the resistivity of the powders, which is dependent on humidity and packing. For dust layers up to 1 inch thick, the relaxation times are calculated using the above relationship.

The measured volume resistivities and the calculated relaxation times for the three materials are presented in Table 7. It is seen that the Composition A-5 sample will hold an electrostatic charge the longest (83.6 sec.). The TNT sample is the second best charge retainer (0.16 sec.) followed by sodium nitrate (0.14 sec.).

It should be noted that the general rule of thumb for evaluating electrostatic charge accumulation hazards is to consider relaxation times of less than one second to be insignificant. Hence, the TNT and sodium nitrate samples would not be considered to be significant static charge generating hazards in an electrically grounded process system. However, Composition A-5 is capable of generating and storing electrostatic charges for a significant period of time.

Minimum Ignition Temperature of Dust Clouds

Results presented in Table 8 reveal that sodium nitrate could not be ignited as a dispersed dust cloud when passed through a 735^{o}C thermal environment.

CONCLUSIONS

Results of the experiments performed on this program are summarized in Table 10. These results reveal that TNT and Composition A-5 can be ignited as a dispersed cloud using an electrical ignition source. Sodium nitrate does not propagate a dust explosion when subjected to an 11,000 volt electrical discharge at dust concentrations up to 2.0 gm/l. Once ignited, the Composition A-5 sample generates pressure at a faster rate than TNT. Composition A-5 and TNT both qualify for a "severe" explosion severity rating.

Composition A-5 is the more hazardous of the two explosives based on its ability to generate and store static electricity, low minimum ignition energy and extremely rapid rate of pressure rise. TNT is not capable of storing electrostatic charges for durations greater than 1.0 second, however, it is sensitive to ESD ignition. Sodium nitrate is not a dust explosion hazard since no ignitions were observed in both the thermal and electrical ignition experiments.

The effect of dispersion systems on results is very significant. Lower minimum concentrations and ignition energies result from using the "1 bar system". Higher explosion severities result from the "6.9 bar system". It is beyond the scope of this report to explain this phenomena. However, it is clear that as dispersed dust cloud concentrations of Composition A-5 exceed 1.00 gm/l, it is possible to have a "detonation" instead of an "explosion".

HAZARDS RESEARCH CORPORATION

Table 1. Minimum explosive concentration for dust clouds three materials-1 bar system

TNT

Concentration (gm/l)	Results +indicates combustion -indicates no combustion
0.100	+
0.090	+
0.085	+
0.085	+
0.080	+
0.075	+
0.075	+
0.070	-
0.070	-
0.070	-
0.070	-

The minimum concentration required for combustion is 0.075 gm/l.

Composition A-5

0.200	+
0.150	+
0.140	+
0.135	+
0.130	+
0.125	+
0.120	+
0.115	-
0.115	-
0.115	-
0.115	-

The minimum concentration rquired for combustion is 0.120 gm/l.

HAZARDS RESEARCH CORPORATION

Table 1. Minimum explosive concentration for dust clouds of three materials-1 bar system (cont.)

Sodium nitrate

Concentration (gm/l)	Results +indicates combustion -indicates no combustion
2.00	-
2.00	-
2.00	-
1.50	-
1.25	-
1.00	-
0.50	-
0.20	-
0.10	-
0.05	-

The sample could not be ignited in the dispersed dust cloud phase at concentrations up to 2.00 gm/l. The test apparatus is not capable of dispersing concentrations of this material above this value.

HAZARDS RESEARCH CORPORATION

Table 2. Minimum explosive concentration for dust clouds of three materials-6.9 bar system

TNT

Concentration (gm/l)	Results +indicates combustion -indicates no combustion
0.150	+
0.135	+
0.130	+
0.125	+
0.120	+
0.115	+
0.110	+
0.105	-
0.105	-
0.105	-
0.105	-

The minimum concentration required for combustion is 0.110 gm/l.

Composition A-5

0.150	+
0.145	+
0.140	+
0.135	+
0.130	-
0.130	-
0.130	-
0.130	-

The minimum concentration required for combustion is 0.135 gm/l.

Table 3. Minimum spark ignition energy for dust clouds of three materials-1 bar system

TNT

Energy (joules)	Results + indicates combustion - indicates no combustion
0.50	+
0.40	+
0.35	+
0.30	+
0.25	+
0.20	+
0.20	+
0.15	-
0.15	-
0.15	-
0.15	-

The minimum spark ignition energy for this sample is 0.20 joules at a 0.70 gm/l dust concentration.

Composition A-5

0.50	+
0.30	+
0.25	+
0.20	+
0.15	+
0.15	+
0.10	-
0.10	-
0.10	-
0.10	-

The minimum spark ignition energy for this sample is 0.15 joules at a 0.60 gm/l dust concentration.

Table 3. Minimum spark ignition energy for dust clouds of three materials-1 bar system (cont.)

Sodium nitrate

Energy (joules)	Results + indicates combustion - indicates no combustion
8.00	-
8.00	-
8.00	-
8.00	-
8.00	-
8.00	-
8.00	-
8.00	-
8.00	-
8.00	-

The minimum spark ignition energy for this sample is greater than the 8.00 joule maximum capacity of the test apparatus. All trials were performed at a 1.0 gm/l dust cloud concentration.

Table 4. Minimum spark ignition energy for dust clouds of three materials-6.9 bar system

TNT

Energy (joules)	Results + indicates combustion - indicates no combustion
0.50	+
0.45	+
0.35	+
0.35	+
0.25	+
0.20	+
0.20	+
0.15	-
0.15	-
0.15	-
0.15	-

The minimum spark ignition energy for this sample is 0.20 joules at a 0.5 gm/l dust concentration.

Composition A-5

0.50	+
0.40	+
0.35	+
0.30	+
0.30	+
0.25	-
0.25	-
0.25	-
0.25	-

The minimum spark ignition energy for this sample is 0.30 joules at a 0.5 gm/l dust concentration.

Table 5. Maximum pressure and rate of pressure rise in explosions of dust clouds of three materials-1 bar system

Concentration (gm/l)	Maximum rise rate (bar/sec.)	Maximum pressure (bar)
TNT		
0.10	59	1.6
0.20	197	2.8
0.50	353	4.6
0.75	579	5.4
1.00	700	5.7
Composition A-5		
0.10	0	0
0.20	211	2.9
0.50	1145	6.3
0.75	1421	9.4
1.00	1628	11.9

HAZARDS RESEARCH CORPORATION

Table 6. Minimum pressure and rate of pressure rise in explosions of dust clouds of three materials-6.9 bar system

Concentration (gm/l)	Maximum rise rate (bar/sec.)	Maximum pressure (bar)
TNT		
0.10	0	0
0.20	378	3.7
0.50	938	6.1
0.75	1214	7.2
1.00	1297	7.6
Composition A-5		
0.10	0	0
0.20	308	3.2
0.50	1448	7.3
0.75	2317	9.4
1.00	2759	12.9
Sodium nitrate		
0.10	0	0
0.20	0	0
0.50	0	0
1.00	0	0
2.00	0	0

This material could not be ignited as a dispersed dust cloud at concentrations up to 2.00 gm/l.

Table 7. Volume resistivity and relaxation time for three materials

Sample	Volume resistivity (ohm-cm)	Relaxation time* (sec.)	Environment	
			Temp. (°C)	Rel. hum. (%)
TNT	$3.9 \times 10^{+11}$	0.16	21	45
Composition A-5	$2.1 \times 10^{+14}$	83.60	25	39
Sodium nitrate	$3.4 \times 10^{+11}$	0.14	25	39

*calculated

Table 8. Minimum ignition temperature of dust clouds of sodium nitrate

Temperature (°C)	Results +indicates combustion -indicates no combustion
735	-
735	-
735	-
730	-
730	-
730	-
730	-
725	-
700	-
700	-
600	-
400	-

The minimum ignition temperature for dust clouds of the sample is greater than 735°C. This material could not be ignited at temperatures up to 735°C in the Godbert-Greenwald furnace.

Table 9. Results of explosion severity experiments

Sample	Dispersion system	Max. explosion pressure (bar)	Max.rate of pressure rise (bar/sec)	Explosion severity (E.S.)
TNT	1 bar	5.7	700	4.4
	6.9 bar	7.6	1297	10.8
Composition A-5	1 bar	11.9	1628	21.4
	6.9 bar	12.9	2759	39.2
Sodium nitrate	6.9 bar	0	0	-
Pitts. coal	6.9 bar	5.7	159	1.0

Table 10. Summary of results

Sample	Min. ign. energy		Min. conc.for expl.		Max. press.rise rate		Maximum Pressure		Explosion Severity		Vol. res.
	1 bar (joules)	6.9 bar (joules)	1 bar (gm/l)	6.9 bar (gm/l)	1 bar (bar/sec)	6.9 bar (bar/sec)	1 bar (bar)	6.9 bar (bar)	1 bar	6.9 bar	(ohm-cm)
TNT	0.20	0.20	0.075	0.110	700	1297	5.7	7.6	4.4	10.8	$3.9 \times 10^{+11}$
Comp. A-5	0.15	0.30	0.120	0.135	1628	2759	11.9	12.9	21.4	39.2	$2.1 \times 10^{+14}$
Sodium nitrate	>8.00	-	*	-	-	0	-	0	-	-	$3.4 \times 10^{+11}$

*This material could not be ignited at dust cloud concentrations up to 2.00 gm/l.

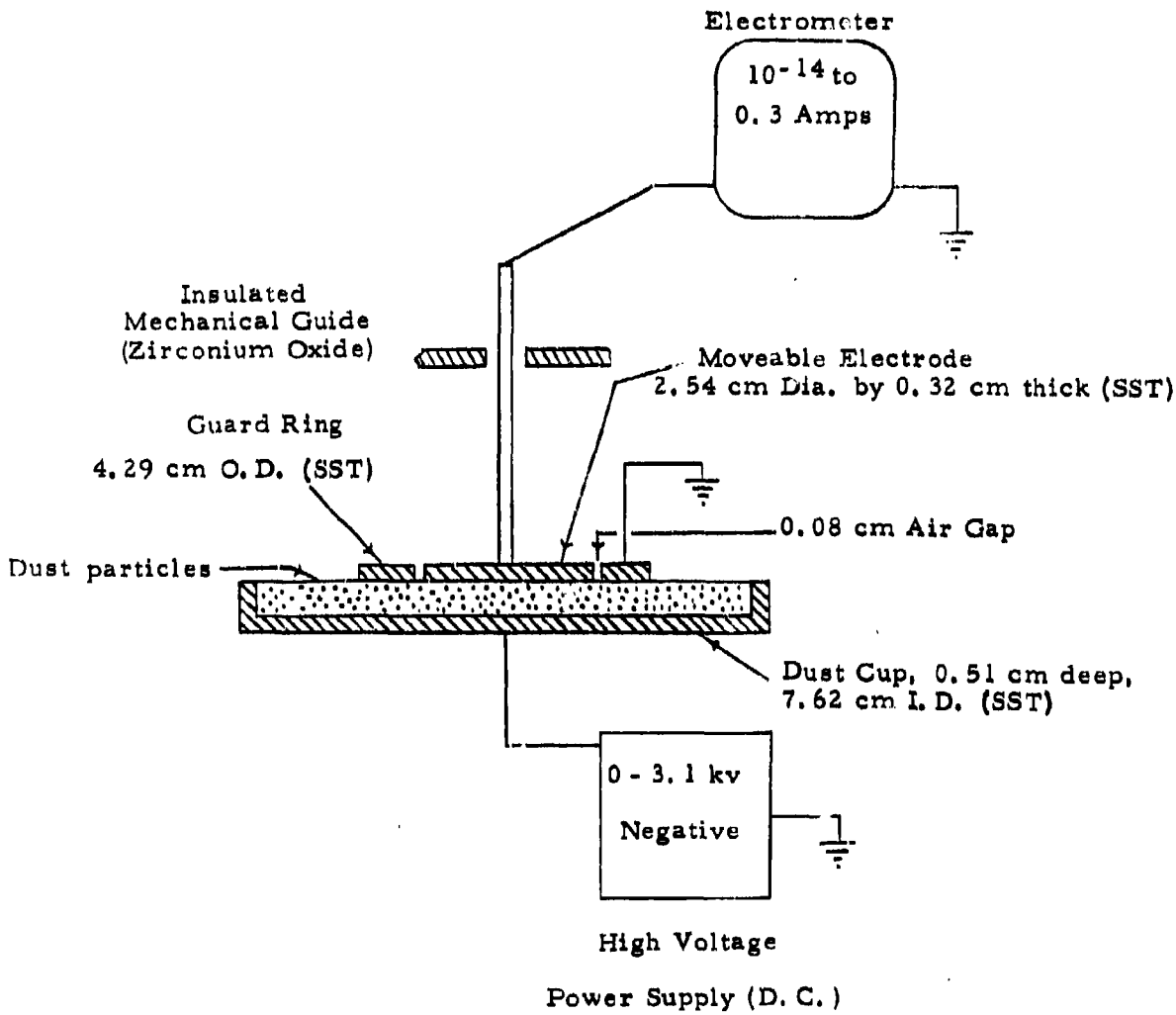

Figure 1. Volume resistivity measurement apparatus

Figure 2. Dust explosion pressure and rate of pressure rise for TNT - 1 bar system

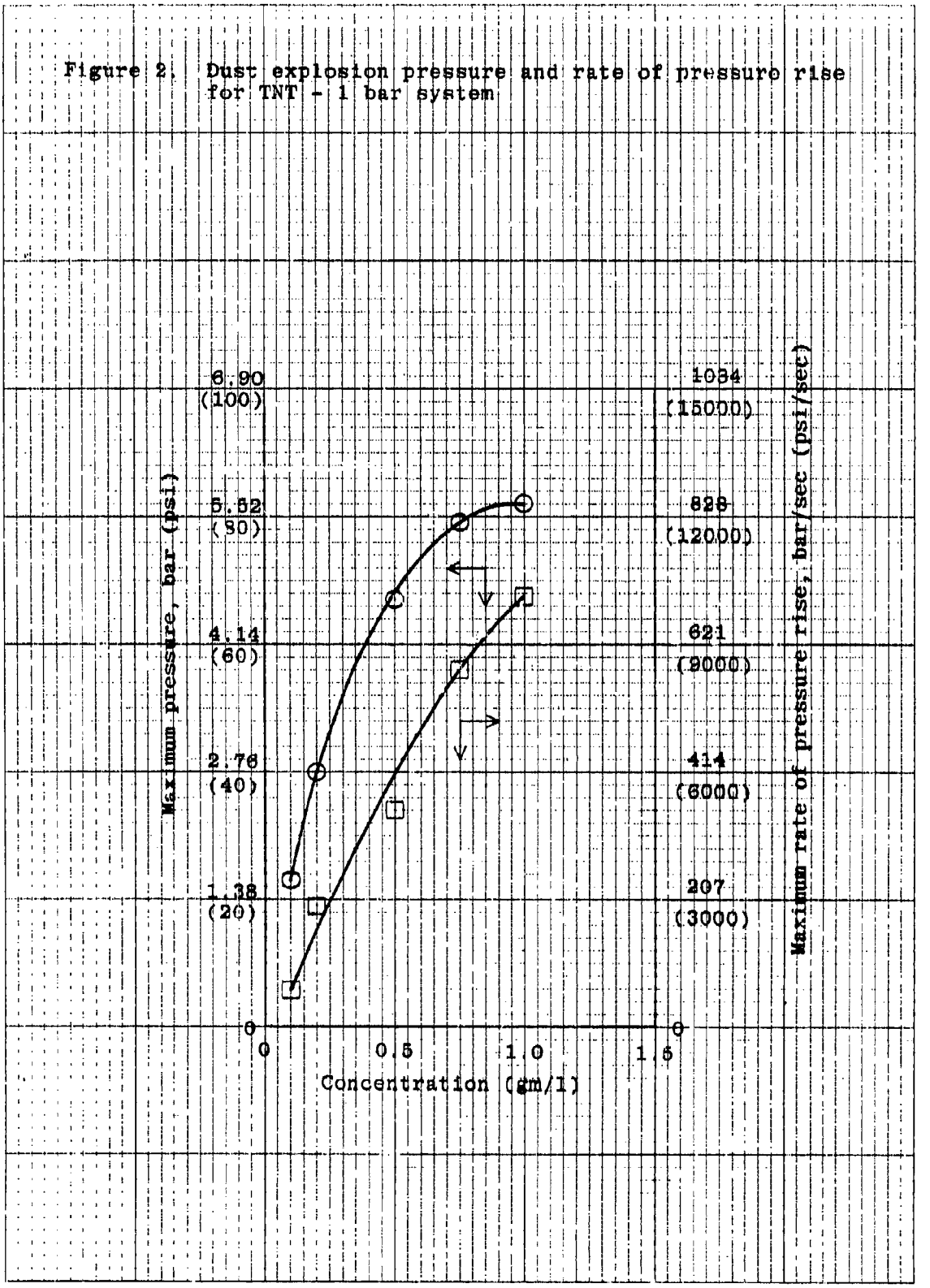

Figure 3. Dust explosion pressure and rate of pressure rise for Composition A-5-1 bar system

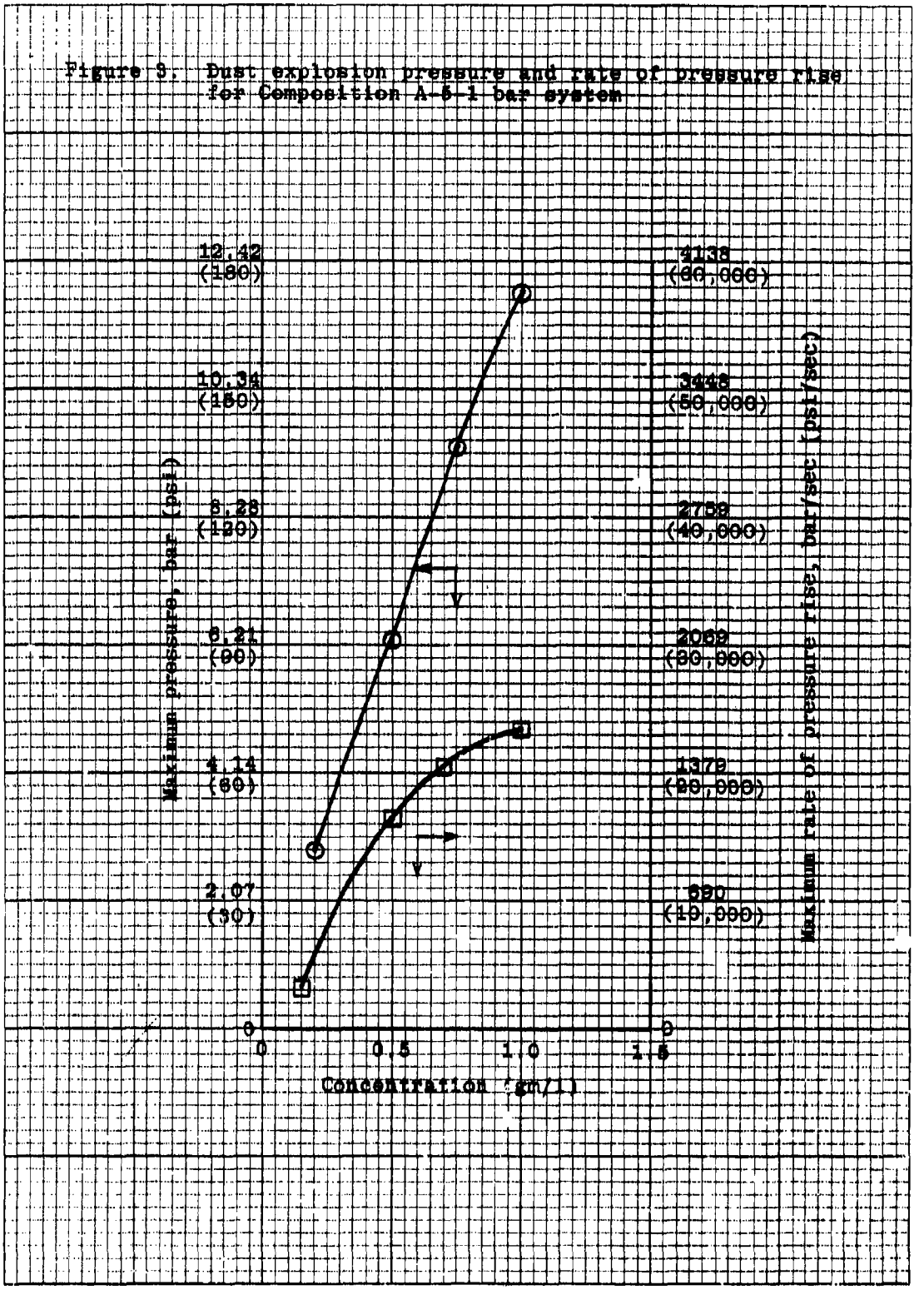

Figure 4. Dust explosion pressure and rate of pressure rise for TNT-6.9 bar system

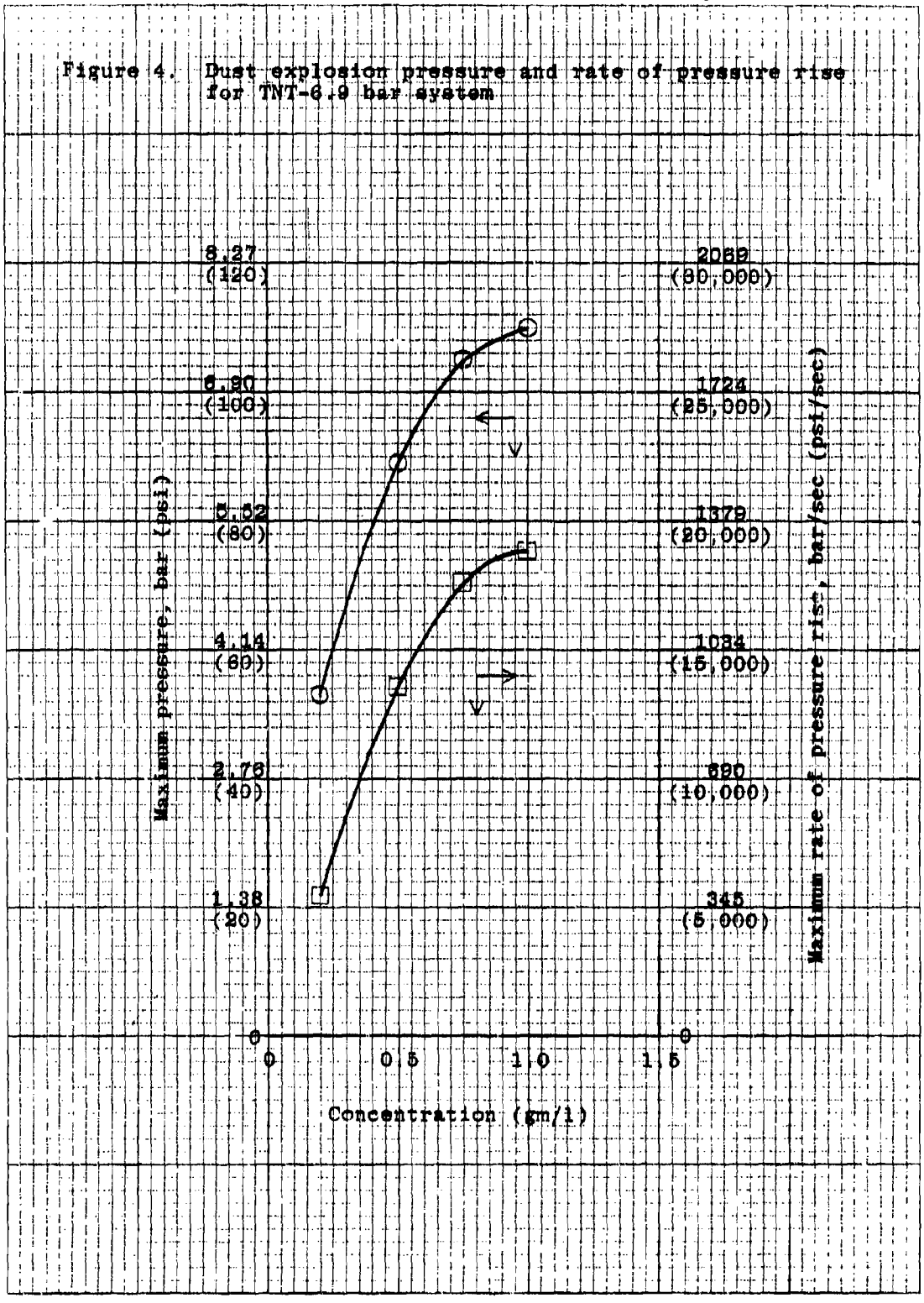

Figure 5. Dust explosion pressure and rate of pressure rise for Composition A-5-6.9 bar system

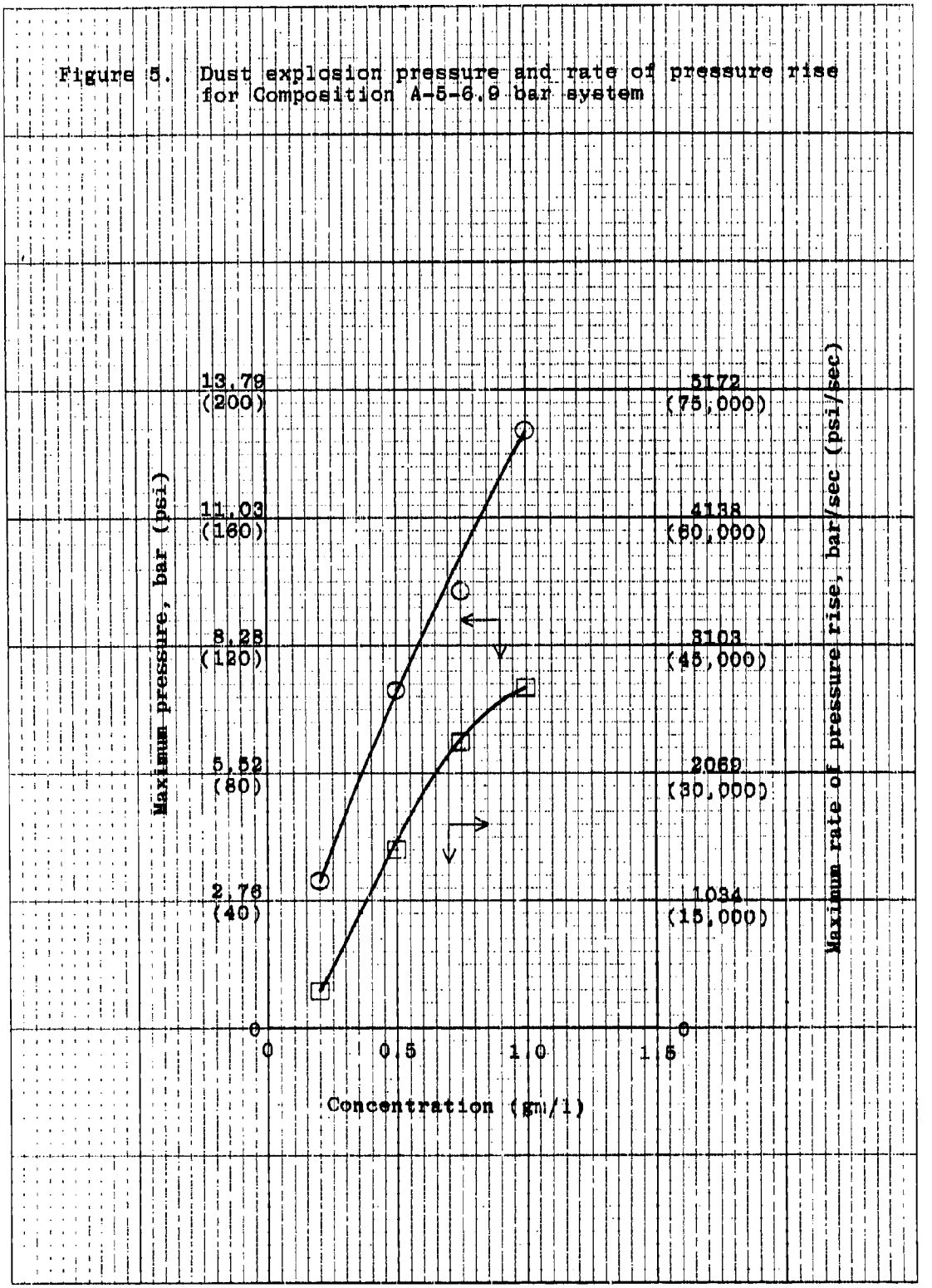

Figure 6. Pressure vs. time traces for various concentrations of TNT-1 bar system

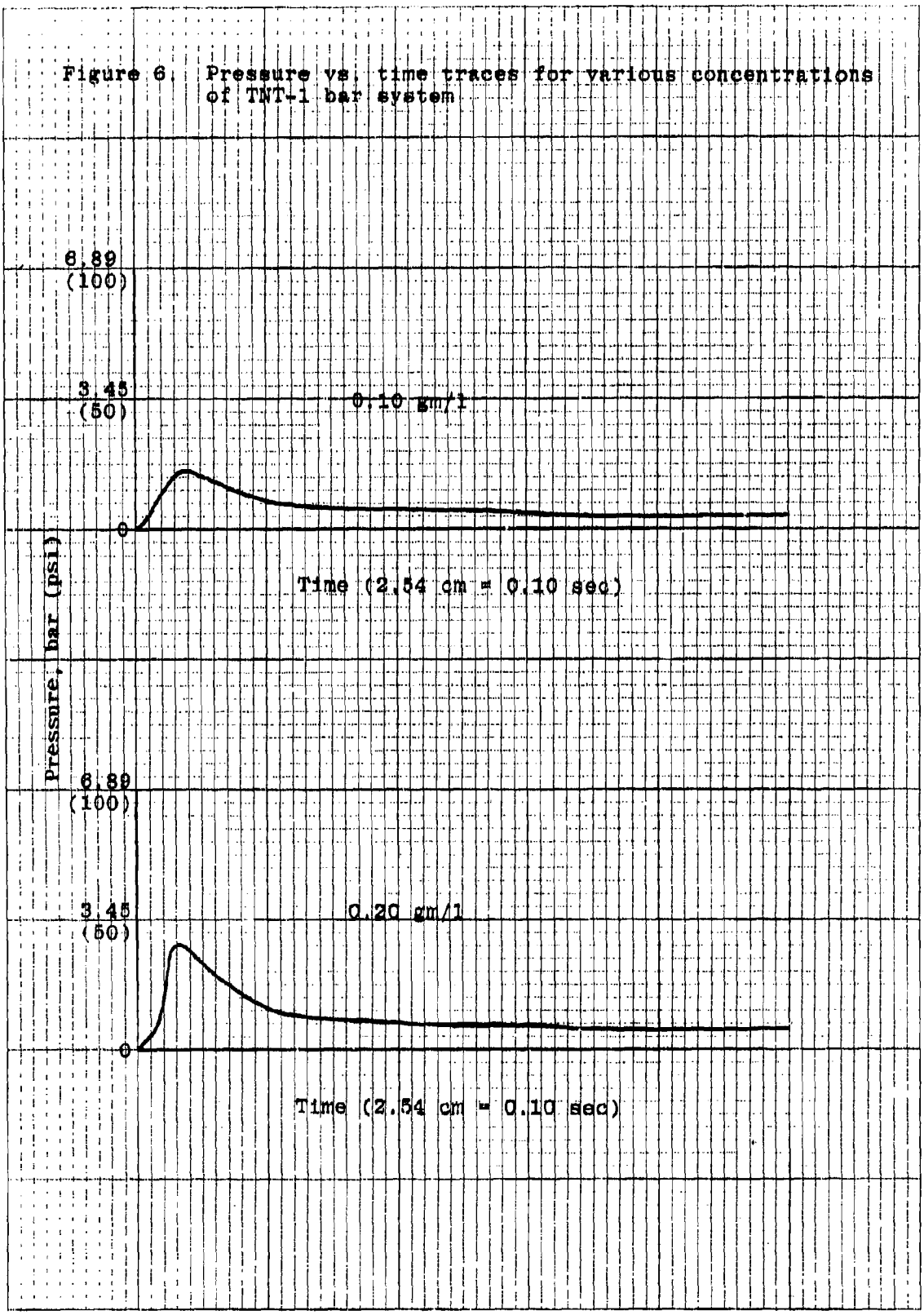

Figure 6. (continued) Pressure vs. time traces for various concentrations of TNT-1 bar system

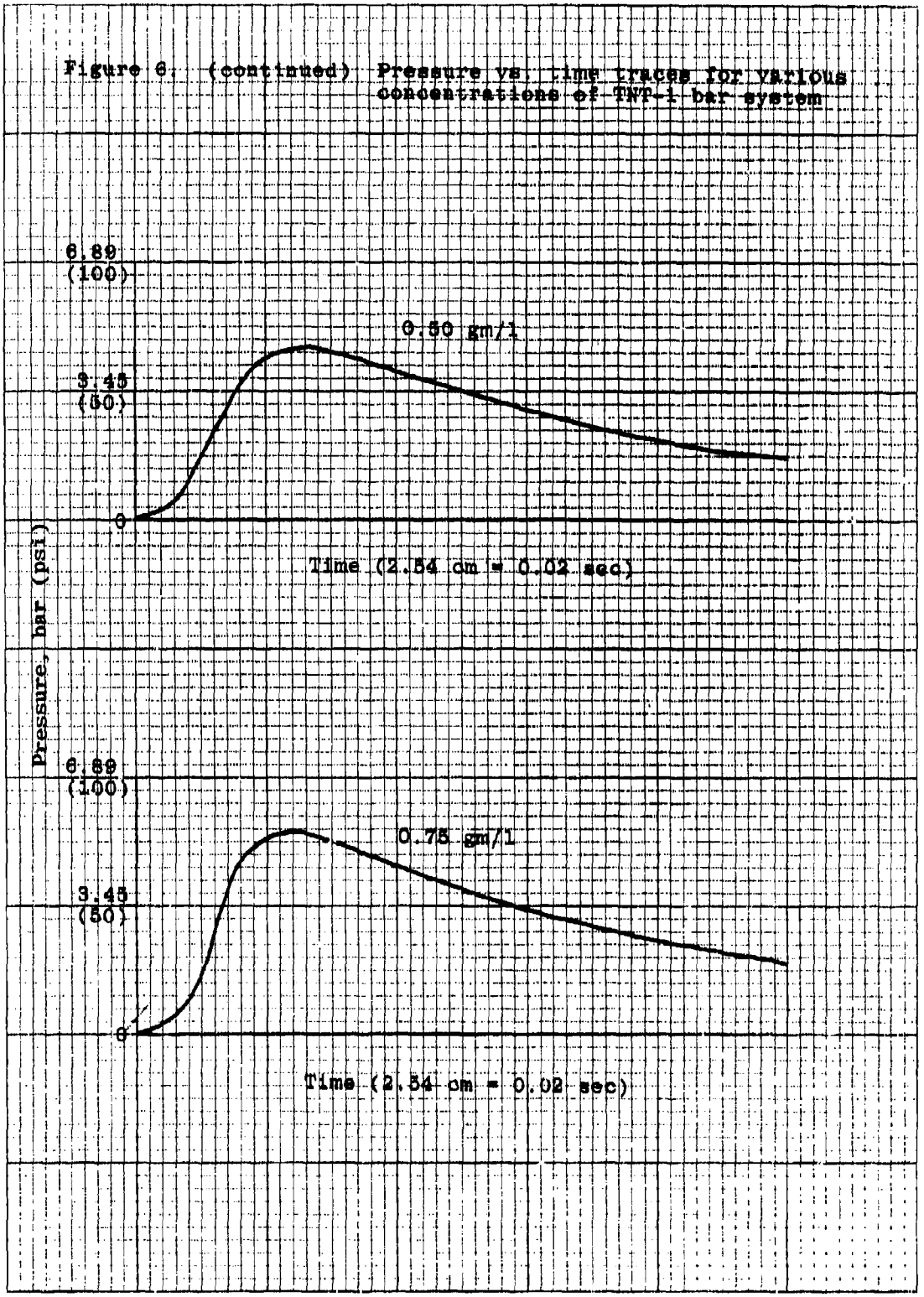

Figure 6. (continued) Pressure vs. time traces for various concentrations of TNT-1 bar system

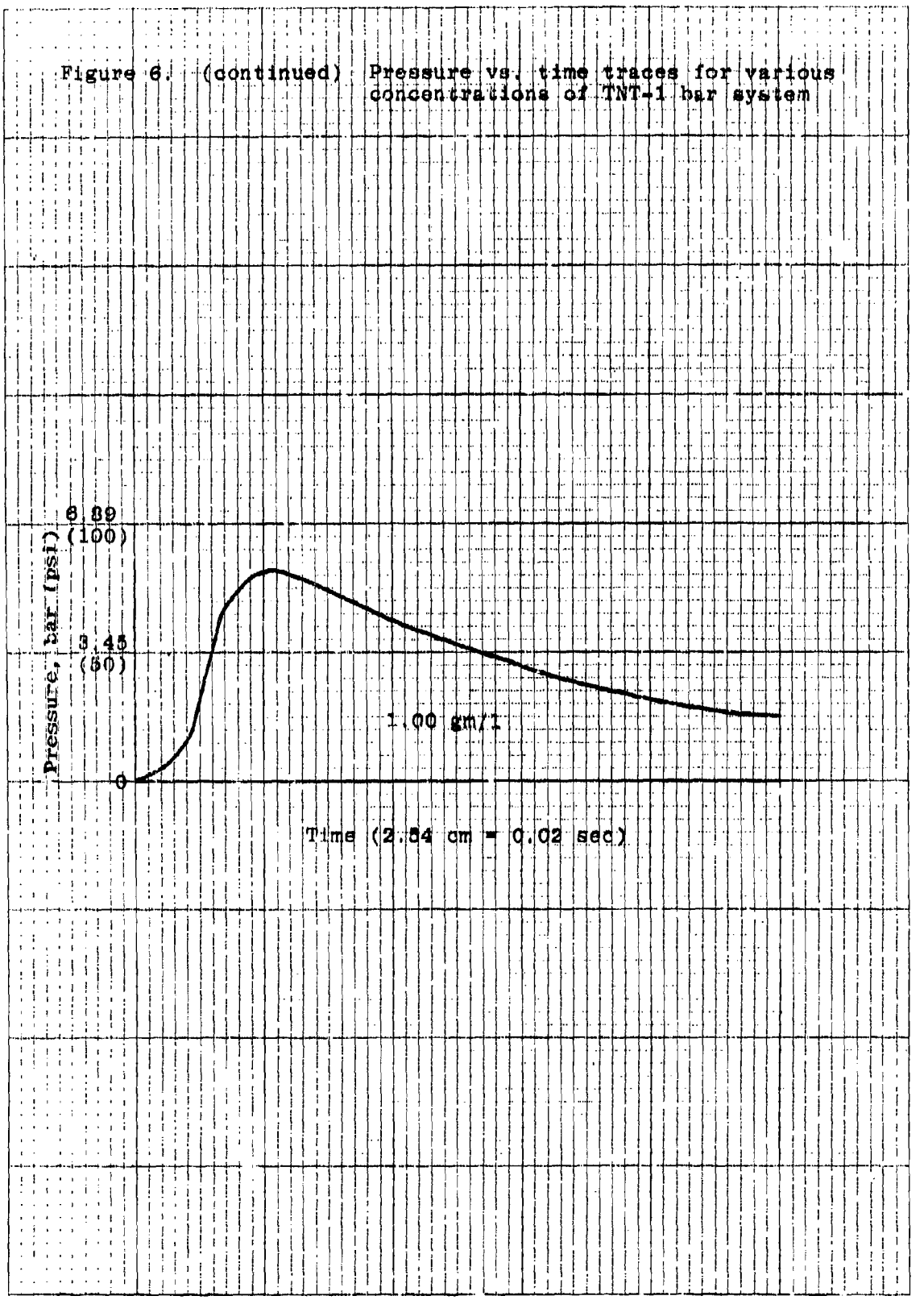

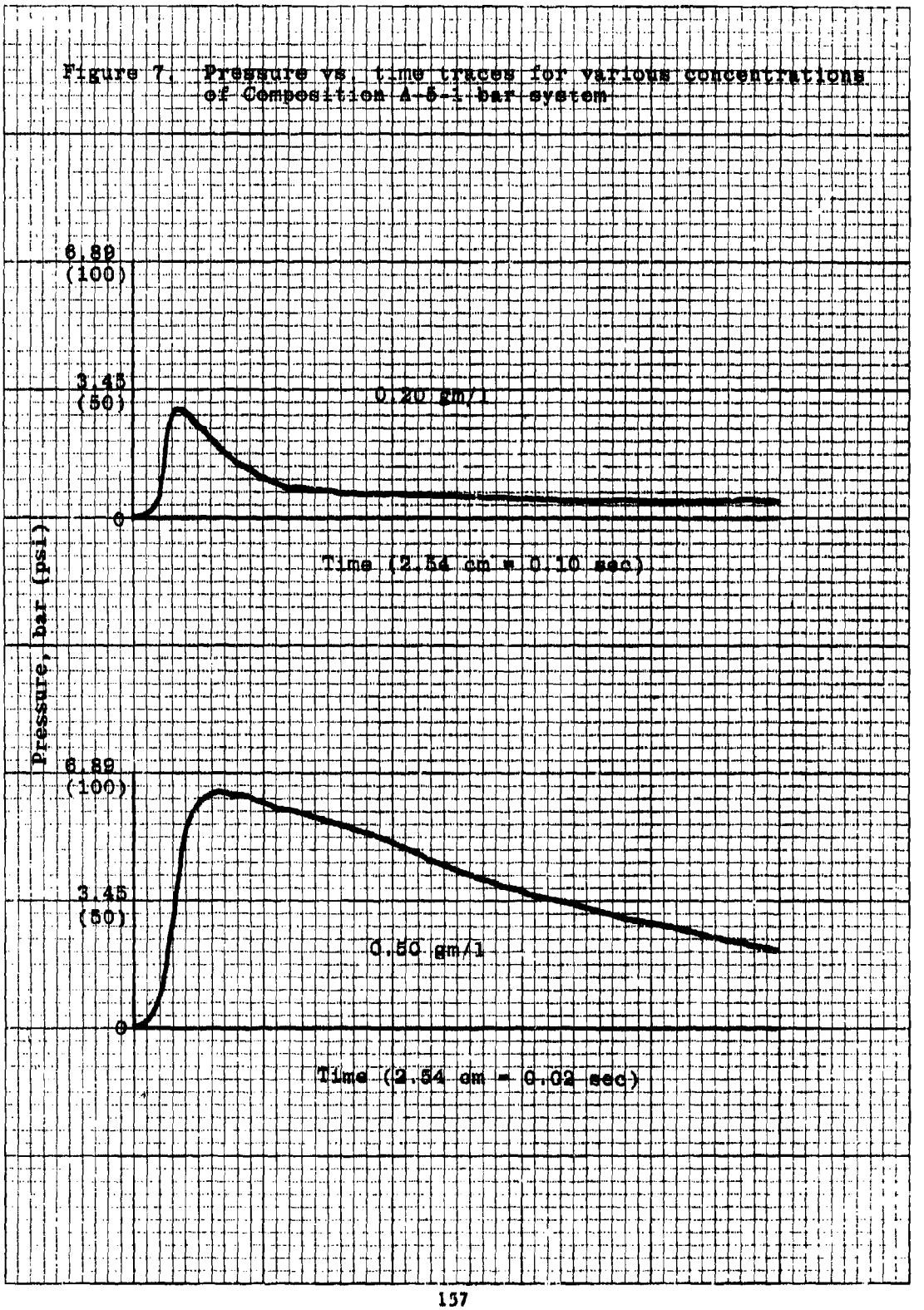

Figure 7. Pressure vs. time traces for various concentrations of Composition A-5-1 bar system

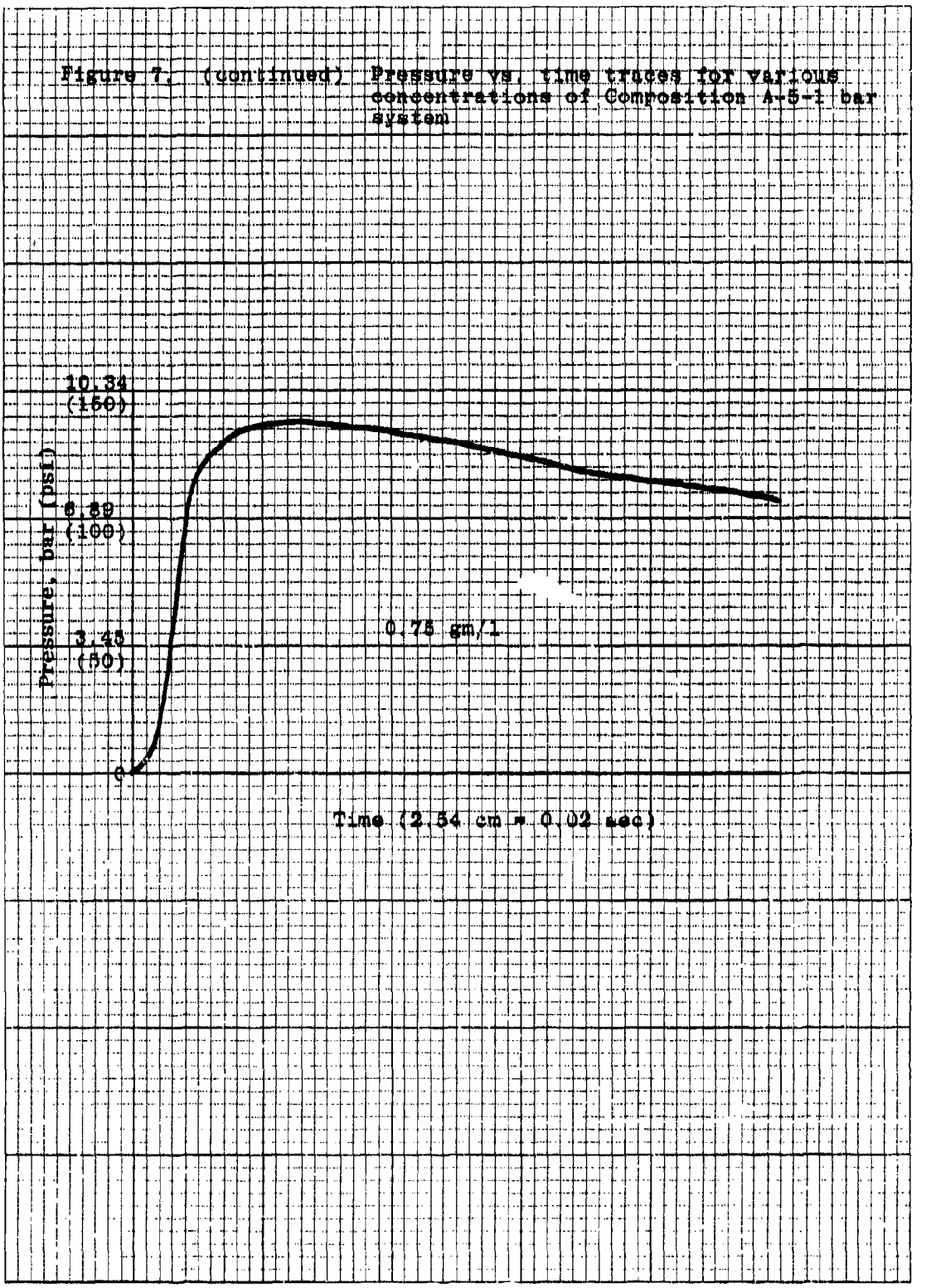

Figure 7. (continued) Pressure vs. time traces for various concentrations of Composition A-5-1 bar system

Figure 7. (continued) Pressure vs. time traces for various concentrations of Composition A-6-1 bar system

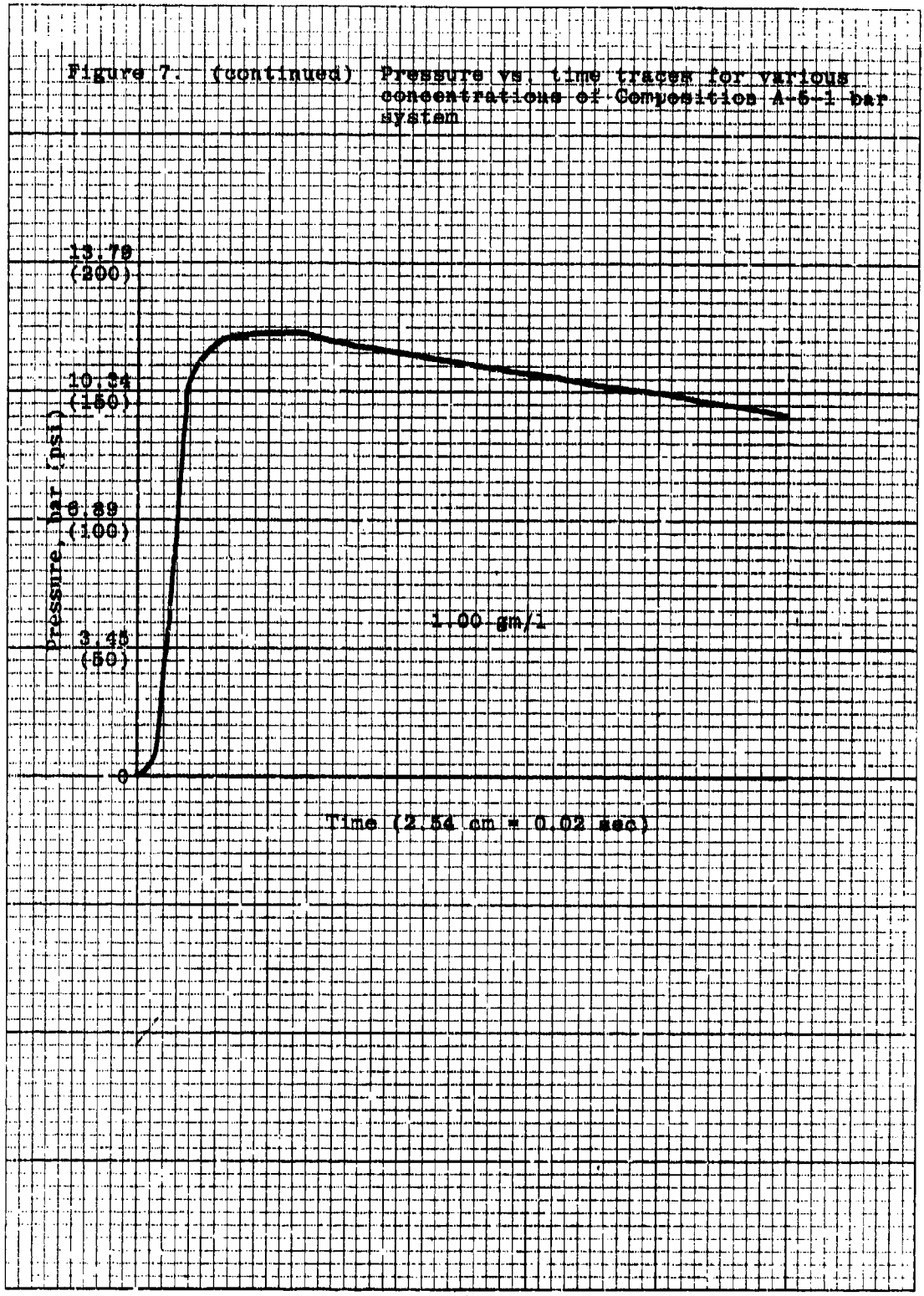

Figure 8. Pressure vs. time traces for various concentrations of TNT-6.9 bar system

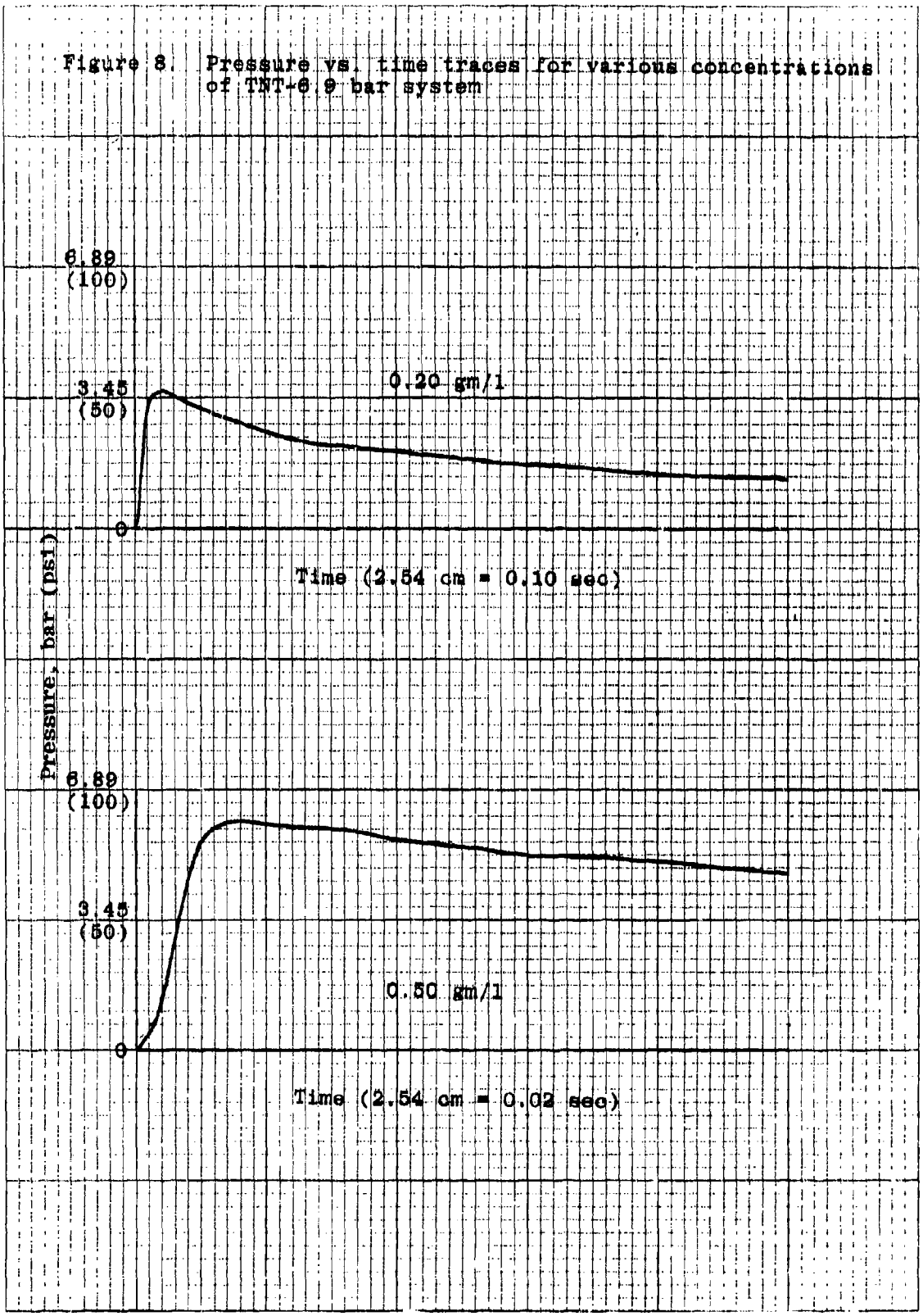

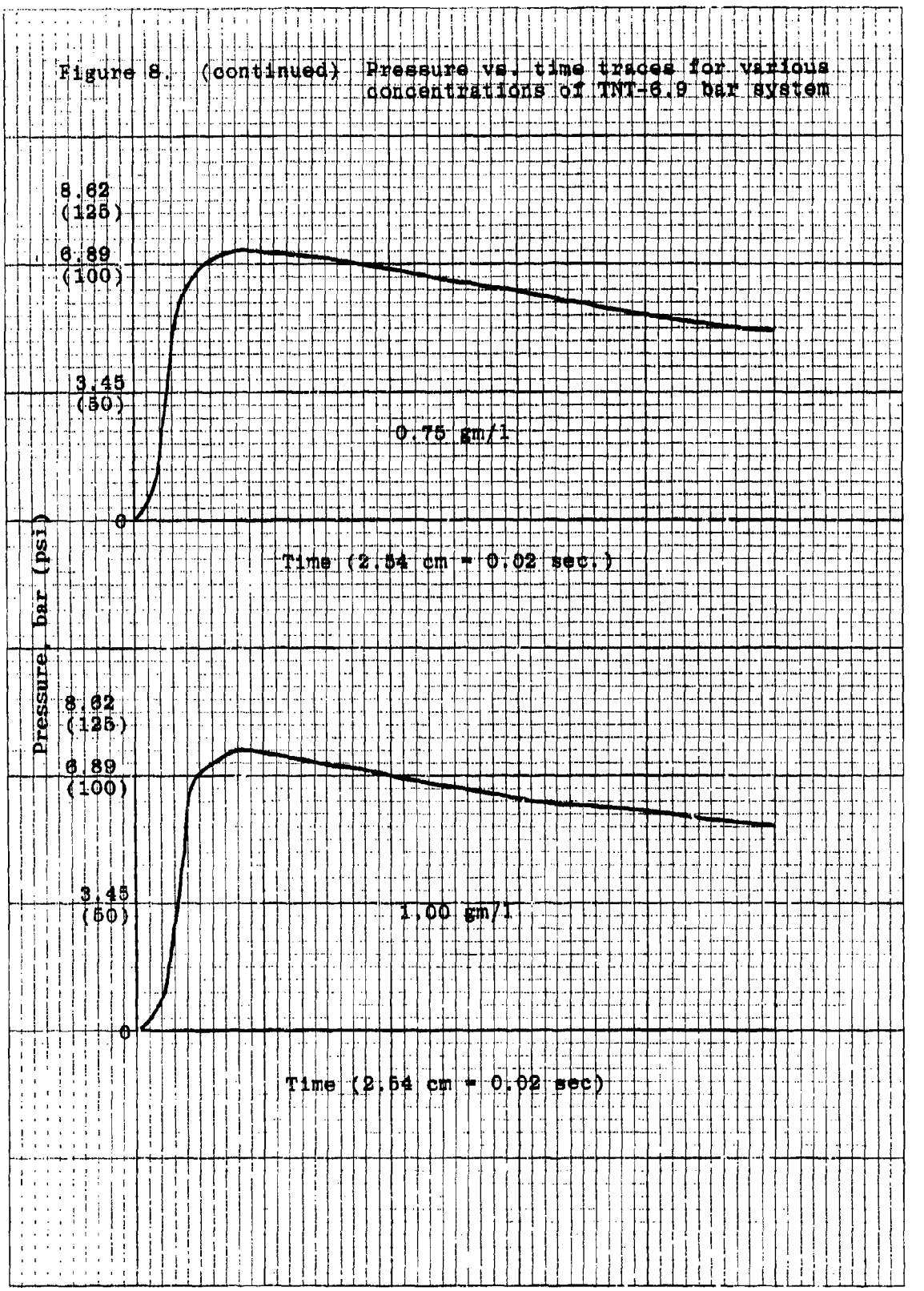

Figure 8. (continued) Pressure vs. time traces for various concentrations of TNT-6.9 bar system

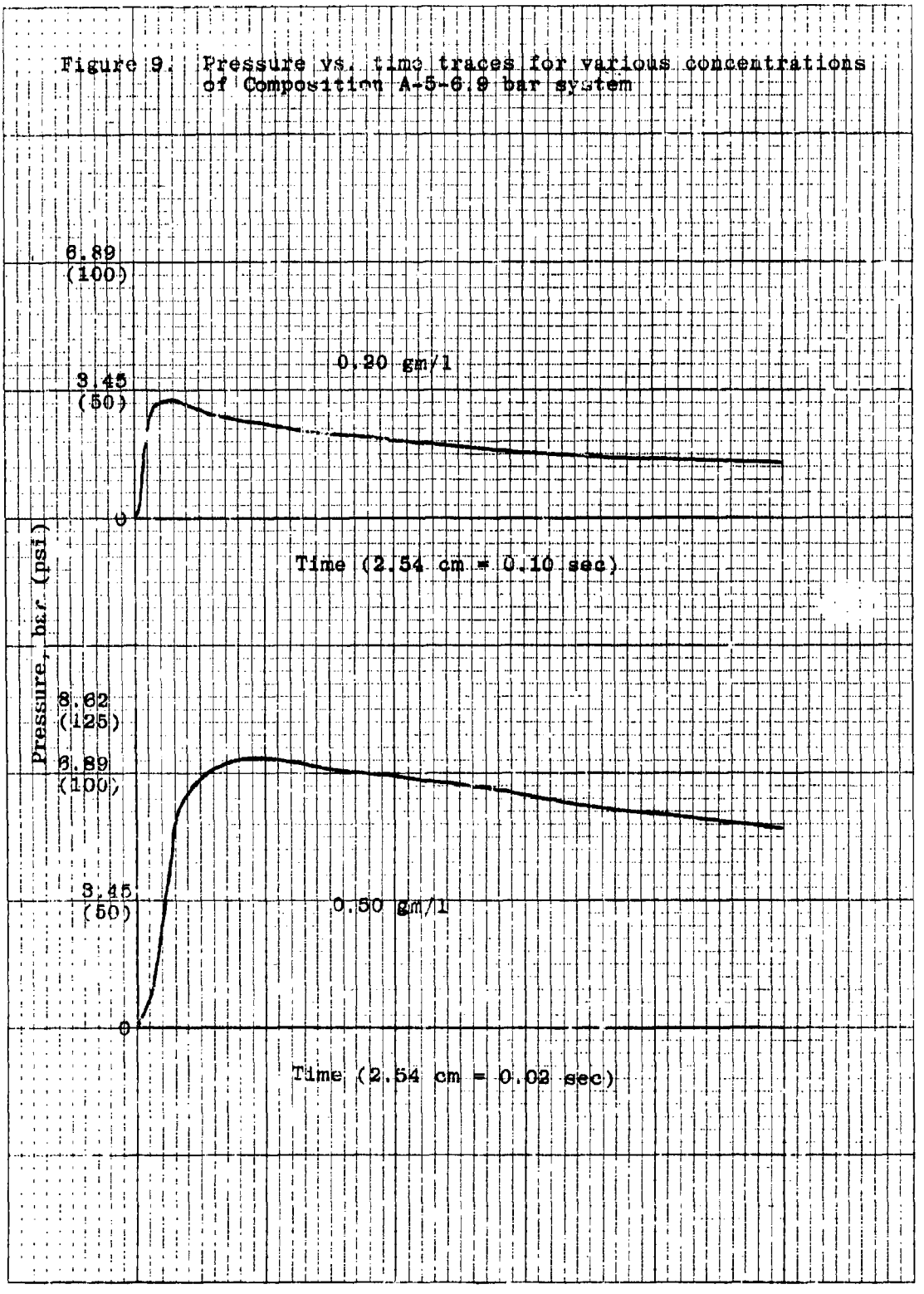

Figure 9. Pressure vs. time traces for various concentrations of Composition A-5-6.9 bar system

Figure 9. (continued) Pressure vs. time traces for varibus concentrations of Composition A-5-6.9 bar system

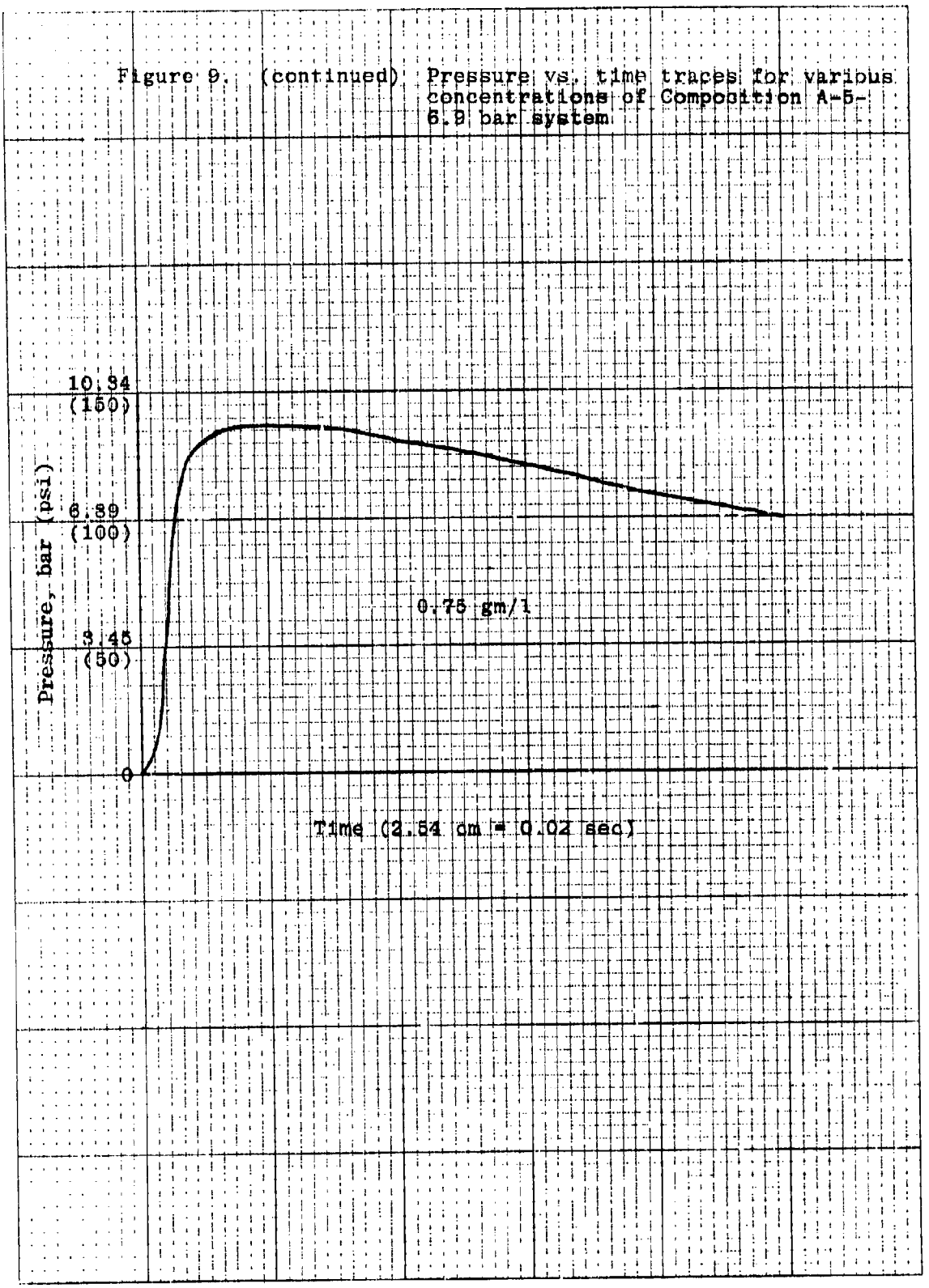

Figure 9. (continued) Pressure vs. time traces for various concentrations of Composition A-5-6.9 bar system

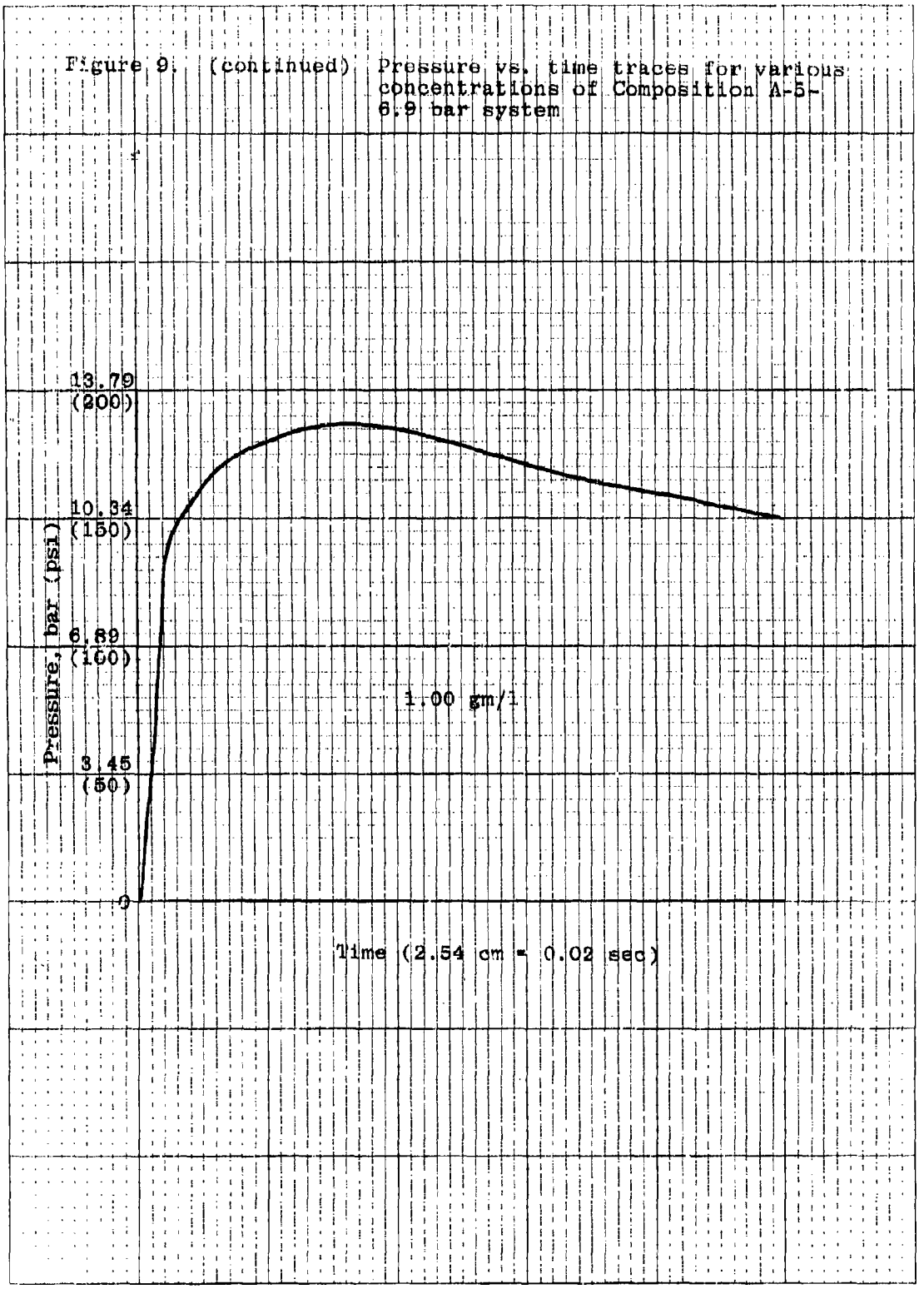

APPENDIX E

Comprehensive Test Data

Comprehensive Test Data

Test	Dust	Mesh Size	Percent Moisture Content	Temp. °F	Relative Humidity (Z)	Ignitor	Delay to Ignition (sec)	Concentration (gm/m^3)	P_{max} (psi)	$\frac{dp}{df}$ ($\frac{psi}{s}$)	Chamber
1	Comp B	-100	<1Z	76	68	AC ARC	0.5	97.6	0	0	Hartmann Bomb
2	Comp B	-100	<1Z	76	68	AC ARC	0.5	195	24.9	225.	Hartmann Bomb
3	Comp B	-100	<1Z	76	68	AC ARC	0.5	301	42.9	667.	Hartmann Bomb
4	Comp B	-100	<1Z	76	68	AC ARC	0.5	488	53.9	1020.	Hartmann Bomb
5	Comp B	-100	<1Z	76	68	AC ARC	0.5	976	75.0	1362.	Hartmann Bomb
6	Comp B	-100	<1Z	76	68	AC ARC	0.5	2.0	90.0	1810.	Hartmann Bomb

Comprehensive Test Data

Test	Dust	Mesh Size	Percent Moisture Content	Temp. °F	Relative Humidity (%)	Ignitor	Delay to Ignition (sec)	Concentration (gm/m^3)	P_{max} (psi)	$\frac{dp}{dt}$ ($\frac{psi}{s}$)	Chamber
65	Comp B	-100	< 1%	54	17	AC ARC	N/A	197	2.7	4.6	40ℓ
67	Comp B	-100	< 1%	34	100	AC ARC	N/A	198	3.0	6.2	40ℓ
69	Comp B	-100	< 1%	34	100	AC ARC	N/A	245	2.1	0	40ℓ
72	Comp B	-100	< 1%	-	-	AC ARC	N/A	262	12.5	71.4	40ℓ
70	Comp B	-100	< 1%	36	93	AC ARC	N/A	271	2.5	0	40ℓ
71	Comp B	-100	< 1%	-	-	AC ARC	N/A	273	40.0	245.0	40ℓ
63	Comp B	-100	< 1%	52	17	AC ARC	N/A	279	2.5	2.8	40ℓ
64	Comp B	-100	< 1%	54	17	AC ARC	N/A	284	43.7	364.0	40ℓ
68	Comp B	-100	< 1%	34	100	AC ARC	N/A	285	58.3	648.0	40ℓ
62	Comp B	-100	< 1%	46	17	AC ARC	N/A	387	75.7	-	40ℓ
66	Comp B	-100	< 1%	60	18	AC ARC	N/A	500	83.3	992.0	40ℓ
33	Comp B	-100	10%			BEM	0.5	213	4.4	68.0	40ℓ
34	Comp B	-100	10%			BEM	0.5	258	19.8	82.3	40ℓ
20	Comp B	-100	10%			BEM	0.5	273	19.4	110.0	40ℓ
26	Comp B	-100	10%			BEM	0.5	316	25.6	101.0	40ℓ
35	Comp B	-100	10%			BEM	0.5	345	30.8	158.0	40ℓ
89	Comp B	-100	< 1%	52	55	BEM	0.5	100	15.9	188.0	40ℓ
88	Comp B	-100	< 1%	40	62	BEM	0.5	148	30.4	223.0	40ℓ
87	Comp B	-100	< 1%	62	29	BEM	0.5	192	31.9	158.0	40ℓ
86	Comp B	-100	< 1%	60	29	BEM	0.5	238	43.7	240.0	40ℓ
85	Comp B	-100	< 1%	59	30	BEM	0.5	286	52.1	334.0	40ℓ
83	Comp B	-100	< 1%	58	36	BEM	0.5	337	60.4	516.0	40ℓ
123	Comp B	-100	< 1%	61	44	AC ARC	N/A	117	0.0	0.0	$1m^3$
124	Comp B	-100	< 1%	62	42	AC ARC	N/A	187	40.0	120.0	$1m^3$
120	Comp B	-100	< 1%	74	51	AC ARC	N/A	250	53.7	231.0	$1m^3$
121	Comp B	-100	< 1%	67	40	AC ARC	N/A	279	62.2	349.0	$1m^3$
122	Comp B	-100	< 1%	67	40	AC ARC	N/A	328	88.6	976.0	$1m^3$

Comprehensive Test Data

Test	Dust	Mesh Size	Percent Moisture Content	Temp. °F	Relative Humidity (%)	Igniter	Delay to Ignition (sec)	Concentration (gm/m^3)	P_{max} (psi)	$\frac{dp}{df}$ ($\frac{psi}{s}$)	Chamber
111	Comp A-5	-100	< 1			BEM	.25	125	7.6	77.9	40ℓ
112	Comp A-5	-100	< 1			BEM	.25	164	11.3	108.6	40ℓ
113	Comp A-5	-100	< 1			BEM	.25	218	19.4	119.4	40ℓ
114	Comp A-5	-100	< 1			BEM	.25	260	26.9	180.0	40ℓ
91	Comp A-5	-100	< 1	58	40	BEM	.25	267	32.7	251.0	40ℓ
100	Comp A-5	-100	< 1	62	69	BEM	.25	274	35.4	259.0	40ℓ
90	Comp A-5	-100	< 1	52	46	BEM	.25	280	33.5	322.0	40ℓ
117	Comp A-5	-100	< 1			BEM	.25	313	25.8	264.0	40ℓ
107	Comp A-5	-100	< 1			BEM	.5	121	6.5	40.0	40ℓ
108	Comp A-5	-100	< 1			BEM	.5	169	5.4	43.7	40ℓ
116	Comp A-5	-100	< 1			BEM	.5	178	7.6	45.0	40ℓ
109	Comp A-5	-100	< 1			BEM	.5	220	13.5	104.0	40ℓ
94	Comp A-5	-100	< 1	62	38	BEM	.5	225	13.2	102.0	40ℓ
110	Comp A-5	-100	< 1			BEM	.5	271	16.2	119.0	40ℓ
97	Comp A-5	-100	< 1	44	85	BEM	.5	315	27.1	189.0	40ℓ
84	Comp A-5	-100	< 1	58	33	BEM	.5	337	28.7	170.0	40ℓ
98	Comp A-5	-100	< 1	47	85	BEM	.5	354	38.2	226.0	40ℓ
73	Comp A-5	-100	< 1	62	38	BEM	.5	378	45.8	352.0	40ℓ
82	Comp A-5	-100	< 1	58	40	BEM	.375	415	41.5	266.0	40ℓ
103	Comp A-5	-100	< 1			BEM	.75	140	0.0	0.0	40ℓ
104	Comp A-5	-100	< 1			BEM	.75	180	1.7	18.7	40ℓ
105	Comp A-5	-100	< 1			BEM	.75	220	5.4	43.7	40ℓ
115	Comp A-5	-100	< 1			BEM	.75	268	9.7	55.3	40ℓ
106	Comp A-5	-100	< 1			BEM	.75	274	3.8	29.2	40ℓ
92	Comp A-5	-100	< 1	60	40	BEM	.75	317	16.8	78.3	40ℓ
79	Comp A-5	-100	< 1	50	62	BEM	.75	333	16.6	85.1	40ℓ
81	Comp A-5	-100	< 1	55	42	BEM	.75	390	22.6	112.0	40ℓ
77	Comp A-5	-100	< 1	49	62	BEM	1.0	275	4.2	64.6	40ℓ
96	Comp A-5	-100	< 1	43	85	BEM	1.0	324	4.3	44.1	40ℓ

DISTRIBUTION LIST

Commander
U.S. Army Armament Research and
Development Command
ATTN: DRDAR-CG
DRDAR-LC
DRDAR-LCM
DRDAR-LCM-S (12)
DRDAR-SF
DRDAR-TSS (5)
Dover, NJ 07801

Commander
U.S. Army Materiel Development and
Readiness Command
ATTN: DRCDE
DRCIS-E
DRCPA-E
DRCPP-I
DRCDL
DRCSG-S
5001 Eisenhower Avenue
Alexandria, VA 22333

Commander
USDRC Installations and
Services Agency
ATTN: DRCIS-RI-IU
DRCIS-RI-IC
Rock Island, IL 61299

Commander
U.S. Army Materiel and
Readiness Command
ATTN: DRSAR-IR (2)
DRSAR-IRC
DRSAR-ISE (2)
DRSAR-IRC-E
DRSAR-PDM
DRSAR-LC (2)
DRSAR-ASF (2)
DRSAR-SF (3)
DRSAR-LEP-L
Rock Island, IL 61299

Office, Chief of Engineers
ATTN: DAEN-MZA-E
Washington, DC 20314

Chairman
Department of Defense Explosives
Safety Board (2)
Hoffman Bldg 1, Room 856C
2461 Eisenhower Avenue
Alexandria, VA 22331

Commander
U.S. Army Munitions Base
Modernization Agency
ATTN: SARPA-PBM-LA (3)
SARPA-PBM-T-SF
SARPA-PBM-EP (2)
Dover, NJ 07801

Director
Ballistics Research Laboratory
U.S. Army Armament Research and
Development Command
ATTN: DRDAR-TSB-S
DRDAR-BLE (C. Kingery) (2)
Aberdeen Proving Ground, MD 21005

Administrator
Defense Technical Information Center
ATTN: Accessions Division (12)
Cameron Station
Alexandria, VA 22314

Commander
U.S. Army Construction Engineering
Research Laboratory
ATTN: CERL-ER
Champaign, IL 61820

U.S. Army Engineer District,
Huntsville
ATTN: Construction Division
HAD-ED (2)
P.O. Box 1600 West Station
Huntsville, AL 35807

Director
U.S. Army Industrial Base
Engineering Activity
ATTN: DRXIB-MT (2)
Rock Island, IL 61299

Director
DARCOM Field Safety Activity
ATTN: DRXOS (5)
Charlestown, IN 47111

Director
U.S. Army Materiel Systems
Analysis Activity
ATTN: DRXSY-MP
Aberdeen Proving Ground, MD 21005

Commander/Director
Chemical Systems Laboratory
U.S. Army Armament Research and
Development Command
ATTN: DRDAR-CLJ-L
DRDAR-CLB-PA
APG, Edgewood Area, MD 21010

Chief
Benet Weapons Laboratory, LCL
U.S. Army Armament Research and
Development Command
ATTN: DRDAR-LCB-TL
Watervliet, NY 12189